Author:
Burford, Rory

Title:
Out of the Blue

An investigation of two alternative sources of deep ice

OUT OF THE BLUE:

AN INVESTIGATION OF TWO ALTERNATIVE SOURCES OF DEEP ICE

Rory Joshua Burford

A dissertation submitted to the University of Bristol in accordance with the requirements for award of the degree of MSc by Research in the Faculty of Science

School of Geographical Sciences, September 2018

Word count: 29,408

Abstract

The direct sampling of deep ice is an invaluable tool for environmental research, however the logistical, technical and financial difficulties associated with many direct sampling approaches renders them unfeasible for all but the largest research collaborations. This thesis considers two alternative sampling approaches, both of which utilise deep ice that has been exposed for surface sampling by the natural flow of glaciers. Namely, it presents the biogeochemical analysis of terminal blue ice from the Marble Hills Blue Ice Area (Antarctica) and calved icebergs from Lago Steffen (Chilean Patagonia). These samples were collected and analysed using straightforward, low-cost methodologies, available to a large number of glaciological researchers. These approaches are evaluated in terms of the usefulness of the data that can be obtained and the availability of potential sample sites for future investigation. In doing so, this thesis sheds light on new methodologies that could be employed to answer questions concerning glacial processes.

As well as exploring novel research approaches, this thesis offers original contributions to the knowledge of natural processes occurring within the vicinity of Horseshoe Valley Glacier (West Antarctic Ice Sheet) and Steffen Glacier (North Patagonian Icefield). The discussion of the Antarctic samples centres on the subglacial origin of the ice, which is indicated by the non-meteoric relationship between $\delta^{2}H$ and $\delta^{18}O$ and the high concentrations of certain nutrients ($CaCO_3$, SO_4^{2-}, DOC) corresponding with subglacial environments. This also reveals the dominant chemical processes occurring at the bed. The discussion of iceberg samples employs similar techniques with a different focus: augmented by samples of local rivers and precipitation, it considers the impact of Steffen Glacier on downstream freshwater systems. This thesis therefore emphasises how readily-available deposits of deep ice can be utilised for a wide range of contemporary research questions.

Dedication and Acknowledgements

I would like to dedicate this thesis to Susan, David, Zara and Tom – my family – without whom I would not have had the courage to make the jump to glaciology, let alone find the confidence to take myself seriously as an academic. To Zara and Tom in particular, I also owe thanks for their constant tips for my development as a postgraduate researcher. Along a similar vein, I would like to thank my supervisor, Professor Jemma Wadham, for offering me the opportunity to pursue this (fascinating) research and leaving me the space to grow as a scientist.

I must also acknowledge the patience and support of Jon Hawkings and Matthew Marshall – my main mentors in the mysterious ways of planning and executing plans in the lab and field – and James Williams, who supported me enormously in bringing the water isotope analyser online against all odds.

Lastly, I owe gratitude to Andy Hein, David Sugden and others at the University of Edinburgh involved in the sampling of the Marble Hills BIA with which I have been working, as well as Ale Urra Gallardo and the PISCES Project collaborators for their parts in organising the February 2017 field season at Lago Steffen. *¡Muchas gracias a todos!*

Author's Declaration

I declare that the work in this dissertation was carried out in accordance with the requirements of the University's *Regulations and Code of Practice for Research Degree Programmes* and that it has not been submitted for any other academic award. Except where indicated by specific reference in the text, the work is the candidate's own work. Work done in collaboration with, or with the assistance of, others, is indicated as such. Any views expressed in the dissertation are those of the author.

SIGNED: .....  ..... DATE:20/12/2018.....

Table of Contents

List of Figures and Tables

Chapter 1 – Why do we need alternative sources of deep ice?

1.1 – Overview

Ice preserves. Deep ice may hold a chemical record of paleoclimatic conditions from the time of precipitation [1], while the deepest ice can preserve the traces of subglacial processes [2]. Both of these records are of interest to the contemporary research community: paleoclimatic reconstructions are used to constrain models of future climate change, whilst the input of glacial meltwaters into marine and freshwater environments is believed to play a significant role in biogeochemical cycles. Glaciochemical studies of deep ice are therefore a versatile tool for environmental research.

Despite their obvious promise, surprisingly few successful deep ice investigations have been published to date. This is because important sampling sites are typically located in remote areas with extreme conditions of temperature (e.g. the Antarctic Ice Sheets) and/or altitude (e.g. the Patagonian Icefields). Such sites are often inaccessible by road, which makes the transport of sampling equipment and establishment of a research base logistically difficult. Once a location is established, most deep ice can only be accessed with sophisticated drilling instruments, which are difficult to obtain and run without mass collaborative efforts such as those within the Scientific Committee on Antarctic Research (SCAR). In short, accessibility is a limiting factor of the utilisation of deep ice for environmental research.

This thesis considers two unconventional sources of deep ice as accessible alternatives to direct sampling for some research purposes. Terminal Blue Ice Samples (TBIS) have been taken from the Marble Hills Blue Ice Area (BIA), where negative surface mass balance (SMB) is known to result in the upwards flow of ancient ice. These terminal samples are likely to have flown from deeper than elsewhere in the BIA – potentially even the subglacial environment, hundreds of metres below. Samples have also been taken from icebergs in Lago Steffen, a proglacial lake in Chilean Patagonia. These icebergs calve from the terminus of Steffen Glacier, exposing englacial and subglacial ice as they rotate in the lake. Both sets of samples were retrieved by a small team with no specialist training and only basic sampling equipment: the methodology could therefore be easily adopted by other researchers. The samples have undergone standard laboratory analyses such as the spectroscopic measurement of water isotopes and ion-exchange chromatography. With these data, this thesis will aim to answer three key questions underlying this project:

1. What can TBIS tell us about the environment beneath the Antarctic surface?
2. What can calved Patagonian icebergs tell us about inaccessible mountain glaciers?
3. What role could alternative sources of deep ice serve in the 21st Century?

The individual analyses are likely to be interesting in their own right: no previous work has ever investigated the subglacial environment of Horseshoe Valley Glacier, nor has there been an estimation of the composition of Steffen Glacier and its impact on downstream ecosystems. However, the questions are phrased more generally to reflect the primary aim of this thesis: to investigate whether or not the methodology employed in this thesis could be adopted more widely by the contemporary research

community. In order to reach this conclusion, there must be evidence that these samples sites are not unique, i.e. there is an appropriate distribution of potential sites for further work to be carried out. It must also be shown that the available glaciochemical data are useful for a range of applications besides the conceptual approach employed in this thesis.

It is not anticipated that direct sampling of deep ice will be replaced overnight: it is unlikely that either the Antarctic or Patagonian samples will be interchangeable with direct samples for every application. However, even a few novel applications could greatly simplify the task of studying deep ice. Given that the impacts of deglaciation will be felt widely across both marine and freshwater environments, 21st Century climate change will bring a demand for an increase in research output from the wider glaciology community. The establishment of new, economical sampling approaches (both in terms of cost and time) could thus play an important role in meeting the demands of a changing world.

1.2 – The utility of deep ice data

1.2.1 – Paleoclimatic records

It has long been known amongst archaeologists and geologists that there is an approximate relationship between the age of a find and the depth at which it is found [3]. When researchers of paleoclimate turned their attention to the cryosphere, they found that the unique conditions of glaciers and ice sheets can preserve hundreds of thousands of years of climate data [4-6]. Indeed, it has been argued that deep ice is the most reliable source of atmospheric data throughout the Quaternary [1]. This is likely due to the continued presence of polar ice sheets since long before the most recent ice age (the expansion of the Antarctic cryosphere may date back to the middle Miocene climatic transition [7, 8]) and the absence of large-scale human populations to disturb the records.

Climate scientists have been aware of the utility of deep ice as dipsticks into past atmospheric conditions for over thirty years, when early pioneers of global warming research extracted a record of changing methane levels from Greenland ice cores [9]. In the decades that followed, successive studies on Antarctic ice cores have extended our knowledge of Pleistocene atmospheric CO_2 levels back more than 800,000 years [10-12], while the $\delta^{18}O$ record observed in low latitude ice caps has been used to estimate tropical sea surface temperatures over much of recorded human history [13, 14]. Temporal records showing 300 years of anthropogenic pollution have been resolved from ice cores in Svalbard [15, 16], the Alps [17, 18], the Saint Elias Mountains [19] and numerous other sites in close proximity (or with indirect exposure) to human activity. These studies all rely upon the principle that snow and firn gradually accumulate on the surface of glaciers and ice sheets, trapping air and ice as they are compressed by the younger firn that collects above them. This preserves a temporally-stratified record of meteoric water and atmospheric composition. According to IPICS (International Partnerships in Ice Core Sciences), ice core records have been collected from every continent except Australia. The available data are however insufficient for a comprehensive climate reconstruction – longer records are required, with better temporal resolution [20].

Much of the available data are from polar regions, where polythermal glaciers dominate and human interference is limited. Net annual accumulation at these latitudes is significantly less than that which is found at lower latitudes: much of the Antarctic continent is essentially a desert [21]. This leads to the build-up of annual layers that are very thin and may not be distinguished from their neighbours, limiting the temporal resolution that can be achieved from Antarctic ice cores. Deep ice from high latitudes does however have a good deal of utility in the study of paleoclimate, where annual resolution is not required. This is due to the relatively undisturbed existence of the polar ice sheets throughout the Quaternary – facilitating the development of continuous records that stretch back hundreds of thousands of years – and the fact that polar glaciers are generally stable all year round, which reduces the risk of mixing between layers of different ages due to melting of the porous upper portion.

For the most part, this thesis will focus on the other uses of deep ice, as described in the following sections. This is not due to a lack of potential for the extraction of paleoclimatic data from alternative sources of deep ice, but rather because work is already underway in this area. Antarctic blue ice areas have attracted the interest of a number of paleoclimatology groups due to their unique ability to horizontally stratify ancient ice. In Chapter 3, blue ice is investigated from a different perspective: the subglacial environment.

1.2.2 – Atmosphere and ecosystems

Not all deep ice is millions of years old, nor are the uses of deep ice data restricted to paleoclimate contexts. In contrast with their polar cousins, temperate glaciers may be better suited to the collection of relatively recent atmospheric data with seasonal resolution [22]. NO_x species, aerosols and other anthropogenic pollutants are often deposited on the surface of low to mid latitude glaciers, marking them out as sites for monitoring the human impact on the environment; these studies will be of growing importance throughout the 21st Century due to the increasing threat expected to be posed by climate change.

In addition to this, many settlements rely directly on temperate glaciers for drinking water, agriculture and the generation of electricity [23-25]. This is especially important in arid locations, where peak flux of glacial meltwaters coincides with the annual rainfall minimum [26]. These areas are thus especially sensitive to climate-induced glacier loss [27]. Populations that do not utilise glacial meltwaters for drinking, power or irrigation may still rely indirectly on the cryosphere as a source of essential nutrients for downstream primary productivity [28-30] and the subsequent sustainable ecosystems upon which many livelihoods depend [31, 32]. Meltwater often differs distinctly from the riverine and coastal waters that it feeds into in terms of composition, salinity, turbidity, temperature and density. Consequently, the rate of glacial melt can significantly affect the biological and chemical systems downstream.

Numerous studies have demonstrated that phytoplankton biomass and diversity is dependent on meltwater in both freshwater and marine environments. For instance, the delivery of growth-limiting nitrogen to glacially-influenced lakes in the Rocky Mountains is associated with five times higher primary productivity than is observed in lakes fed by snowpack alone [33]. A similar case is found in the Southern Ocean (SO), where the supply of bioavailable iron is a well-established limit on primary productivity [34-39]. Other studies of the SO have noted that the dilution of saline water caused by glacial runoff is associated with

changes in microbial community structure [40]. Moreover, glaciers can affect primary production through alteration of the physical properties of the water. For example, increased turbidity may limit the rate of photosynthesis for all but the most specialised producers [41, 42], while the density differences between meltwater and the ocean result in a stratified surface layer, the extent of which may again influence the community structure of primary producers [43]. The chemical composition of inaccessible glaciers can therefore influence fields such as aquatic ecology.

The chemical impact of glacial meltwater is generally less visible than the swirling phytoplankton blooms that correlate with Greenland Ice Sheet runoff [44]; there are nevertheless myriad ways in which the cryosphere can affect the composition and subsequent chemistry of downstream systems. Subglacial meltwaters in particular are a major driving force behind chemical change. These streams are known to contain more dissolved species than their supraglacial counterparts [45], and carry chemically-active reagents released by subglacial processes. For instance, high concentrations of sulphate and insoluble iron hydroxide are released into the water by the chemical weathering of pyrite [46, 47]. Iron hydroxide adsorbs soluble reactive phosphate, effectively removing a significant chemical substrate from solution [47]. Sulphuric acid is also produced by this process, and can provide protons for acid hydrolysis, a major source of base cations in glacial systems [48]. These interconnected processes may dominate the geochemistry of glacial streams.

In addition to the relatively irreversible reactions discussed above, ion-exchange may take place between the meltwater and the stream bed, contributing to weathering rates [49, 50]. Along with gas exchange at the air-water interface, these processes form part of a larger group of rapid reversible reactions occurring in glacially-fed streams. To further complicate things, Tranter et al. [51] proposed that solute acquisition most often occurs through the concerted action of fast and slow reactions. An illustrative example is the reversible dissolution of CO_2 in glacial waters:

$$CO_{2(g)} \rightleftharpoons CO_{2(aq)} \qquad \text{Equation 1}$$

$$CO_{2(aq)} + H_2O_{(l)} \rightleftharpoons H_2CO_{3(aq)} \qquad \text{Equation 2}$$

$$H_2CO_{3(aq)} + H_2O_{(l)} \rightleftharpoons {HCO_3}^-_{(aq)} + {H_3O}^+_{(aq)} \qquad \text{Equation 3}$$

$${HCO_3}^-_{(aq)} + H_2O_{(l)} \rightleftharpoons {CO_3}^{2-}_{(aq)} + {H_3O}^+_{(aq)} \qquad \text{Equation 4}$$

Alone, this process will merely reach a thermodynamic equilibrium with the atmosphere, limiting how much solute can be acquired by the stream. Under most conditions, the point of equilibrium will be quite far to the left. However, the few hydronium ions which are formed by equations 3 and 4 will quickly be used up by other reactions – most notably, the acid dissolution of minerals. This destabilises the equilibrium and drives further dissolution of CO_2, as per Le Chatelier's Principle, leading to net acquisition of Ca^{2+} and Mg^{2+} (from dissolved minerals), as well as HCO_3^- ions (by-products of the original equilibrium). Consequently, the concentrations of major cations and carbonate anions have been found to correlate significantly both with each other and with increasing distance downstream [52].

Over different locations and timescales, climate change may have very different impacts on glacially-supported ecosystems. Clearly, it has the potential to augment these chemical outputs through increased

surface melt. It also has the potential to reduce precipitation over the accumulation areas of alpine glaciers, decreasing glacial outputs [53]. It even threatens to halt them altogether in locations such as Glacier National Park (Montana, USA), where glaciers may become extinct by 2030 [54]. An understanding of the biological and chemical influence of glaciers on downstream ecosystems is therefore essential for the accurate prediction of (and subsequent response to) the local impact of climate change. In Chapter 4, calved iceberg samples are analysed alongside riverine samples in order to explore the influence of glacial ice on downstream communities and ecosystems.

1.2.3 – Subglacial processes

The deepest glacial ice may hold clues to the subglacial environment. Due to pressure-induced melting and refreezing underneath many of the world's ice sheets and glaciers, ice that has been in contact with the subglacial bed may have mixed with solute-heavy subglacial water. Such processes may also lead to the incorporation of biologically-active sediment into the basal layer. Biogeochemical studies of these deep samples are consequently invaluable in the identification of the processes taking place under the ice. Accessible sources of such ice would not only improve our ability to characterise the subglacial environment, but would also help us to predict the effect of glacial runoff on the downstream environment, as discussed above.

The relative abundance of nutrients carried by subglacial waters is largely due to weathering and denudation taking place at the glacial bed. Nutrients are released through a combination of both physical and chemical processes, the fluxes of which have been shown to be interdependent [55]. This typically begins with abrasion of the underlying rock, followed by comminution of suspended grains, creating glacial flour. A dramatic increase in surface area results from this grinding of inorganic particles; it can also put minerals under enough strain to instigate local deformation of the lattice [56]. These processes enhance reaction with the aqueous subglacial environment and may explain the limited effect that the low temperatures of glacial environments seem to have on rates of chemical weathering [57].

Of course, not all subglacial weathering takes place by purely physical and chemical means. Microbial communities have been observed virtually everywhere that glacial ice occurs, from the Greenland ice sheet [58] to mountain glaciers in Canada [59], New Zealand [60] and low-latitude Venezuelan ice caps [61]. Recently, researchers have established extensive evidence for a microbial ecosystem under the Antarctic Ice Sheets (AIS), in a biome that has been cut off from the atmosphere for more than a million years [62-65]. This life is most likely surviving in diverse hydrological systems at the subglacial bed, rather than in the midst of the englacial zone [66]. In fact, the common factor in all of these studies are that microbe communities were found to live underneath the ice (although cells are also known to survive on the surface, particularly in cryoconite holes [67, 68]). It might seem counter-intuitive that life can persevere in such harsh conditions: light levels are negligible and temperatures can be lower than the pressure-induced melting point of the ice above [69, 70]. It is nevertheless commonly accepted that microorganisms are both present and exceedingly well adapted to life under the cryosphere.

Much of the evidence for subglacial ecosystems comes from observations of biogeochemistry. A series of incubation experiments carried out by Skidmore et al. [59] found that measurements of NO_3^- and SO_4^{2-} – both of which can act as terminal electron acceptors for cellular respiration – decreased during anaerobic incubation of basal ice, while thawed englacial samples showed no such change. The same study found that biological activity persisted even at basal temperature conditions (ca. 0°C), indicating that the cells responsible remained viable *in situ*. Further roles for sulphate in metabolism have been indicated by investigations of Haut Glacier d'Arolla (Switzerland), where biological activity can drive anoxic conditions and subsequent metabolic reduction of SO_4^{2-} in place of O_2 [71, 72]. Conversely, the resulting anaerobic environment enables the oxidation of S_2^- by Fe^{III} via both biotic and abiotic mechanisms [73, 74]. The discovery of these interdependent biological and chemical processes has led to a considerable shift in our understanding of subglacial weathering.

Where biological activity is great, there is often an abundance of metabolic by-products. In the sulphate reduction example there is no build-up of the reduced product, as the corresponding oxidation reaction occurs at a much greater rate [72]. This is not the case for all subglacial biological processes; microbial respiration, for example, has been suggested as a cause for the excess of HCO_3^- found in Haut Glacier [75, 76]. The mass production of key chemical species can be of significance for global biogeochemical cycles, creating ice-bound reservoirs that may or may not remain stable in the face of climate change. Furthermore, these processes are likely to differ throughout the cryosphere due to the various factors that control the composition and growth of cellular communities [77, 78]. A thorough understanding of the biological weathering processes occurring beneath glaciers worldwide would therefore be beneficial in predicting the response of global biogeochemical cycles to climate change.

The AIS alone are expected to play an important role in the biogeochemical cycles of Fe, C, N, P and Si [79]. We have already encountered one of the best-studied cycles under glacial influence: the iron cycle. Iron hydroxide can be liberated from pyrite through a number of chemical processes, largely driven by the oxidation of sulphide [73]. Within the glacial environment, this oxidised iron serves as an important terminal electron acceptor in chemolithoautotrophy [74], as well as an oxidising agent in anoxic chemical systems [71]. However, free iron is not necessarily (nor even mostly) in the aqueous state – a great deal forms colloidal species that are carried beyond the subglacial bed [39, 80]. Major sources of iron in the oceans include riverine input (of which meltwater can be a significant component [81]), through the melting of icebergs [82] and through direct discharge from the AIS [83]. As mentioned earlier, the input of iron to the Southern Ocean results in a huge boost in primary productivity [84]; indeed, Martin's famous 'Iron Hypothesis' explores the possibility of iron-controlled photosynthesis leading to significant changes in atmospheric composition [34]. The iron cycle is expected to change with global warming, as local temperatures affect the partitioning between Fe^{II}/Fe^{III} oxidation states [85], the rate of biological processes and the volume/distribution of meltwaters. Even for this well-studied cycle, additional quantitative data regarding both the flux and partitioning of iron into the oceans are required to improve current models [39, 86].

Lastly, we ought to appreciate that analyses of deep ice can be a window to yet deeper temporal records and ongoing processes beneath the subglacial bed. For one, there is evidence that some subglacial

lakes may even predate the current ice sheets [69]. This has attracted much interest from the paleoclimate research community, as sampling from these features may give insight into pre-glaciation history [87]. Furthermore, it has been speculated that there are large reservoirs of methane lying underneath the AIS, with significance for future greenhouse gas emissions [88, 89]. Methanogenic archaea beneath the AIS are yet to be identified, however numerous studies have found that the deeper portions of the subglacial environment may be anoxic, wet, and with a depleted supply of sulphates and other common electron acceptors [2, 70, 79]. This suggests an ideal environment for the growth of methanogens [90]. Moreover, methanogenic archaea have been found in the subglacial sediments of a mountain glacier in the Northern Hemisphere [91], while an ammonia-oxidising archaeon, Candidatus *Nitrosoarchaeum*, is known to reside in the Antarctic Subglacial Lake Whillans [92]. Such stores of an active greenhouse gas would be of obvious significance to climate models because release of methane from the margins of a retreating ice sheet would likely augment global warming through a positive feedback loop [90]. There are currently no recorded observations of subglacial biogenic gas below the AIS; this may be identified through the entrapment of methane in basal ice samples.

To summarise, deep ice may be of extreme utility across a number of research topics. Gas, sediment and the isotopes of water and solutes may all hold clues to climatic conditions stretching back hundreds of thousands of years, while the biogeochemical influence of the cryosphere may play a fundamental role in climate over the next century. Glacial meltwaters sustain human communities and affect ecosystems both downstream and within glaciers; indeed, much of the cryosphere may be deemed a unique biome in its own right [93]. The findings of deep ice studies have even been used in the research of extra-terrestrial life [94]. With all this information available from studies of deep ice, it raises the question: why are they not more commonplace?

1.3 – Difficulties in sampling deep ice

It took almost forty years and a great deal of international collaboration before scientists could study the deepest ice found on Earth. The characteristics of the Antarctic subglacial environment were originally inferred from remote techniques such as radio-echo sounding (RES) in the 1970s. It was with RES that scientists first uncovered the existence of subglacial lakes under the AIS [95, 96]. These lakes and their associated hydrology are of great interest for research into both microbiology [2, 63, 97] and into Antarctic deglaciation [98] and ice flow [99]. The mean thickness of the AIS is, however, 2126m – approaching 4 km within the central EAIS (from BEDMAP2 [100]). Because of this, it was not until the 1990s that the Scientific Committee on Antarctic Research (SCAR) began to investigate the possibility of direct exploration of any of these Antarctic subglacial lakes, eventually founding the Subglacial Antarctic Lake Exploration Group of Specialists (now known as SALE) in the year 2000 [101, 102]. That subglacial lakes underwent such a transition from scientific novelty to viable research target is likely due to the use of RES data for the characterisation of Subglacial Lake Vostok and the identification of a large number of new subglacial lakes [102-104]. By the turn of the millennium, a plan had been drafted for drilling at three such lakes: Subglacial Lake Vostok (SLV),

Subglacial Lake Ellsworth (SLE) and Subglacial Lake Whillans (SLW) [105]. The ambitious multimillion dollar operations that followed have contributed to our understanding of the atmospheric conditions of the last 420,000 years [11], the microbial ecosystems of the cryosphere [66] and the requirements of deep ice core drilling [106]. Nevertheless, the operation exemplifies the great risk, expense and hardship associated with sampling deep ice in Antarctica.

Early on, the project was faced with a compromise: practicality versus contamination. Contamination is a primary concern of any deep ice investigation, due to the low cell count typical of such environments. This leads to samples which are especially sensitive to external influence and – more importantly – it means that unclean sampling technique could risk contaminating the entire subglacial system [107]. This is commonly referred to as forward-contamination: a term used by astrobiologists to describe the introduction of foreign microorganisms to extra-terrestrial bodies via inadequately sterilised equipment [108-110]. Drilling had begun at the SLV site prior to the formation of SALE, but was suspended in 1998 after reaching a depth of more than 3500 m. This was due to concerns that the kerosene drilling technique in use was not microbiologically clean [111]. Whilst the cleanest option would have been to begin from scratch with a different drilling technique, this was rejected by the Arctic and Antarctic Research Institute (AARI) and the St. Petersburg State Mining Institute (SPSMI) on the grounds of the significant financial, organisational and logistical difficulties that it would incur [112].

In 2004, drilling in borehole 5G recommenced [112]. The six year hiatus was intended to allow for the development of a cleaner alternative to the kerosene-based drilling technique previously in use there [111]. This was no easy task, as the immense pressures of the surrounding ice sheet are known to close the hole if not counterbalanced by a high pressure fluid. Ultimately, the chosen method relied upon the activation of three simultaneous processes at a critical moment: use of a thermal drill to breach the upper surface of SLV; injection of an organic silicon fluid at the lake-borehole interface (to keep the drilling fluid separate from the lake water); and reducing fluid pressure at the top of the borehole, allowing the lake water to displace the liquid in the borehole, forcing it upwards. The first contact with subglacial lake water took place on 5th February 2012, almost fifteen years after the completion of the draft plan and twenty-two years since drilling at the site had begun [113]. As planned, the pressurised lake water forced the kerosene-Freon mixture back up the borehole, preventing forward-contamination of the lake. However, the accreted samples retrieved from the borehole were contaminated both chemically and biologically by the drilling fluid [114, 115].

Contamination was not the only difficulty faced by the drilling team at SLV. On two occasions, the drill became stuck at the bottom of the hole; on the second of these, the team were unable to recover it. As a result, the final drilling attempt had to deviate from the original angle [113, 116]. Furthermore, the pressure differences between SLV and 5G caused the lake water to rise around 600m up the hole before refreezing – significantly further than the team had calculated, due to incorrect assumptions regarding the pressure of the lake water [113, 117]. Certainly, this is better than the alternative: a reversed pressure gradient would have forced the drilling fluid down into the lake, rather than back up the borehole. Nevertheless, it demonstrates the unpredictable nature of drilling operations into an environment for which there are insufficient data.

The SLE drilling expedition – the second of three SALE targets – commenced on 1st December 2012 [118]. This operation was to use a newly-developed hot-water drilling technique to melt through more than 3 km of ice in 72 hours, penetrating the roof of the lake in a chemically and microbiologically clean manner [119, 120]. The team however suffered a number of equipment failures, and eventually had to abandon the attempt after less than four weeks [118]. Several issues with the boiler have been attributed to the harsh conditions of the Antarctic continent, such as cracked valves and the freezing of the pressurisation pumps; the low temperatures were also responsible for the freezing of the umbilical cord (required to recycle water around the system) [118, 120]. There were other instances of equipment failure. Non-functional load cells prevented the team from knowing when the hose had reached the bottom of the borehole. This resulted in slight damage to the drill head, bending it so that the main hole was not drilled vertically [114].

A multi-stage procedure was required for the transport of food, fuel, survival gear, electrical equipment, several kilometres of hose and anything else that might be required throughout the operation. Because of this, relatively straightforward technical issues were often compounded by logistical difficulties. The team was crippled by two instances where control panels short-circuited – due to the remote nature of the drilling site, replacements could not be delivered for ten days [114]. Moreover, the operation was ultimately cancelled due to insufficient fuel; a resource that had to be tightly budgeted to reduce waste and unnecessary transportation [121, 122].

Technical and logistical problems are not limited to the study of subglacial lakes, and examples can be found in most studies of deep Antarctic ice. Deep ice coring operations at both Dome C (European Project for Ice Coring in Antarctica, EPICA) and Dome Fuji (Japanese Antarctic Research Expedition, JARE) encountered similar technical issues, whereby drill performance was decreased or completely halted. This was due to the production of ice chips at sub-zero temperatures [6, 123]. Furthermore, much of the polar cryosphere is difficult to access via manned land expeditions – even successful coring expeditions acknowledge the enormous undertaking of the task [124, 125]. The lack of population density (less than 1% of the world's population lives outside of the central latitudes between 60°N and 60°S [126, supplementary information]) means that the vast majority of provisions and machinery used for high latitude coring must be transported great distances to the research station. It also gives little incentive for governments to build and maintain roads in such areas, which subsequently necessitates the use of specialist transport. This all has obvious implications for polar studies in terms of both time and expense.

The situation is not much better at lower latitudes, although there is a different set of difficulties for researchers to overcome. In contrast with ice sheets, temperate glaciers do not pose such a risk of cold-induced equipment failure; nor do they come close in terms of thickness of ice through which to drill. Deep ice studies in such regions are constrained primarily by accessibility: approach may be hindered by topographical barriers (such as steep cliffs), biological barriers (in particular, dense forestation) or even political barriers [127]. Indeed, the latter may put a restriction on aerial photography [128]. The high altitudes of glaciers in the Himalayan and Andean mountain ranges may be closer to human populations in terms of straight-line distance, however they may be considered equally remote in terms of travel time and infrastructure. Furthermore, there is very limited availability of flat, open spaces upon which to set up

equipment. Consequently, specialised, portable drilling systems are required to take deep ice samples from temperate glaciers [129].

It is generally agreed that the benefits of deep ice sampling outweigh the risks, however there is enough evidence of hardship to suggest that alternative sources of deep ice would prove beneficial to the wider research community. This project identifies two such alternatives, weighing their usefulness and their limitations against mainstream approaches in terms of expense, time cost and reliability.

1.4 – An Antarctic solution: blue ice areas

Ultimately, most of the difficulties faced by expeditions in the Antarctic are derived from the thickness of the ice sheets. Scientists rely on complicated (and error-susceptible) equipment only because a long pilot hole must be melted or removed before sampling; large amounts of fuel are required only because it takes a long time to drill so deep. Conversely, many of the difficulties described above could be circumvented if the desired ice was found on the surface. Indeed, data are relatively abundant for research into cryoconite holes and firn chemistry because expeditions do not need to be planned to the same scale as the SALE missions. The upper layer of an ice sheet is principally composed of firn, a crystalline form of snow. This is clearly not a suitable substitute for deep ice: it is neither dense enough to contain trapped air bubbles, old enough to interest paleoclimatologists, nor has it ever been in contact with the unique hydrological and biological systems of the subglacial bed. However, firn is not the only form of water that can be found atop the AIS. Dense ice is present on around 1% of the surface of Antarctica, in regions known as Blue Ice Areas (BIAs) [130].

BIAs are found uniquely on the Antarctic continent. As the name might suggest, they are most easily distinguished from the surrounding ice sheet by their blue colouration and low albedo. Nevertheless, the defining feature of BIAs is that their annual net change in surface mass is negative [130, 131]. This negative mass balance is caused by the removal of surface material, which explains the lack of firn in such regions. Some definitions explicitly state that the major ablative process should be sublimation; this is done to exclude regions of bluish ice that are produced by surface melt rather than by sublimation, such as those found in Dronning Maud land [132]. The precise reasons for a net reduction in surface mass are numerous, hence BIAs can usually be subdivided into four categories (Table 1) [130]. All of these categories are linked in some way to topography, so it should be unsurprising that the majority of BIAs are located in the vicinity of moraines and mountainous regions [133].

Table 1 – Classification of BIAs by origin.

Category	Cause of negative surface mass balance
Type I	A protruding surface behaves as an obstacle to accumulative snowdrift
Type II	Katabatic winds along a valley glacier sublimate ice from the surface of the BIA
Type III	Katabatic winds down a steep slope sublimate ice from the surface of the BIA
Type IV	Surface snow is removed by winds that accelerate down into a glacier basin

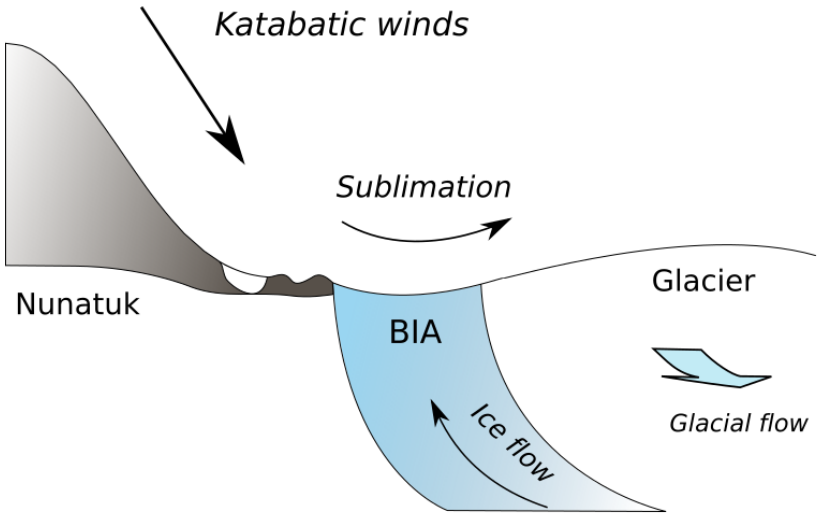

Figure 1 – Vector graphic demonstrating flow in a cross section of a blue ice area.

The negative SMB of BIAs leads to some very interesting properties. In 1969, the 10th Japanese Antarctic Research Expedition (JARE) discovered nine meteorites apparently stranded upon the surface of the South Yamato BIA [134]. This was a momentous find – only four meteorites had been discovered across the entire continent prior to the expedition [135]. Early interest in BIAs was consequently focused on their status as meteorite stranding surfaces; the JARE discovery instigated a series of systematic searches and the subsequent identification of more than 25,000 such specimens over the next thirty five years [136]. This was soon followed by studies of flow in regions of blue ice, given that the apparent accumulation of meteorites could be explained if the usual patterns of glacial movement were absent in BIAs.

The essential findings of these investigations were that – unlike most other ice on the Antarctic continent – there is a net upward component in the flow of ice into a blue ice area [137, 138]. This upward flow is what makes blue ice areas such excellent meteorite stranding surfaces – meteorites falling on the Antarctic continent are gradually incorporated into the ice sheets, sinking below the surface as the surrounding ice is covered by fresh accumulations. Any meteorite which falls in the vicinity of blue ice may move into the path of upward ice flow, eventually emerging on the surface of the blue ice field when katabatic winds remove the surrounding ice. Once a BIA has formed, it tends to remain relatively stable; the smooth surface hinders further accumulation of windblown ice, while the additional energy absorbed by blue ice (due to a lower albedo) can increase the rate of sublimation [130]. This allows for the accumulation of a large number of meteorites upon the surface of blue ice areas.

Naturally, the discovery of regions of easily accessible, ancient ice stirred interest amongst the paleoclimatology community [139]. In a closed BIA (one which is dammed completely by nunataks or other topographical feature), the surface ice is both ancient and horizontally stratified, with the oldest ice occurring towards the snout [131, 137, 138]. This unusual distribution of ancient ice opens the possibility that horizontal

ice cores may be collected from a number of blue ice areas around Antarctica. These are theorised to have very high temporal resolution relative to vertical ice cores, and require only a fraction of the drilling [140].

As mentioned in section 1.1, the potential of blue ice to yield useful paleoclimate data has already been demonstrated. Korotkikh et al. (2011) used high resolution samples taken horizontally from the Mount Moulton BIA in order to investigate the Eemian, while Spaulding et al. (2013) [141, 142] dated blue ice along a 5 km transect of the Allan Hills BIA. However, no study has yet investigated the potential of blue ice sampling as a source of information about the subglacial environment and its impact on global biogeochemistry.

The third chapter of this thesis describes the chemical composition of Terminal Blue Ice Samples (TBIS) taken from the surface of the Marble Hills blue ice area in Horseshoe Valley, Antarctica. A number of glaciochemical measurements are considered with a view to establishing the history of ice flowing into the terminus of the Marble Hills BIA. The proposed glacial history of the TBIS is then discussed in light of the first objective of this thesis: what can TBIS tell us about the environment beneath the Antarctic surface?

1.5 – An alpine solution: calved icebergs

A different solution is required for the study of mountain glaciers. For one, blue ice areas are not found north of 65°S. For another, the main issue in sampling at mid to low latitudes is one of accessibility, not of ice thickness. There is a notable absence from the literature of ice sampling data from major mountain ranges such as the Andes and the Himalaya. These ranges are home to thousands of glaciers, many of which cannot be directly accessed on foot, let alone with heavy scientific equipment. While it is true that access may improve over time – courtesy of advancements in infrastructure and drilling technology – it is unlikely that these improvements will come quickly enough. Many mountain glaciers are rapidly retreating: digital elevation models and aerial imagery reveal increasing rates of melt across the Patagonian icefields and the European Alps [143, 144], while some climate models project that glaciers will be extinct from Glacier National Park (Montana, USA) as soon as 2030 [54]. As glaciers thin over the next few decades, many natural climate records will be lost with them. Furthermore, fast action is required if scientists are to use glaciochemical data in order to best support glacially-dependent communities during the coming period of uncertainty: changing rates of runoff will inevitably induce a shift in the chemical composition of some freshwater systems. In light of such time pressures, an ideal sampling method would be one that requires no development of new technology, nor a lengthy period of organisation. Consequently, it may be wise to take advantage of another naturally-occurring source of deep ice: calved icebergs.

The majority of glaciers in Patagonia are calving glaciers, including all of the most major glaciers in terms of both size and their importance to communities. The glaciers themselves are outlets of the Northern and Southern Patagonian Icefield; surrounded by mountains and uncultivated vegetation, they are difficult to reach. In contrast, their calved icebergs collect at low altitudes, in the fjords and lakes where they terminate. These areas are far more accessible by research teams: thanks to the human predilection to build beside water sources, travel can be conducted mostly or entirely by boat and by road. Moreover, the tendency for icebergs to rotate after calving can expose a vertical cross section of the glacier, making it easier

to take samples representative of the glacial terminus. Given the typical path of glacial flow (see Figure 2), the exposed ice is likely to be stratified by age and depth.

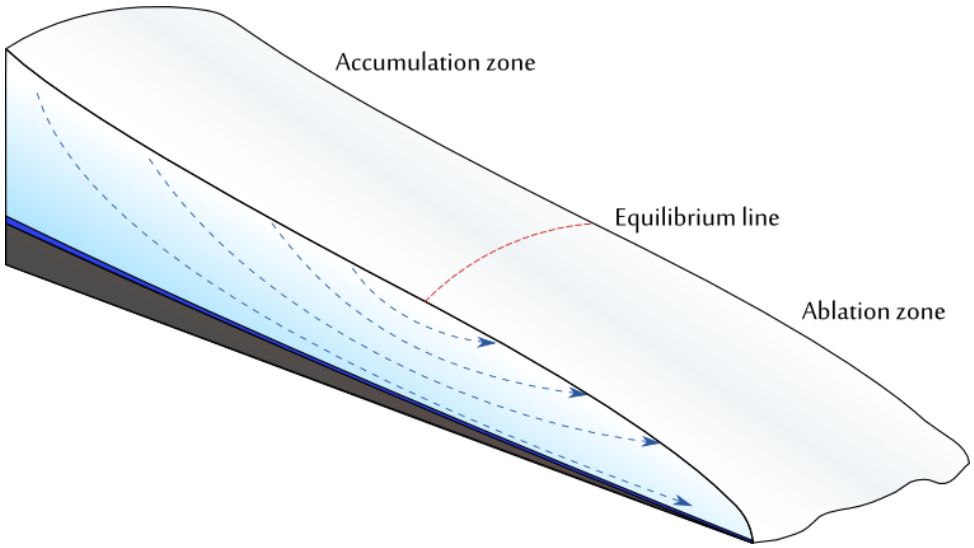

Figure 2 – Diagram of flow paths within alpine glaciers. Dotted blue lines represent the path of ice along the glacier. Precipitation from higher altitudes travels deeper and has longer retention within the glacier.

At the time of writing, there do not appear to have been any published attempts at sampling from calved terrestrial icebergs. This may be because of concerns that samples cannot not be useful if their exact origin is unknown: the unpredictability of iceberg movement makes this impossible without constant monitoring between calving and sampling. Alternatively, it may be due to the assumption that the iceberg contribution to glacial rivers and fjords is negligible. Neither of these assumptions have been tested, however extensive evidence that icebergs can significantly affect the chemistry of the Southern Ocean [82, 145, 146] does at least legitimatise the hypothesis that they may also be influential in glacial rivers. Furthermore, given there is no known process that should alter their composition post-calving, iceberg sampling has the potential to elucidate the composition of the glaciers themselves. Even if individual samples cannot be traced back to the part of the glacier from which they originated, a sufficiently large cohort of icebergs should be representative of the glacier as a whole.

The fourth chapter of this thesis presents glaciochemical data from twenty-four iceberg samples from Lago Steffen. These data are used to discuss ongoing processes affecting the composition of Steffen Glacier. $\delta^{18}O$ and $\delta^{2}H$ values are also compared with samples from semi-glacial (Rio Huemules) and non-glacial (Rio Quince) sources in order to estimate the varying influence of Steffen Glacier on the downstream freshwater system. These two parts are synthesised by a discussion of the dominant processes by which Steffen Glacier affects the chemistry of the Rio Huemules.

Chapter 2 – Methodology

2.1 – Overview of field sites

2.1.1 – Marble Hills BIA

The Heritage Range forms the southern half of the Ellsworth Mountains, on the edge of the WAIS. TBIS were collected from the Marble Hills BIA (80.25317 S, 82.07148 W, 861.9m), which lies at the southern edge of Horseshoe Valley, approximately 50 km from the Filchner-Ronne ice shelf. Sampling was also conducted at the Patriot Hills BIA (80.32899 S, 81.26820 W, 752m); this second set of samples has been prepared for gas extraction and further chemical analysis. These sample sites were selected largely for their logistical convenience: the Patriot Hills BIA is a short flight from Rothera Station, and already has an established landing strip for light research aircraft.

As with other known regions of blue ice, negative SMB has been observed at the Patriot Hills site [147, 148] and is likely due to the strong katabatic winds of up to 30 ms^{-1}[149] which flow down into the valley. A similar situation is expected at the Marble Hills. This results in compensatory ice flow from Horseshoe Valley Glacier – which flows NE towards the Filchner-Ronne ice shelf – towards the nunataks to the south [150]. Given that the continued flow of ice is blocked by the Patriot and Marble Hills, these blue ice areas may be described as 'closed'.

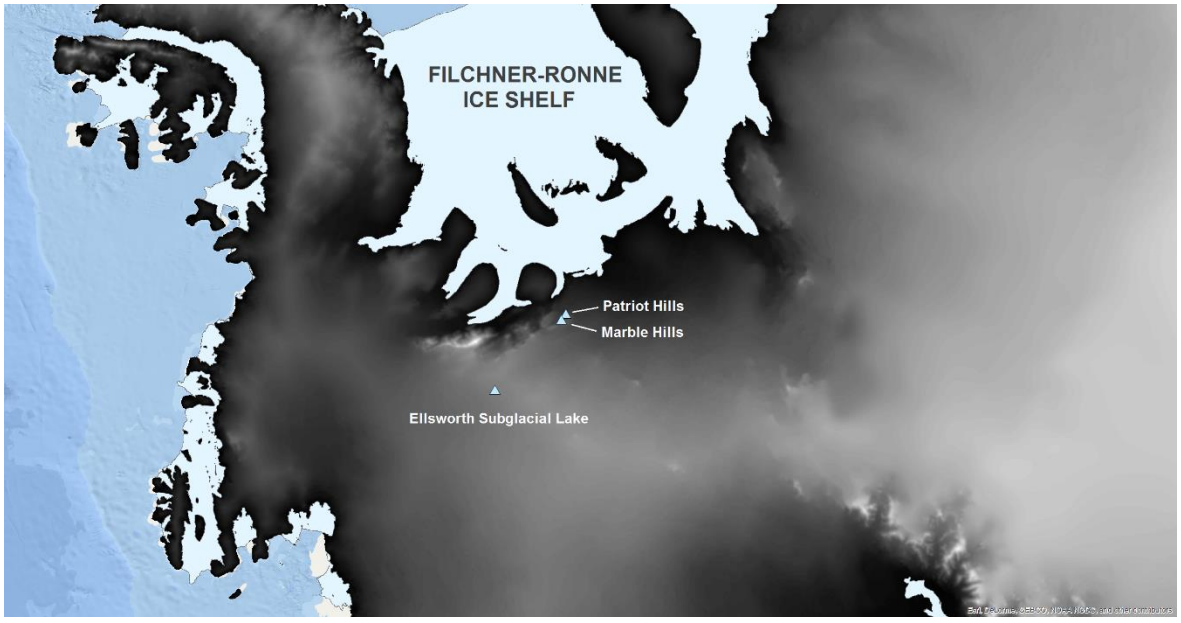

Figure 3 – ArcGIS map of Antarctic sample sites. Elevation data from BEDMAP2 [100].

2.1.2 – Subglacial Lake Ellsworth

The experimental work also utilised a firn core taken from above SLE. This was used to estimate the local meteoric water line (LMWL) and to gauge the chemical composition of non-subglacial ice. The sampling site is around 70 km west of the Ellsworth Mountains, in Ellsworth Land. The ice sheet surface here is relatively uninterrupted by nunataks, which may have implications for the local weather systems that bring snow to the site. Consequently, the firn core data in this thesis are always considered alongside relevant examples from the literature.

2.1.3 – Lago Steffen, Patagonia

Steffen Glacier (*Glaciar Steffen*) is the southernmost glacier in the North Patagonian Icefield (NPI), with a latitude of 47.49°S. It is also the most substantial outlet along the southern edge of the icefield [151]. Like most Patagonian glaciers, Steffen is a calving glacier – a class known to be especially dynamic – and may undergo rapid retreat due to positive feedbacks between calving rates, ice thinning and water depth [152, 153]. It has a historic length of 50.4 km [154], however has been in retreat since the mid-20th Century, losing 12 km^2 of surface area between 1979 and 2001 [155]. A report conducted by the Japanese Aerospace Exploration Agency (JAXA) found that the main terminal had retreated approximately 2.1 km between 1987 and 2010, including more than a kilometre in the first three years of the 1990s [156, 157]. The sensitivity of the Patagonian Icefields to climate change is a global concern: they make a contribution to sea level that is disproportionately large and increased markedly over the 20th Century [143, 158].

The glacier calves into a remote proglacial lake (Lago Steffen), presumably dammed by moraines left behind as the glacier retreats (PISCES bathymetry data, unpublished). Water from the lake feeds the Rio Huemules, ultimately flowing into the fjord system surrounding the Baker Channel. Many livelihoods rely upon this water; most notably those of Caleta Tortel, a farming/fishing community to the east of the Steffen fjord and the administrative centre for the Tortel area. Communities in Chilean Patagonia are exceedingly remote (the residents of Tortel are a 10-hour drive away from the nearest hospital), and so are especially sensitive to local environmental changes.

Study of Patagonian glaciers is similarly hindered by the remoteness of their location, and the biggest obstacle encountered by any study of the Patagonian icefields is a lack of data. Steffen Glacier is no exception: extreme hills and dense forest inhibit approach on land, while approach from the lake is prevented by the aggregation of icebergs at a bottleneck around 2 kilometres from the calving front. Given that direct glacial sampling is all but impossible for small-scale operations, the study of Steffen's contribution to the downstream geochemistry and ecology requires an alternative approach. It should be noted that due to the apparent sensitivity of calving glaciers, interpretation of paleoclimatic data is likely to be hindered by "non-climatic noise" [153]. Nevertheless, the dependence of local communities on a fast-retreating glacier should be sufficient justification for the study.

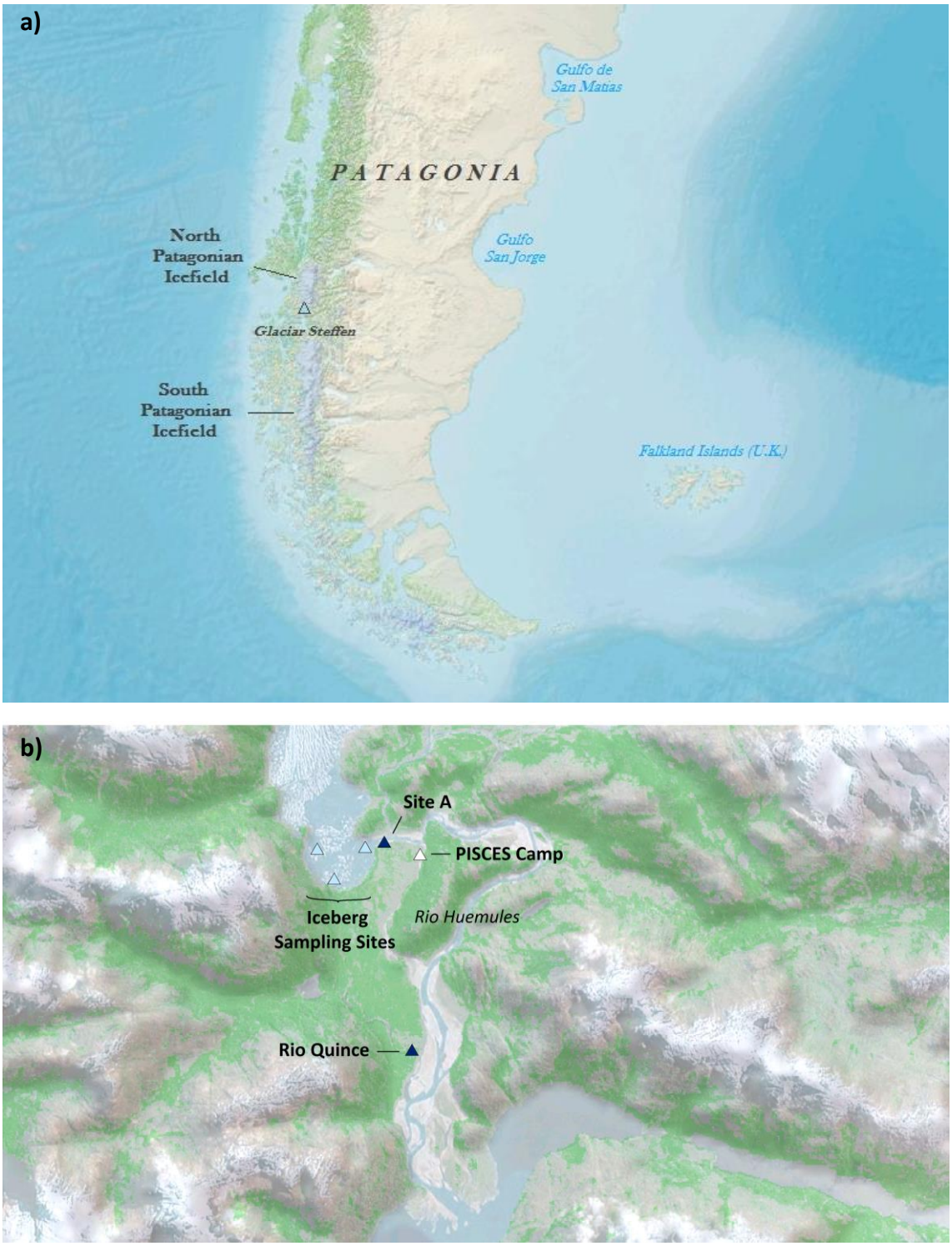

Figure 4 – ArcGIS maps of Patagonian sample sites. (a) Steffen Glacier is situated at the southern tip of the North Patagonian Icefield. (b) Icebergs were sampled from three locations in Lago Steffen, while river sampling took place a few hundred metres downstream of the lake, at Site A, and in the Rio Quince, a nearby non-glacial river. Sources: ESRI, USGS, NOAA.

2.2 – Collection and preparation of samples

Antarctic blue ice

The Marble Hills and Patriot Hills BIAs were sampled in January 2014 during an expedition led by the University of Edinburgh. Extraction was via chainsaw and ice axe, followed by the removal of 5-10 cm of ice from the exposed topside. These were packed into insulated boxes before shipping to Bristol, where they were stored at -20°C in the Low Temperature Experimental Facility (LOWTEX) until required.

The blue ice arrived as two large slabs (approximately 30 kg from the Patriot Hills and 15 kg from the Marble Hills). Each slab was sectioned into six small columns with a pre-cleaned stainless steel Bosch S 1211 K sabre saw (Figure 5). The same saw was then used to further divide the blocks at 4 cm intervals along the vertical axis. The result was that each of the original monoliths was transformed into six samples for every 4 cm in depth; in all, there were 40 samples from the Patriot Hills BIA and 36 for the Marble Hills, with average masses of 720 g and 375 g respectively. These were stored in sterile polyethylene (Whirl-Pak) bags.

Samples were incubated for twenty-four hours at -6°C before cleaning (Appendix 1). The ice was rinsed with ultrapure water in a laminar flow hood, transferred to fresh polyethylene bags (Whirl-Pak) and left at ambient temperature for the outer layer to melt away. They were then transferred to fresh polyethylene bags and allowed to melt fully. Liquid samples were filtered on pre-rinsed cellulose nitrate filter paper (0.45 µm pore, 25 mm diameter) in a reusable filter holder so that both filtrate and sediment could be retained for later analysis. Filtrate was transferred to an acid-cleaned HDPE bottle, while the sediment was placed in polyethylene bags. Both were stored at -20°C until further analysis could take place.

Figure 5 – Photograph of BIA block during initial sectioning. Each of the blocks pictured weights approximately 3 kg. Additional till samples (Whirl Pak bags) were also included in the storage container.

Figure 6 – Photograph taken during the second stage of blue ice sectioning. Each of columns were divided into six samples from different depths (note that the column pictured is turned on its side). The two large circular holes are remnants of the original sampling procedure. The variable colouration results from uneven levels of debris interspersed throughout the block.

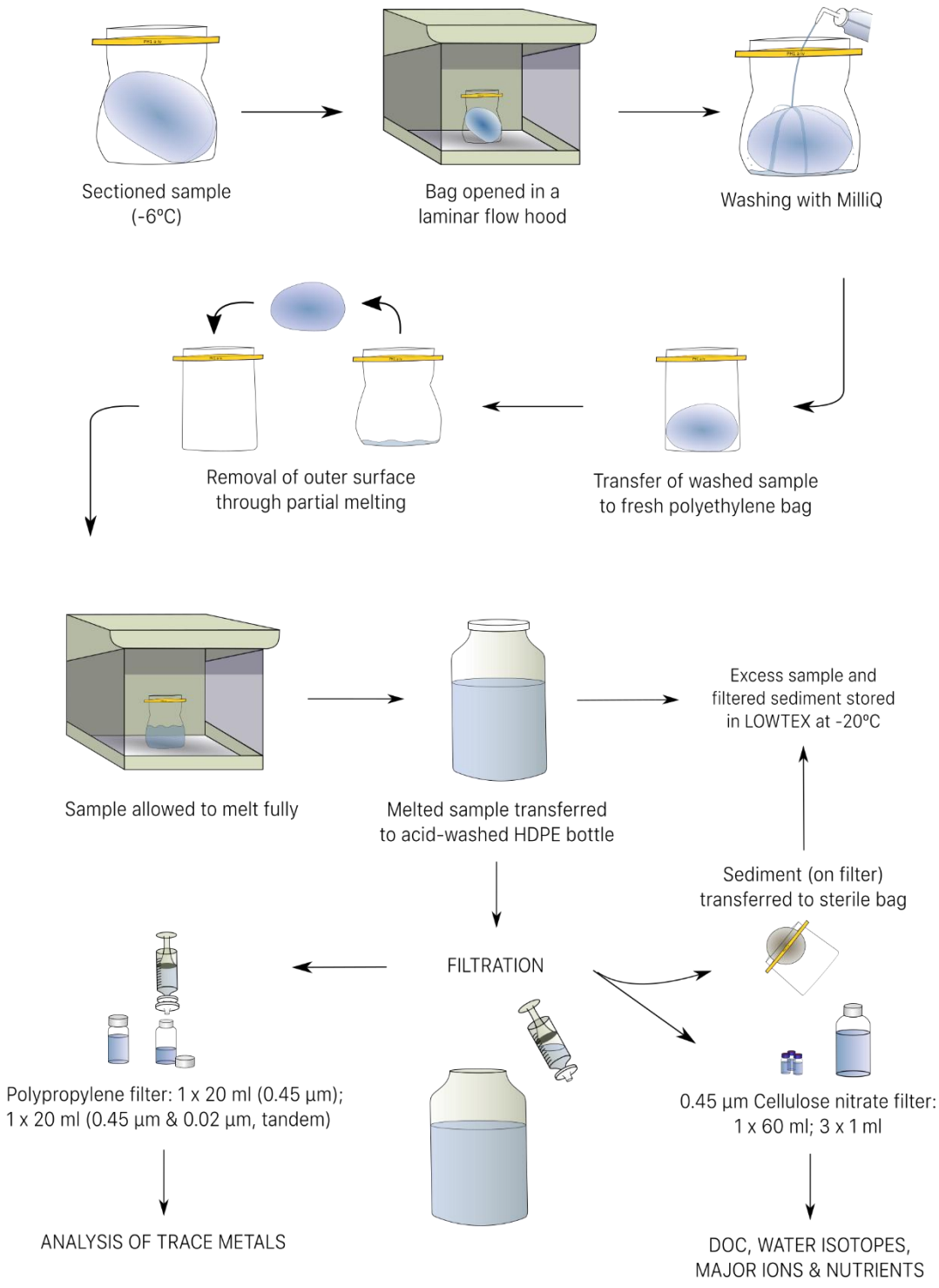

Figure 7 – Schematic diagram of the methodology for processing TBIS. The stages shown in the upper portion include washing, melting and filtration of the sectioned samples. Analysis of the stable isotopes of water, major ions and DOC were all performed as part of this thesis; the filtered sediment and the remaining filtrate have been stored for future analyses.

Ellsworth Firn Core

The firn core used in this project is one of three firn cores drilled from the surface above Subglacial Lake Ellsworth during the 2007-08 austral summer in preparation for the SALE-coordinated drilling operation [159]. The original core was cut into cylinders of approximately 40 cm in length before transport to LOWTEX, where they were stored at -20°C for several years prior to sample preparation.

Fifteen small segments (approx. 5 ml each) were removed at 8 cm intervals from the core. The incisions were made with the use of a pre-cleaned stainless steel sabre saw; the same saw was used to scrape away the potentially contaminated outer surface before taking samples. This alternative cleaning method was used because the extremely porous nature of the firn means that techniques involving partial melt and/or washing with deionised water could contaminate the isotopic signatures of the sample (Appendix 1). Segments were placed in resealable bags and left to melt at room temperature. Melted samples were then filtered (cellulose nitrate, 0.45 µm pore, 25 mm diameter), stirred, and transferred to ampoules for isotope analysis. A further eight segments were later taken for ion chromatography.

Calved Patagonian icebergs

Samples were retrieved from eight icebergs in the glacial lake in February 2017, and were processed in the field. The icebergs varied greatly in appearance and consistency, presumably due to experiencing different pressures and ice-rock contacts along their different flow paths along the glacier. In order to test whether or not these physical differences correlated with chemical differences, the icebergs were divided into three categories, referred to as “Blue”, “Grey” and “White” (see Table 2).

Table 2 – Categorisation of blue, grey and white icebergs via observable properties.

Colour	***Density***	***Visible sediment***	***Other observations***
Blue	*Very high*	*Very low, very fine*	*Some small air bubbles*
Grey	*Fairly low*	*Abundant, varied particle sizes*	*Exposed collections of silt or pebbles*
White	*Intermediate*	*Intermediate*	*Very small hydrological channels*

Categorisation of the icebergs is important because – in the event that these categories are found to be discrete populations – the results should be weighted according to the abundance of each iceberg type. For this small pilot study, the ratio of blue : white : grey icebergs was estimated by counting the icebergs in the southern half of Lago Steffen, and was found to be 3:2:3 (n=32). Samples were then collected in the same ratio; arithmetic means can therefore be considered representative of the calving front, regardless of whether or not category is a significant factor in iceberg chemistry.

Three samples were taken from each of eight icebergs, giving twenty-four samples in all. The outer 3 cm of the surface was removed and discarded so as to reduce the risk of contamination. Around 1200 cm^3 of ice was then collected into a sterile polyethylene bag. In order to further reduce the likelihood of surface contamination affecting the final samples, the outer 1cm of ice was left to melt at ambient temperatures and

then removed (see Appendix 1 for a brief discussion of the chosen method of cleaning). A second melting step occurred before the clean ice was transferred to new sterile polyethylene bags and left to melt fully.

Samples were filtered (0.45 µm, cellulose nitrate), and both the sediment and the filtrate were retained. The sediment was transferred to sterile polyethylene bags and frozen for later analysis of sediment-bound nutrients. Filtrate from each sample was partitioned into acid-washed HDPE bottles for measurement of water isotopes, DOC, ions and nutrients. For sixteen samples, 2 x 10 ml of filtrate was also put through additional filtration steps using 0.45 µm / 0.02 µm polypropylene inline syringe filters. These were stored in clean 20 ml bottles for trace element analysis and acidified with 100 µl 7% nitric acid. The remaining filtrate (up to 1 litre per sample) was retained for ^{14}C DOC analysis.

2.3 – Water isotope analysis

2.3.1 - Method

Isotope composition was determined by off-axis integrated cavity output spectroscopy (Los Gatos Research T-LWIA 45-EP). More detailed descriptions of this technique can be found in Baer (2002) and Berman (2013), based upon the principle outlined in Paul (2001) [160-162]. The T-LWIA instrument measures raw $^{2}H/^{1}H$, $^{18}O/^{16}O$ and $^{17}O/^{16}O$ isotopic ratios simultaneously, with an interval of around 96s between individual injections. At the beginning of each sample measurement, 950 nl of sample is injected into the heating block by a PAL autoinjector (CTC analytics). The aqueous sample is vaporised and then passed into a measurement cell within the optical cavity. Two near-infrared tuneable diode lasers ($\lambda_1 \approx 1388$ nm, $\lambda_2 \approx 1397$ nm) are directed into the cavity off-axis, giving an optical path that is several kilometres in length. Absorption is measured by comparing the outputs of two photodetectors (one proximal to the optical cavity, and one distal), while effective path length is monitored *in silico* by recording the delay between laser deactivation and the absence of a signal on the second photodetector. Path length and absorption across the two narrow spectra are then used in a modified version of the Beer-Lambert absorption equation to calculate raw isotope ratios for that injection. These are expressed in terms of delta values, calculated relative to VSMOW:

$$\delta(X) = 1000 \times [\ (R_{sample} / R_{VSMOW}) - 1\ ]\ ‰ \qquad \text{Equation 5}$$

where X is the isotope of interest (^{2}H, ^{18}O or ^{17}O) and R is the isotopic ratio of X relative to the most common stable isotope ($^{2}H/^{1}H$, $^{18}O/^{16}O$ and $^{17}O/^{16}O$).

Due to fluctuating conditions within the instrument, these raw delta values are relatively meaningless; they must be calibrated against a set of standards, interspersed throughout the run (Table 3). Each standard was measured a minimum of three times per run: individual standards were spaced regularly amongst the sample measurements (one standard every 2-4 samples), and a full standard set was measured at the beginning and end of each run. This design enabled the use of a cubic spline standardisation method in post-processing, which was found to best take into account drift within the instrument.

Post-processing was conducted with the recommended LGR software (LWIA Post Analysis v.4.5.0.6). For a cubic spline standardisation, the software creates an individual curve for each standard, interpolating

between the different measurements in order to estimate what the response variable would have been if that standard were measured for any given injection. Each injection is then measured relative to a unique calibration curve constructed from the estimated response variables of each standard at that point in the run. This standardisation technique therefore accounts for drift in the response variable over the course of a run. The post-processing software also calculates metrics for accuracy, precision and reliability, and produces an array of diagnostic plots.

Table 3 – List of standards used to with the T-LWIA. Secondary standards were established relative to the primary standards prior to the onset of sample measurement. The reported delta values for secondary standards are taken from the average of at least fifty measured injections. Unknown samples were measured alongside a standard set of five (Antarctic samples) or seven (Patagonian samples) standards, as well as one reliably measured internal control (either an additional secondary standard or a previously measured sample).

Name	1°/2°	Source	$\delta^{2}H$	$\delta^{18}O$	$\delta^{17}O$
SLAP2	Primary	IAEA, Austria	-427.5	-55.5	-
IA-R065	Primary	Iso-Analytical, UK	-270.3	-34.1	-
lgr1c	Primary	Los Gatos Research, USA	-154.0	-19.5	-10.3
lgr2c	Primary	Los Gatos Research, USA	-123.7	-16.2	-8.6
lgr3c	Primary	Los Gatos Research, USA	-97.3	-13.4	-7.1
lgr4c	Primary	Los Gatos Research, USA	-51.6	-7.9	-4.2
lgr5c	Primary	Los Gatos Research, USA	-9.2	-2.7	-1.4
LW	Secondary	West Antarctica Ice Sheet	-272.8	-34.4	-
GRN	Secondary	Greenland Ice Sheet	-234.1	-29.0	-
FRA	Secondary	Alps, France	-107.5	-14.4	-7.6
SG1618	Secondary	Lago Steffen, Chile	-100.3	-14.1	-7.4
SWI	Secondary	Alps, Switzerland	-98.6	-13.7	-7.1
SCI	Secondary	Lago Steffen, Chile	-91.8	-12.6	-6.6
SVP	Secondary	*Unknown*	-88.0	-12.6	-6.6
SG1314	Secondary	Lago Steffen, Chile	-77.6	-10.6	-5.5
EGB	Secondary	Engabreen, Norway	-62.6	-9.0	-4.7
MQ	Secondary	LOWTEX, UK	-35.8	-5.2	-2.7

2.3.2 – Quality control data

The *accuracy* of any given run can be inferred from the standards: the higher the accuracy achieved by the instrument, the closer each standard measurement will be to the known ("true") value. There are several ways to quantify accuracy; in this thesis, the accuracy of delta values will be calculated using the metric recommended by the instrument manufacturer (Los Gatos Research). This is the weighted average of the difference between each standard measurement and the true value. This is a relatively conservative accuracy metric when compared with other methods as it takes into account every standard measurement, which removes the possibility of cherry-picking an accurate midrange standard.

The standard set is newly measured alongside every run, which means that each run has its own accuracy metrics. This is a useful tool for verifying that the performance of an individual run was acceptable:

a poor accuracy metric is indicative of a poor standard set, which would in turn necessitate that the standards are checked and the run repeated. In all, twenty-two runs were necessary in order to reliably measure all one hundred and sixty-eight samples used in this project. When evaluating a dataset as a whole, it may be more convenient to have a single value for accuracy. For example, the thirty-six samples from the Marble Hills BIA were measured across eight different runs, each with their own quality control data. A single accuracy metric for the Marble Hills dataset was obtained by taking the weighted mean of its eight constituent runs: these average deviations from known were weighted according to the number of sample injections that were accepted from each run (i.e. all measured injections which bypassed the filters in post-analysis) (Table 4).

Table 4 – Accuracy and precision metrics for water isotope analysis. The metrics were calculated for individual runs and then a weighted mean was taken according to the number of accepted sample injections from each run. The chosen accuracy metric was the average deviation of each measured standard injection from its known value; the chosen precision metric was the standard deviation of individual sample injections from the replicate average.

Dataset	No. samples	Sample injections	Accuracy metric / ‰			Precision metric / ‰		
			δ^2H	$\delta^{18}O$	$\delta^{17}O$	δ^2H	$\delta^{18}O$	$\delta^{17}O$
Marble Hills	36	591	0.231	0.145	n/a	0.181	0.061	n/a
Ellsworth firn	15	227	0.296	0.131	n/a	0.090	0.061	n/a
Calved icebergs	24	407	0.130	0.086	0.030	0.143	0.078	0.049
Glacial rivers	93	1492	0.201	0.124	0.076	0.131	0.095	0.045
Total	168	2717	0.205	0.124	0.066	0.140	0.082	0.046

The *precision* of an analytical technique is the extent to which values will spread if the same sample is measured multiple times. One way to quantify precision is to take the average standard deviation of replicate injections (i.e. injections taken from the same sample). As with the accuracy metric above, this is a very conservative estimate of precision, because it is influenced by every sample in the run. This method takes into account the drop in precision brought about by natural heterogeneity in the source, as it compares injections from different (albeit replicate) ampoules, which were collected at the same time and site, however may technically differ in composition. Moreover, by using the processed injection data, this technique accounts for any imprecision introduced during standardisation. Consequently, this metric should be considered the precision of the entire process – from sample collection to post-analysis – rather than merely the precision of the instrument itself.

As with accuracy, the LGR software automatically generates a precision metric specific to a single run. The precision metrics listed in Table 4 are weighted averages of the sample injection standard deviation for all of the runs comprising each of the four groups of samples.

Unlike many other types of instrumental analysis, data regarding the limits of detection and quantification (LOD and LOQ respectively) for water isotope analyses are extremely difficult to obtain. The simplest measurement of LOD or LOQ is based on the standard deviation of several blank measurements. These are relatively easy to obtain when measuring nutrients, because ultrapure water (such as MilliQ) can be generated on-site for use as blanks; it is however far less realistic when measuring isotopic ratios, for which

a “blank” sample would be one of pure isotopic composition. This also excludes the possibility of using signal-to-noise ratios to calculate LOD and LOQ, as noise is typically estimated from blank samples. LOD/LOQ can be determined via the slope of the calibration curve, but only if the standard deviation of the response is known for low concentrations of solute (or in this case, low isotopic ratios of $^{2}H/^{1}H$, $^{18}O/^{16}O$ and $^{17}O/^{16}O$). It would be inappropriate to assume that SLAP2, the most depleted standard, has a sufficiently low isotopic ratio in order to calculate the response; it is a universal standard used in water isotope analysis (second only to VSMOW in terms of importance), and is well above the limit of quantification.

2.4 – Ion chromatography (IC)

2.4.1 – Method

Cation and anion-exchange chromatography were carried out simultaneously using a Dionex ICS-5000 instrument connected to a personal computer running Chromeleon 7 data system software. 1000 mg/l stock solutions of Na^{+}, NH_3^{+}, K^{+}, Mg^{2+} and Ca^{2+} were mixed and then diluted with MilliQ ultrapure water to make up standards for cation exchange chromatography; the anion standards were made from 1000 mg/l stock solutions of F^{-}, Cl^{-}, NO_2^{-}, SO_4^{2-}, NO_3^{-} and PO_4^{3-}.

The dilutions were conducted gravimetrically: a laboratory balance (Kern ABT 220-4M) was used to weigh quantities of stock solution and MilliQ to ±0.00005 g precision. The smallest measured quantity in any step was 7.4131 g, corresponding with a relative uncertainty in the measurement of less than 0.001 %, and no standard underwent more than four serial dilutions from the primary stock. Standards were freshly made within 48 hours of the run, and ranged from 8 ppb to 2000 ppb. An appropriate set of seven or more standards were selected from this range, depending on the samples being measured; for instance, the TBIS were measured against a more concentrated set of samples.

During the pilot runs, it was established that the cation and anion peaks could be adequately resolved using methods with isocratic elution. Cation exchange was conducted using a Dionex IonPac CS12A column (2x250 mm). The eluent was methylsulphonic acid (20 mM), with a flow rate of 0.0080 ml/min and a duration of 15 minutes. Anion exchange was conducted using an IonPac AS11-HC column (2x250mm), a potassium hydroxide (20 mM) eluent, a flow rate of 0.015 ml/min and a run time of 12 minutes per sample.

Calibration

The output of the IC instrument is the area underneath the each of the peaks (min*µS) on a graph of signal against time. A full set of standards (ranging from 8-2000 µg dm^{-3}) was included alongside unknown samples, which enabled the calculation of a calibration curve from which the response variable could be manually converted to concentration. Calibration curves and subsequent concentrations were calculated independently for each ion. At the completion of each run, the range of concentrations among the samples was estimated by comparison of observed areas with those of the standard set.

Once rough concentrations were known, irrelevant standards were excluded from either (or both) extremes of the spectrum: this reduced the likelihood that the calibration curve would be affected by high leverage outliers, whilst retaining a core set of standards (average = 7.2) that comfortably encompassed the

range of concentrations in the samples. These standards were tested for normality (Shapiro-Wilk test), and plotted on a graph of response variable versus concentration. An appropriate regression method was then used to estimate this relationship: least squares linear regression for normally-distributed sets, or the Theil-Sen estimator for non-normal distributions. The resulting linear equation was applied to the areas observed during sample measurement, yielding concentration data in units of μg dm^{-3}.

2.4.2 – Quality control data

Every run on the IC featured five consecutive blanks of ultrapure water (MilliQ). The standard deviation and mean of these five measurements can be used to calculate the Limit of Blank (LoB), as described in Armbruster & Pry (2008, [163]). The LoB is the highest measurement that can be reasonably expected when measuring a solution containing negligible concentrations of analyte. Put another way, if a LoB is calculated for the 95% confidence interval, then it is expected that all but 5% of blank measurements will be less than or equal to the LoB. Assuming that the measurements are normally distributed, then the LoB is calculated as:

$$LoB = \bar{x}_0 + 1.645\ \sigma_0 \qquad \text{Equation 6}$$

where $\bar{x}_0$ and σ_0 are the mean and standard deviation of the blank measurements, respectively. The coefficient 1.645 is derived from a Gaussian distribution with tail area, $\alpha = 0.05$.

Since it is calculated purely from blank measurements, it should be clear that the LoB can only indicate the likelihood of Type I errors, wherein a negative solution is measured as if it contained some quantity of analyte (commonly referred to as a "false positive"). When determining the composition of glacial ice and meltwaters, we are also interested in Type II errors, which occur when extremely dilute samples cannot be sufficiently distinguished from blank solutions. The Limit of Detection (LoD) sets a threshold value above which analyte concentrations greater than zero can be reliably detected. There are several schools of thought regarding the calculation of LoD; this thesis once again adopts the method described by Armbruster & Pry (2008, [163]):

$$LoD = LoB + 1.645\ \sigma_{[Low]} \qquad \text{Equation 7}$$

where $\sigma_{[Low]}$ is the standard deviation from several measurements of an extremely dilute standard (for most ions, this was around 8 mg dm^{-3}). This is preferable to other limits of detection present in the literature because it utilises both the LoB and observations of a non-zero solution: other methods, which rely solely on blank measurements (e.g. $LoD = 3 \times \sigma_0$) provide no empirical evidence that dilute solutions can actually be detected at the LoD. In contrast, Equation 7 implies that, for a solution of actual concentration equal to the LoD, 95% of measurements will be above the LoB and will therefore be distinguishable from a blank sample (Figure 8). If the mean measurement for any given sample is greater than or equal to the LoD, it can be stated with 95% confidence that the concentration of analyte is greater than zero.

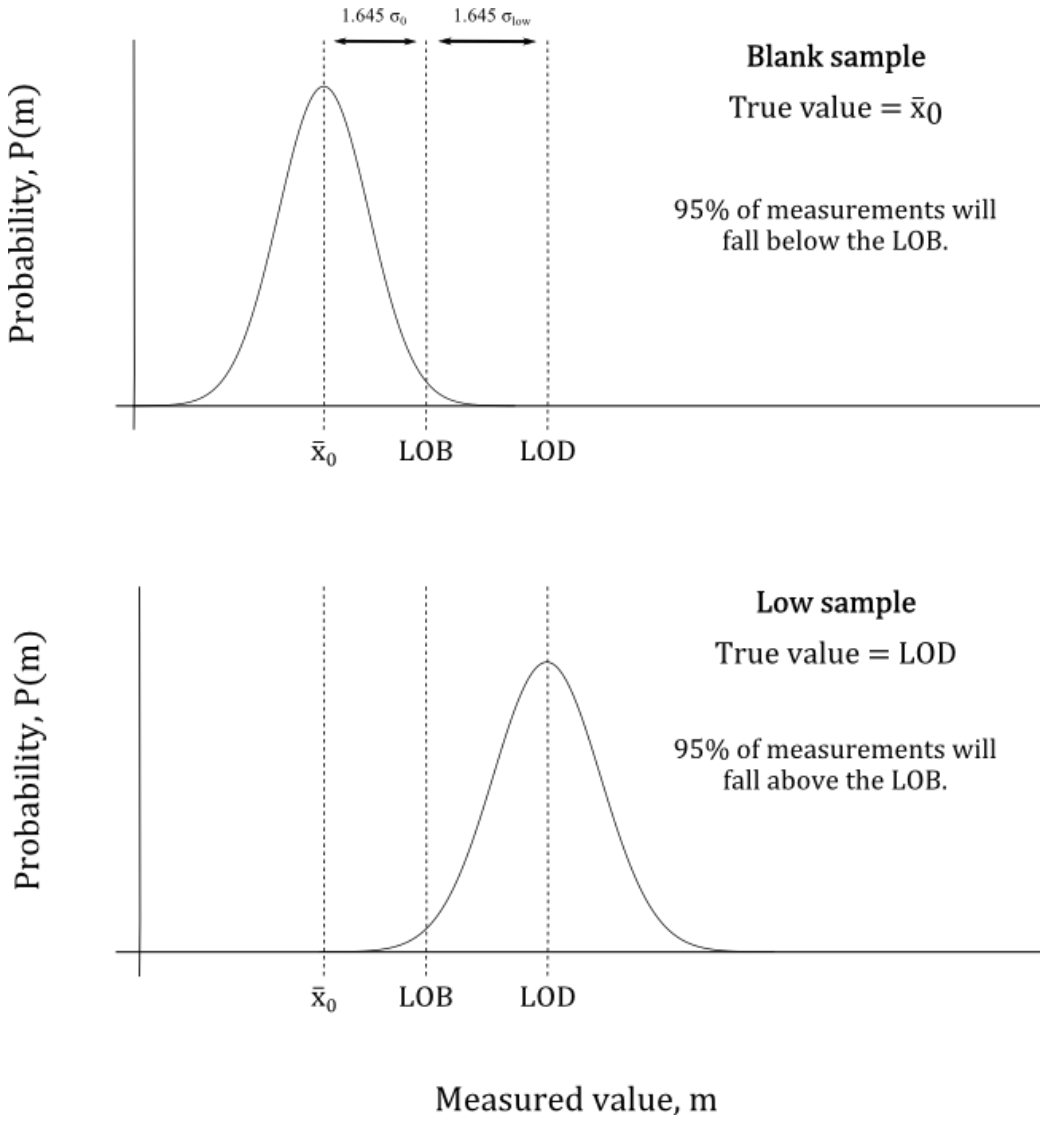

Figure 8 – Illustration of the limits of blank and detection. Measurements of a given sample should have a normal distribution about the true value. The LOD used in this method is the lowest value for which 95% of measurements will be distinct from blank samples (i.e. above the LOB).

The limit of quantification (LoQ) adds another layer to the argument. Whilst it may be possible to detect concentrations as low as the LoD, measurements at this extreme may lack sufficient accuracy or precision (both of which scale with magnitude) for reliable quantification. As with the LoD, there are a number of ways in which LoQ may be estimated. At its simplest, LoQ can be defined by the concentration of the lowest standard that is greater than the LoD and for which the pre-defined accuracy and precision targets are also met. This approach is unsuited to experiments where the calibration curve was optimised for samples within a given range of concentrations. While the calibration may well hold below the range of standards used in its calculation, it cannot be assumed that quantification will remain satisfactory. The least concentrated standard may be detectable, however if it was not used in the calibration curve, then it should not be used to set the limit of quantification. Conversely, it would be preferable to use a method that derives the LoQ from the calibration curve itself.

An appropriate LoQ for this analysis can be calculated as:

$$LoQ = 10\,\sigma_{res} / m_{cal} \qquad \text{Equation 8}$$

where m_{cal} and σ_{res} are respectively the gradient and the standard deviation of the response for the calibration curve. Note that the standard deviation of the response should not be confused with the standard error of the estimate, which is calculated with one additional degree of freedom (n-1 rather than n-2). This method is based on the principle that quantification is possible where the signal/noise ratio is greater than ten. In this case, the deviation of any one measurement from the calibration curve is assumed to be due to noise; given the observed noise in the calibration, Equation 8 calculates the concentration at which this noise is more than one tenth of the signal. Compared with other signal/noise approaches – which focus on a single blank or standard measurement – this method of LoQ calculation is based upon a significantly larger pool of data. This reduces the impact of natural stochasticity on the calculation, resulting in a more realistic LoQ. Note that the LoQ must be greater than or equal to the LoD: an undetectable quantity can clearly not be quantified. Consequently, the two are considered equal in cases where an excellent signal/noise ratio results in a LoQ that is below the LoD.

The accuracy of each run on the ion chromatograph was calculated based upon the standard curve. As with the water isotope analysis (above), this was to make the accuracy valid across the entire measurement range, as opposed to calculating accuracy from a single standard. The difference between measured and known concentration was calculated for each standard in the calibration curve. These values were divided by the known concentration and expressed as percentage inaccuracy; this was averaged across the standards to give an inaccuracy metric for the calibration as a whole. For obvious reasons, standards were excluded from the accuracy calculation if they were below the limit of quantification.

Precision was once again estimated by dividing the average of several measurements by their standard deviation. These measurements were all replicates of a single standard (approx. 100 ppb), which was measured at least five times. The discrepancy between this and the precision quoted for the water isotope analysis – which was averaged across the whole calibration curve – is due to the limitations of the two instruments. In general, more variability is observed between repeated injections when using the T-LWIA than the ion chromatograph. However, the T-LWIA can rapidly measure several injections of each standard, whereas the Dionex instrument takes upwards of fifteen minutes to measure each injection.

This means that while water isotope measurements generally require upwards of twelve measurements per standard, it is rarely necessary to include more than two replicates of each standard when designing a calibration curve for ion chromatography. With only two replicates, the standard deviations (and subsequent precision values) are relatively meaningless for the majority of standards in the calibration curve. Consequently, each run finished with several of repeat measurements of a standard containing a low-mid concentration of analyte. Given that the imprecision metric scales inversely with concentration, and that the majority of samples contained greater concentrations of analyte than this standard, the quoted level of imprecision should be an overestimate (i.e. actual precision is likely better than stated).

Table 5 – Limits, accuracy and precision metrics for the analysis of major ions. Each sample group was measured in a separate run, with its own calibration curve. This allowed each calibration to be tailored to a smaller range of concentrations, thus increasing the accuracy within the anticipated concentration range for each set of samples. The chosen accuracy metric was the average deviation of each measured standard injection from its known value; the chosen precision metric was the standard deviation found from five or more consecutive measurements of a mid-range standard. Where the calculated Limit of Quantification is less than the Limit of Detection, it has been assumed to equal the LoD.

Sample	**Quality control**	**Na^+**	**NH_4^+**	**K^+**	**Mg^{2+}**	**Ca^{2+}**	**F^-**	**Cl^-**	**NO_2^-**	**SO_4^{2-}**	**NO_3^-**	**PO_4^{3-}**
Ellsworth Firn Core (n=8)	Inaccuracy / %	1.98	2.08	1.88	3.20	1.41	4.87	1.73	2.58	3.24	3.03	1.29
	Imprecision / %	0.25	0.44	0.65	0.46	1.31	1.28	1.54	0.46	1.51	0.81	0.31
	LoB / M eq.	2.76	0.05	0.58	0.19	0.96	0.45	2.34	0.00	0.24	1.39	0.00
	LoD / M eq.	2.79	0.09	0.59	0.21	1.69	0.55	2.43	0.01	0.27	1.40	0.04
	LoQ / M eq.	5.82	0.99	1.13	1.93	4.27	1.31	2.43	1.22	0.62	2.80	0.26
	Quality control	**Na^+**	**NH_4^+**	**K^+**	**Mg^{2+}**	**Ca^{2+}**	**F^-**	**Cl^-**	**NO_2^-**	**SO_4^{2-}**	**NO_3^-**	**PO_4^{3-}**
Lago Steffen Icebergs (n=24)	Inaccuracy / %	3.18	4.49	3.88	4.06	2.02	2.66	3.78	2.50	1.85	1.55	2.53
	Imprecision / %	4.69	4.47	4.92	5.42	4.03	2.38	2.75	0.69	1.19	0.88	2.54
	LoB / M eq.	0.47	0.34	0.26	0.62	0.21	0.35	0.08	0.09	0.08	0.09	0.29
	LoD / M eq.	0.51	0.50	0.33	0.72	0.30	0.41	0.15	0.10	0.10	0.13	0.41
	LoQ / M eq.	1.26	0.92	0.53	1.27	0.89	1.03	0.30	0.29	0.14	0.18	0.34
	Quality control	**Na^+**	**NH_4^+**	**K^+**	**Mg^{2+}**	**Ca^{2+}**	**F^-**	**Cl^-**	**NO_2^-**	**SO_4^{2-}**	**NO_3^-**	**PO_4^{3-}**
Marble Hills TBIS (n=36)	Inaccuracy / %	1.94	3.36	1.64	0.74	0.93	4.51	2.46	1.28	1.77	1.83	2.28
	Imprecision / %	1.03	2.24	2.45	1.60	0.90	0.35	5.64	1.82	1.62	1.70	6.23
	LoB / M eq.	2.43	0.01	0.88	1.18	0.14	0.43	1.47	0.07	2.00	1.28	0.09
	LoD / M eq.	2.45	0.02	0.89	1.19	0.17	0.45	1.50	0.07	2.02	1.30	0.44
	LoQ / M eq.	10.18	0.25	1.32	3.49	4.20	1.22	2.83	1.27	4.63	1.30	0.44

2.5 – Dissolved organic carbon (DOC)

2.5.1 – Method

Concentrations of non-purgeable organic carbon (commonly considered DOC) were measured using a Shimadzu TOC-L CPH/CPN instrument. As with the other analyses, samples were analysed one at a time, and were delivered via autoinjector. Each 100 µl injection then underwent a three-step process. Firstly, inorganic carbon was converted to $CO_{2(g)}$ and removed from the samples via sparging with 1.5 µl of 1.0 M $HCl_{(aq)}$ for 5 minutes. The remaining non-purgeable organic carbon was then oxidised to $CO_{2(g)}$ through heating to 680°C over a platinum-coated glass wool catalyst. Lastly, an infrared gas analyser was used to detect the quantity of carbon dioxide gas released by the combustion.

During the run, the instrument measured a minimum of two injections per vial. As with the ion chromatograph, the result of each injection was reported as an area (signal strength multiplied by time). An additional injection was automatically carried out if both the standard deviation and the coefficient of variation of the first two measurements were greater than predetermined critical values (0.1 and 2%, respectively). The mean of the accepted areas was then reported as the value for that given sample. Conversion of the response variable to a meaningful concentration was carried out in post-processing, using the equation of a calibration curve.

Calibration

A 1000 mg/l TOC stock solution was diluted by mass (Kern ABT 220-4M) to create a large set of standards, ranging from 10 ppb to 625 ppb. Every run, these were measured alongside the unknown samples, and the values of the response variable (mean measured area) were plotted against the known concentrations of the standards. Simple least squares linear regression was then applied to a minimum of seven data pairings (average = 8.0) in order to calculate a calibration curve for the run. This equation was used to calculate the DOC concentration of the unknown samples.

2.5.2 – Quality control data

Accuracy and precision metrics were calculated as for the ion chromatography analysis (see above), as were the LoB, LoD and LoQ (Table 6). Where multiple runs were required in order to measure an entire sample set, the accuracy and precision metrics presented are a weighted average between the runs. It would be inappropriate to average the LoB, LoD and LoQ, and so the highest (i.e. most conservative) limits were used. In practice, all DOC measurements were found to be significantly above the limits.

Table 6 – Limits, accuracy and precision metrics for the NPOC analyses. As with the ion chromatography, the two groups were measured separately so that the calibration curves could be tailored to a more specific smaller range of concentrations, thus increasing accuracy. The chosen accuracy metric was the average deviation of each measured standard injection from its known value; the chosen precision metric was the standard deviation found from five or more consecutive measurements of a mid-range standard. Where the calculated Limit of Quantification is less than the Limit of Detection, it has been assumed to equal the LoD.

Quality Control	Inaccuracy %	Imprecision / %	LoB / ppb	LoD / ppb	LoQ / ppb
Marble Hills	1.74	3.32	24.0	35.0	52.8
Steffen Glacier	1.22	4.58	17.7	25.4	25.4

2.6 – Suspended debris

Whilst sampling icebergs from Lago Steffen, collections of debris were observed in all iceberg classes (Figure 9). Most sediment appeared to be fine particulate matter and was either brown or grey in colour. Sediment deposits were visibly larger and more abundant in grey icebergs (and was almost certainly the cause of their grey colouration); much less debris was observed in the blue icebergs.

After sampling, debris was captured on pre-weighed cellulose nitrate filter paper (0.45 µm) and stored in pre-weighed polyethylene bags (Whirl-Pak). Sediment samples were frozen (-20°C) and transported back to Bristol. Once in LOWTEX, these samples were weighed (still frozen) and the quantity of wet sediment in each sample bag was calculated. Most of the samples were set aside for future analyses of sediment-bound nutrients, however a subset of samples – a little over 16% by mass – were defrosted and the contents of the polyethylene bags (filter and sediment) were transferred to clean pre-weighed glass vials. The mass of wet sediment in each vial was once again weighed. The samples were then dried overnight (105°C) and the dry mass was determined. The results of this process were used in a linear regression of dry mass vs wet mass, wherein the constant (which is negative) represents the mass of water held by a wet filter paper with no sediment. The equation for this relationship is as follows:

$$m_{Dry} = (0.8016) \times m_{Wet} - 0.2895\ g \qquad \text{Equation 9}$$

Given the very good fit of Equation x with the data ($R^2 = 0.9999$), this relationship was deemed acceptable to estimate the quantity of dry sediment in the rest of the samples.

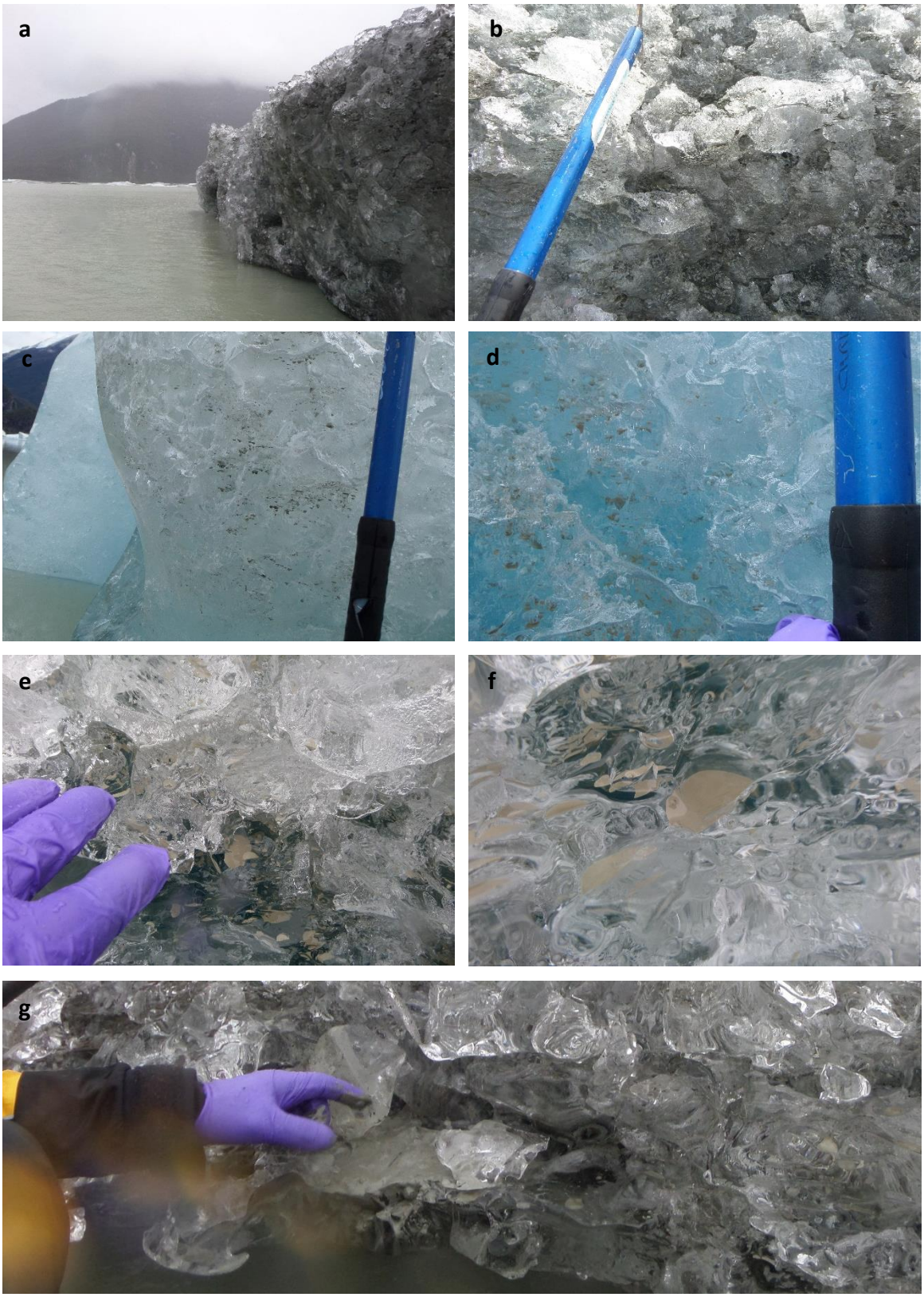

Figure 9 – Photographs of sediment deposits in calved icebergs. a) & b) Icebergs 3 and 8, classified as “grey”. c) & d) Iceberg 6, classified as “blue”. e) & f) Iceberg 1, classified as “white”. Similar deposits were observed in all eight icebergs, although they varied in size (approximately 1 – 30 mm) and abundance. g) Larger deposits (up to 300 mm wide) were uncovered during removal of the outer surface of the icebergs. Samsung WB200F camera, February 2017.

Chapter 3 – What can we learn from Terminal Blue Ice Samples?

Terminal Blue Ice Samples (TBIS) were collected from the surface of the Marble Hills BIA, proximal to the nunataks. The bare ice in this location contained visible bands of suspended debris, unlike the nearby non-terminal blue ice. This suggests that the TBIS may have taken a slightly distinct flow path compared with the rest of the BIA. The majority of analyses were therefore chosen to investigate the origin of these unusual samples, beginning with the determination of δ^2H and δ^{18}O values.

3.1 – Water isotope analysis

Relative to ocean water, glacial samples are typically depleted in the heavier isotopes of oxygen and hydrogen. Fractionation initially occurs during evaporation from the ocean surface, as heavier water molecules (most notably $^2H^1H^{16}O$ and $^1H_2{}^{18}O$) form stronger intermolecular bonds and thus evaporate less readily than $^1H_2{}^{16}O$. The heavier isotopes of water also condense more quickly, meaning that: a) water vapour becomes gradually more depleted in ^2H, ^{18}O and ^{17}O over time; and b) the isotopic signature of precipitation depends on temperature, altitude and distance inland. Despite this variability in isotopic signature, it has been found that there is a consistent relationship between δ^2H and δ^{18}O in precipitated waters:

$$\delta^2H = 8.0 \times \delta^{18}O + 10 \text{ ‰} \qquad \text{Equation 10}$$

This is known as the global meteoric water line (GMWL) [164]. Water/ice that has not undergone further fractionation since precipitating will lie somewhere close to this line, and is termed *meteoric*. Conversely, samples that have undergone additional fractionation processes can often be identified by their non-meteoric water isotope signatures. The stable isotopes of water can therefore provide insight into the journey undertaken by water molecules before they reach the sample site.

Changes of phase may induce further fractionation. Experimental studies of Weertman regelation, for instance, have identified a replicable fractionation that, compared with the precipitation effect, acts to deplete δ^{18}O more strongly than δ^2H [165]. Hubbard and Sharp (1993) modelled this process, showing that the "refreezing slope" would typically fall within a range the 4.5-6.9 [166]. This is consistent with field measurements such as those found by Gordon et al. (1988), who found a regression coefficient of 5.5 in the basal debris layer of "Flutes Glacier", Norway, where local melting and refreezing had taken place [167]. Horseshoe Valley Glacier is significantly larger than the small mountain glaciers where Weertman regelation has been observed, and likely has a different thermal structure. Nevertheless, it is not improbable that basal ice will melt in certain areas due to the immense pressure of the overlying ice: around 9 MPa at the Marble Hills, where the ice is almost 1000 m thick. Furthermore, accretion is known to occur all over the AIS. This means that basal ice in Horseshoe Valley Glacier may undergo some kind of regelation process, gradually melting and then refreezing downstream. Consequently, if the TBIS are comprised of basal ice, then we can expect to observe a δ^2H/δ^{18}O relationship that is markedly different from that of meteoric ice.

Measured δ^2H and δ^{18}O values for the Marble Hills BIA samples are displayed in Table 7. Isotope composition was determined by off-axis integrated cavity output spectroscopy (Los Gatos Research T-LWIA 45-EP). See Methodology chapter for a description of the instrument calibration.

Table 7 – Spectroscopically-determined water isotope content of 36 TBIS. Isotopic ratios and associated errors are both given in delta values per mil, and are relative to VSMOW. Error is the standard deviation calculated from approximately 16 measured injections for each sample, rounded to one significant figure.

Alphanumeric labelling in the left-hand column denote where each sample was located in the original slab: Latin letters indicate proximity to the Marble Hills (A-B); Arabic numerals indicate proximity to the mouth of Horseshoe Valley (1-3); Roman numerals indicate depth below the surface (i-vi). These respectively correspond with the x, y and z axes used in the spatial analysis. The chosen origin was the upper southeast corner (the outside vertex of A1 i). The distance from the centre of the sample to a face containing the origin is used to quantify location along a given axis.

	Distance from origin / cm			**Delta values / ‰**			
	x-axis	**y-axis**	**z-axis**	**δ^2H**		**$\delta^{18}O$**	
A1 i	4.5	5.8	2.0	-309.6	±0.5	-39.4	±0.4
A1 ii	4.5	5.8	6.0	-310.5	±0.3	-39.6	±0.1
A1 iii	4.5	5.8	10.0	-307.7	±0.4	-38.97	±0.06
A1 iv	4.5	5.8	14.0	-309.2	±0.3	-39.23	±0.01
A1 v	4.5	5.8	18.0	-310.2	±0.4	-39.5	±0.4
A1 vi	4.5	5.8	22.0	-308.7	±0.3	-39.3	±0.5
B1 i	13.5	5.8	2.0	-310.5	±0.4	-39.52	±0.4
B1 ii	13.5	5.8	6.0	-308.9	±0.3	-39.2	±0.1
B1 iii	13.5	5.8	10.0	-309.9	±0.2	-39.30	±0.03
B1 iv	13.5	5.8	14.0	-310.8	±0.2	-39.56	±0.04
B1 v	13.5	5.8	18.0	-310.62	±0.06	-39.55	±0.03
B1 vi	13.5	5.8	22.0	-311.2	±0.1	-39.5	±0.1
A2 i	4.5	17.5	2.0	-310.7	±0.1	-39.45	±0.07
A2 ii	4.5	17.5	6.0	-311.5	±0.2	-39.62	±0.04
A2 iii	4.5	17.5	10.0	-311.0	±0.5	-39.6	±0.4
A2 iv	4.5	17.5	14.0	-307.7	±0.2	-39.10	±0.03
A2 v	4.5	17.5	18.0	-310.2	±0.2	-39.52	±0.07
A2 vi	4.5	17.5	22.0	-309.3	±0.2	-39.46	±0.06
B2 i	13.5	17.5	2.0	-310.0	±0.1	-39.54	±0.07
B2 ii	13.5	17.5	6.0	-309.6	±0.5	-39.5	±0.1
B2 iii	13.5	17.5	10.0	-310.5	±0.2	-39.55	±0.07
B2 iv	13.5	17.5	14.0	-310.4	±0.4	-39.40	±0.07
B2 v	13.5	17.5	18.0	-310.61	±0.08	-39.46	±0.03
B2 vi	13.5	17.5	22.0	-309.3	±0.1	-39.35	±0.02
A3 i	4.5	29.2	2.0	-305.5	±0.4	-38.92	±0.06
A3 ii	4.5	29.2	6.0	-308.8	±0.4	-39.2	±0.2
A3 iii	4.5	29.2	10.0	-309.8	±0.2	-39.56	±0.03
A3 iv	4.5	29.2	14.0	-308.75	±0.02	-39.12	±0.02
A3 v	4.5	29.2	18.0	-309.5	±0.3	-39.3	±0.3
A3 vi	4.5	29.2	22.0	-307.3	±0.1	-39.07	±0.03
B3 i	13.5	29.2	2.0	-310.7	±0.2	-39.53	±0.04
B3 ii	13.5	29.2	6.0	-310.56	±0.06	-39.53	±0.02
B3 iii	13.5	29.2	10.0	-310.28	±0.09	-39.38	±0.06
B3 iv	13.5	29.2	14.0	-309.9	±0.1	-39.29	±0.03
B3 v	13.5	29.2	18.0	-304.5	±0.1	-38.6	±0.3
B3 vi	13.5	29.2	22.0	-307.9	±0.1	-39.10	±0.05

3.1.1 – Estimating the local meteoric water line

The isotopic composition of meteoric water reflects a brief history of the air masses in a given locality. The $\delta^2H/\delta^{18}O$ ratios of all meteoric water within the same region will therefore be linked. The LMWL is an approximate linear relationship between the δ^2H and $\delta^{18}O$ values for meteoric water from a defined area; this is likely to be a better fit to the data than the global meteoric line, because local atmospheric processes can shift isotopic ratios away from the global mean. Such relationships can be used to evaluate whether or not an unknown sample has undergone further fractionation processes since falling as precipitation. In the following section, a vertical firn core and a horizontal transect are used to calculate two potential meteoric lines for the Marble Hills BIA.

The firn above SLE lies at a higher elevation than the Marble Hills BIA (at 1928 m and 1049 m respectively). Meteoric ice at this elevation is likely to be more depleted in ^2H and ^{18}O than in Horseshoe Valley [168]. This does not necessarily make the Ellsworth firn core unsuitable for the calculation of a LMWL: elevation should merely shift samples to a more depleted position along the same line. Similarly, the Ellsworth sampling site is around 100 km further from the coast and around 1.3° lower in latitude; these should have small effects on the isotopic ratios of ^2H and ^{18}O, but no overall effect on the LMWL. Whether or not the Ellsworth firn core shares a meteoric line with Horseshoe Valley therefore depends entirely on whether or not their precipitation originates from similar air masses.

Fifteen samples of meteoric firn were used to calculate the LMWL for the region around SLE (see Table 8). Ordinary least squares regression gives a LMWL of:

$$\delta^2H = 7.28529 \times \delta^{18}O - 24.12857 \text{ ‰} \qquad \text{Equation 11}$$

$$R^2 = 0.93650$$

This simplistic technique is based upon the principle that each data point is given equal value. The high R^2 value is consistent with a strong correlation, as can be seen in a plot of δ^2H vs $\delta^{18}O$ (Figure 10). A vertical firn core is preferable for calculating a LMWL because variation in isotopic composition is brought on by temporal and not spatial differences: for instance, due to different sea surface temperatures during the initial evaporation process. It is, however, worth noting that SLE is situated around 70km west of the Ellsworth Mountains. The topography around Horseshoe Valley may have a significant effect on atmospheric currents, which may lead to slight differences in the LMWLs. Consequently, it is necessary to cross-check the Ellsworth meteoric line with samples from within the Ellsworth Mountains themselves.

Fortunately, isotope data are available from the 1990 International Trans-Antarctica Expedition (ITAE) [169]. Surface snow samples were taken from 105 stations across the AIS – including several in the vicinity of the Ellsworth Mountains. Table 9 displays the delta values for the seven samples closest to the Ellsworth firn core, one of which was collected within 5 km of the Patriot Hills BIA, Horseshoe Valley. These data have a meteoric relationship:

$$\delta^2H = 8.07399 \times \delta^{18}O + 7.60401 \text{ ‰} \qquad \text{Equation 12}$$

$$R^2 = 0.99287$$

Table 8 – Tabulated δ 2H and δ 18O values for fifteen samples from the Ellsworth firn core, sorted by depth of origin below the surface. σ is the standard error of all measurements of a given sample, rounded to one significant figure.

Depth / cm	δ^2H / ‰	σ (δ^2H) / ‰	δ^{18}O / ‰	σ (δ^{18}O) / ‰	# Injections
0	-244.6	± 0.3	-30.4	± 0.1	30
8	-242.10	± 0.02	-29.8	± 0.1	10
1738	-266.27	± 0.07	-33.36	± 0.01	10
1746	-251.4	± 0.2	-31.65	± 0.03	10
1754	-252.56	± 0.05	-31.55	± 0.03	10
1762	-250.56	± 0.06	-30.87	± 0.01	9
1806	-272.37	± 0.09	-33.6	± 0.1	10
1814	-266.3	± 0.2	-33.3	± 0.1	33
1822	-257.13	± 0.05	-31.55	± 0.09	10
1830	-267.09	± 0.03	-33.04	± 0.02	10
1838	-265.0	± 0.2	-33.1	± 0.1	10
1851	-255.71	± 0.03	-32.30	± 0.02	10
1859	-261.77	± 0.02	-32.95	± 0.03	9
1867	-255.0	± 0.1	-31.4	± 0.1	7
1875	-250.5	± 0.1	-31.0	± 0.1	49

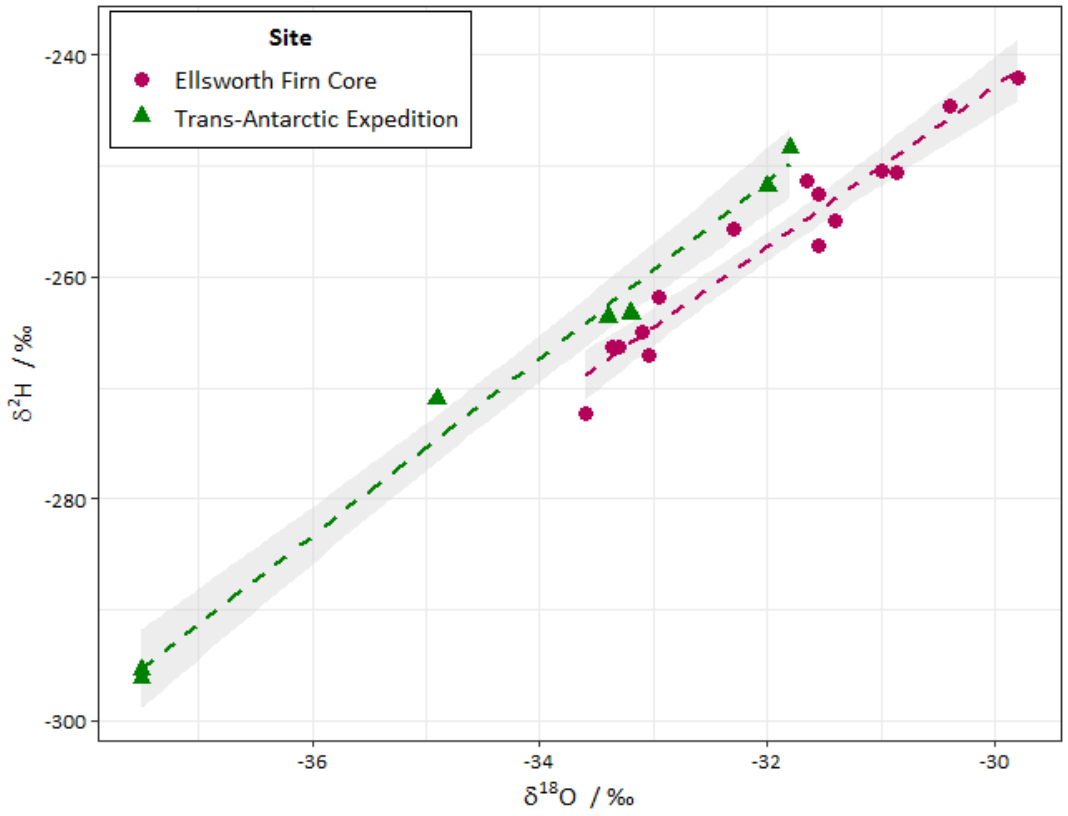

Figure 10 – Comparison of Local Meteoric Water Lines in the Ellsworth Mountains region. LMWL were calculated from the δ^2H and δ^{18}O values measured in the Ellsworth firn core and by the 1990 International Trans-Antarctica Expedition [169]. Standard error at the 95% confidence interval is shown in grey. ANCOVA found a statistically significant difference in intercepts but not gradient.

Table 9 – Tabulated $\delta^{2}H$ and $\delta^{18}O$ values from the International Trans-Antarctica Expedition (1990, [169]). Distances between sampling locations and the site of the Ellsworth firn core were estimated from coordinate data using ArcGIS.

	Latitude / °	Longitude / °	Distance from firn core / km	Altitude / m	$\delta^{2}H$ / ‰	$\delta^{18}O$ / ‰	Nearest landmark
1	-77.65	-87.12	163.75	1500	-248.4	-31.8	Gromshin Heights
2	-78.20	-87.65	105.47	1650	-251.9	-32.0	Probuda Ridge
3	-78.82	-87.23	72.50	2050	-295.4	-37.5	Bastien Range
4	-79.17	-86.85	80.43	1800	-263.3	-33.2	Founders Peaks
5	-79.75	-85.30	136.78	1680	-296.2	-37.5	Soholt Peaks
6	-80.30	-81.35	232.65	700	-263.6	-33.4	Patriot Hills
7	-80.75	-81.25	264.69	900	-271.0	-34.9	-

In Figure 10, the stable water isotope data from the 1990 ITAE are compared with the Ellsworth firn core data. At first appearance, these appear to be overlapping data series. Analysis of covariance (ANCOVA) can be used to test this via two null hypotheses:

$$H_0^1: m_2 = m_3 \qquad H_0^2: \bar{Y}_2 = \bar{Y}_3$$

Where m_i is the gradient of the true meteoric line $y_i = m_i x_i + c_i$ and $\bar{Y}_i$ is the adjusted mean (the predicted value of y given the grand mean x value). Essentially, this is a test for a) a difference in slope and then b) a difference in intercept. If both null hypotheses are accepted, then there is no significant difference between the two LMWLs. Full details of the ANCOVA are given in Appendix 2. The results can be summarised as follows:

1. H_0^1 is accepted at the 5% significance level ($F = 1.3913$, $p = 0.25$, $\alpha = 0.05$, $df_1 = 1$, $df_2 = 18$). The relationship between $\delta^{2}H$ and $\delta^{18}O$ does not differ significantly between the datasets, meaning that the two LMWLs may be assumed to have the same gradient.
2. H_0^2 is rejected at the 5% significance level ($F = 17.206$, $p = 0.0005465$, $\alpha = 0.05$, $df_1 = 1$, $df_2 = 19$). The two datasets differ significantly in terms of $\delta^{2}H$ even when the covariant ($\delta^{18}O$) is taken into account. This was based upon a second model that assumed a shared gradient (from the previous result), and so the difference between the datasets must be due to a significant difference in their intercepts.

Consequently, the original hypothesis is rejected: the two calculated LMWLs are not exactly the same. Nevertheless, given the insignificant difference in gradients, it appears safe to assume that the $\delta^{2}H$-$\delta^{18}O$ gradient for the true LMWL is between 7.3 and 8.0.

3.1.2 – Comparison of blue ice with the local meteoric water line

The relationship between $\delta^{2}H$ and $\delta^{18}O$ for the BIA sample is shown in Figure 11. Although there is some spread in the data, there appears to be a reasonably strong positive correlation. Statistical analysis revealed that the data are not normally distributed, therefore violate the assumptions of a simple "least squares" linear regression. Instead, a non-parametric regression was chosen. Analysis using the Theil-Sen estimator (Appendix 3) found the following statistically significant regression line:

$$\delta^{2}H = 5.6302 \times \delta^{18}O - 87.9885 \text{ ‰} \qquad \text{Equation 13}$$

$$s_{est} = 0.5548362$$

The coefficient of $\delta^{18}O$ (5.6) is strikingly less than that which was found in any of the three meteoric lines (local or global). Interestingly, it is consistent with the slopes for ice that have undergone Weertman regelation, as modelled by Hubbard and Sharp (1993, [166]) and observed by Gordon et al. (1988, [167]).

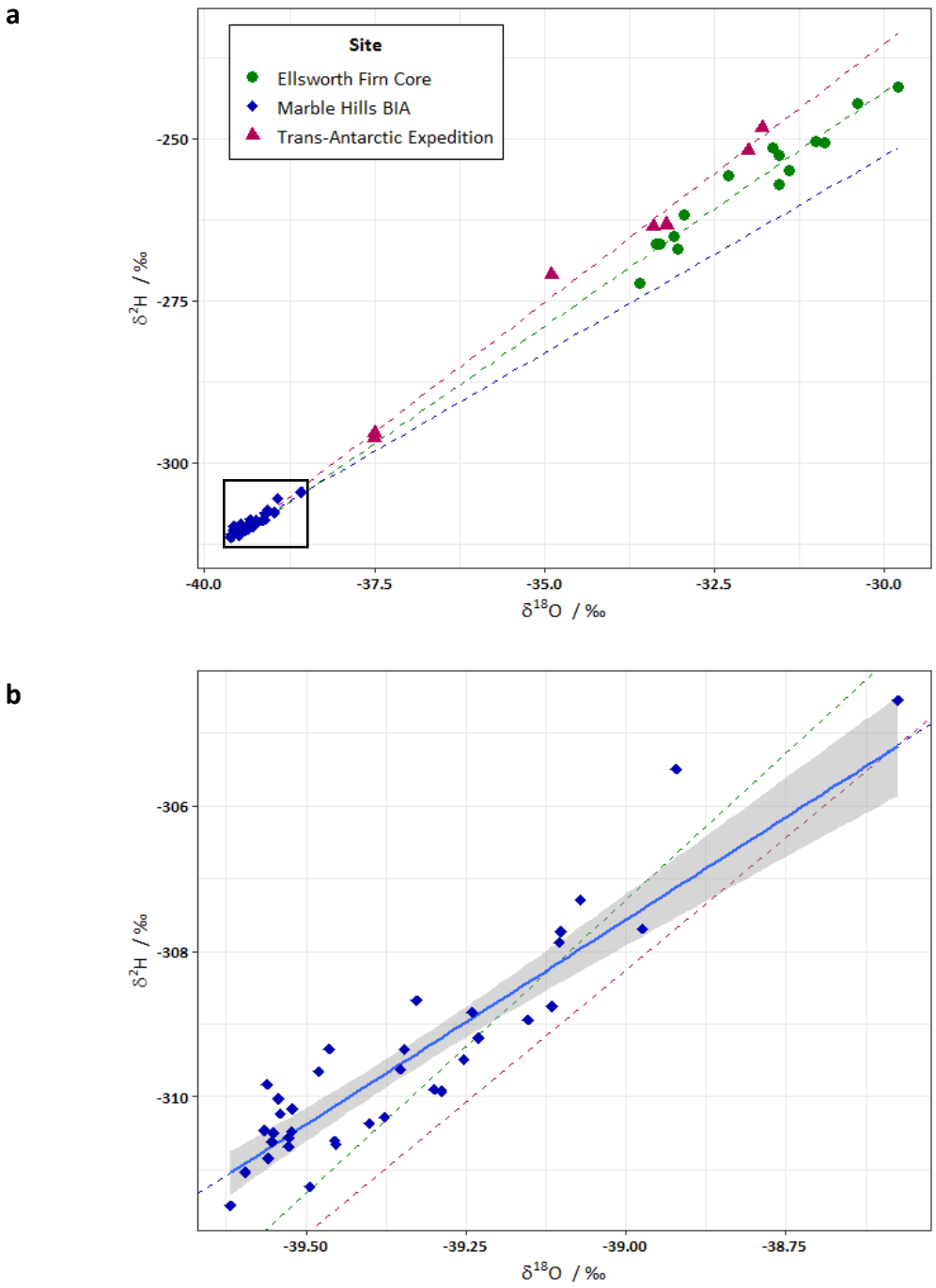

Figure 11 – Scatterplots of δ^2H against $\delta^{18}O$ for blue ice from the Marble Hills BIA. a) Comparison of the TBIS and LMWL datasets. The green and purple lines represent the parametric linear models in Equations 11 and 12 (firn data and ITAE data, respectively). The black box denotes the axes of b), a plot scaled to display only the TBIS data, with median-based regression line and confidence intervals (Equation 13) calculated with the Theil-Sen Estimator. This model fits the data well (s_{est} = 0.5548362) and has a gradient consistent with ice that has undergone subglacial melting and refreezing.

It is difficult to test statistically whether or not Equation 13 is significantly different from the two LMWLs calculated in section 3.1.1. This complication arises from two circumstances. Firstly, the Marble Hills isotope data are not normally distributed. This violates the assumptions of parametric tests such as ANCOVA, which are susceptible to the effects of extreme values. Secondly, the three datasets are unbalanced: each was generated from a different number of data points. This eliminates the possibility of using Quade's rank analysis of covariance, the non-parametric equivalent of ANCOVA. One plausible way to quantitatively evaluate the fit of the three equations to the data is to analyse the residuals. This removes the issue of unbalanced design, as each model generates the same number of residuals. Moreover, these groups were found to be normal, and so valid subjects for parametric tests. Consequently, this approach opens up the possibility of comparing the fit of the three equations to the Marble Hills data using a simple one-way ANOVA.

Appendix 4 describes the process of using $\delta^{18}O$ measurements to generate fitted $\delta^{2}H$ values for each of the three equations (and subsequently a list of residuals) in RStudio. One-way ANOVA found that the three residual datasets were significantly different ($F = 35.8534 > 3.0829$, $df_1 = 2$, $df_2 = 105$, $\alpha = 0.05$, $p << 0.0001$). Post-hoc application of Tukey's Honest Significant Difference test revealed that all three groups were significantly different from each other ($p < 0.001$ in all cases):

```
                            diff        lwr        upr     p adj
Equation 8-Equation 7 -0.6960300 -1.0532396 -0.3388205 0.0000308
Equation 9-Equation 7 -1.2703901 -1.6275997 -0.9131805 0.0000000
Equation 9-Equation 8 -0.5743601 -0.9315696 -0.2171505 0.0006518
```

Calculation of residual sum of squares and the standard error of the estimate then confirmed that Equation 9 was a much better fit for the data than the two LMWLs:

```
                              Equation.7 Equation.8  Equation.9
Slope                        7.285290  7.9805616   5.6301775
Intercept                   -24.128573  3.9898488 -87.9885488
Residual sum of squares      74.799096 28.2893639  11.0823567
Standard error of the estimate  1.441441  0.8864624   0.5548362
```

Given that the residuals generated by Equation 9 are both smaller than, and significantly different to, those of Equations 7 and 8, it is reasonable to deduce that the model represented by Equation 9 is significantly better than those represented by the LMWLs. Nevertheless, it should be noted that the statistical analysis cannot strictly prove that this improvement is due to the difference in gradient of the $\delta^{2}H$ / $\delta^{18}O$ relationship, only that the equation represents a significantly better model; the intercept could, in theory, be the only significantly different component (although a 40% difference in gradient between Equations 8 and 9 suggests otherwise). Consequently, it is important to corroborate the water isotope analysis with other glaciochemical signatures before drawing conclusions on the origin of the sample from the Marble Hills BIA.

3.1.3 – Spatial distribution of water isotopes

The original block of ice was sectioned into thirty-six samples, each of which was labelled according to its location (Table 7). This enabled analysis of the spatial distribution of water isotopes. There were no significant relationships between delta values, depth, distance downstream or proximity to the nunatak (Appendix 5).

3.2 – Major ions

Measurements of major ions have long been a staple of glaciochemical studies [170-172]. There are two main sources of ions in ice and firn: sea spray aerosols – created when wind disperses small droplets from the surface of oceans or sea ice – and highly weathered continental dust [173, 174]. Due to the many ways in which aerosol can be created, the profile of different ions in a given sample can shed light on the rates of certain natural or anthropogenic processes at the time of deposition. For example, in the majority of Antarctic samples, it can be assumed that the Na^+ fraction originated almost entirely from sea spray [172]. In contrast, Cl^- arises both in sea spray and as a secondary atmospheric aerosol (from HCl), while Ca^{2+} is derived largely from mineral dust. By comparing the measured concentration of Na^+ with the reliably established ionic ratios of bulk seawater (e.g. Na^+/Cl^-), it is possible to estimate the sea spray component of a particular ion in a given sample. It follows that subtracting sea spray Cl^- and Ca^{2+} fractions from their total concentrations will indicate the HCl and mineral dust fractions of the Cl^- and Ca^{2+} records. Such relationships can be used to study changes in natural and anthropogenic processes over time.

In samples of subglacial ice, ions may be acquired from a third source: subglacial weathering processes. The major ions released by physical weathering are likely to be similar in composition to those contained in continental dust – albeit in greater concentrations, and derived from a much less diverse array of rock types. However, chemical and biological processes at the subglacial bed may oxidise or reduce these crustal ions, generating species that are not observed in continental dust. One example of this is the sulphide ion, which is typically reduced in continental dust but may be oxidised to sulphate in microbial respiration. Such metabolic by-products are indicative of subglacial processes. Ionic composition can therefore be used to test the hypothesis laid out in the previous section: if the TBIS have undergone some kind of subglacial melting/refreezing process, then they are likely to contain excess crustal species and the products of chemical/biological weathering.

The concentrations of five major cations (Na^+, K^+, Mg^{2+}, Ca^{2+}, NH_4^+) and six major anions (F^-, Cl^-, NO_2^-, SO_4^{2-}, NO_3^- and PO_4^{3-}) were determined by ion chromatography (Dionex ICS-5000). The results of these analyses are displayed in Table 10. All data are given in units of micro-equivalents per litre (μ eq. L^{-1}), as calculated through division of the concentration (initially found in μg L^{-1}) by the molar mass (in g mol^{-1}) for any given ion and then multiplying the result by the magnitude of the ionic charge (in units of elementary charge, ***e***). A value of 1.00 μ eq. L^{-1} is therefore equivalent to ± 1.00 μmol ***e*** L^{-1}, or ± 0.0965 C L^{-1}.

Table 10 – Results of ion chromatography on Antarctic samples. Outliers were excluded from the reported value according to Tukey's Fences (1.5 times the interquartile range beyond the 1st or 3rd quartiles). Ions that could be reliably detected but not quantified are reported < *LoQ*; ions below the detection limit are reported < *LoD*.

	Marble Hills BIA		**Ellsworth Firn Core**	
	Concentration / µ eq. L^{-1}	σ / µ eq. L^{-1}	Concentration / µ eq. L^{-1}	σ / µ eq. L^{-1}
Ca^{2+}	79.1	24.4	12.8	5.9
Mg^{2+}	19.1	5.4	< LoQ	0.6
Na^{+}	13.7	2.1	9.3	4.9
K^{+}	1.7	0.3	3.2	1.6
NH_4^{+}	1.2	0.2	< LoD	0.0
Cations	114.8		25.3	
SO_4^{2-}	30.8	9.7	2.2	1.2
Cl^{-}	4.1	0.7	6.7	3.5
NO_3^{-}	2.3	0.4	12.0	3.8
F^{-}	< LoQ	0.2	< LoD	0.5
NO_2^{-}	< LoD	0.0	< LoD	0.0
PO_4^{3-}	< LoD	0.0	< LoD	0.0
Anions	37.1		20.9	

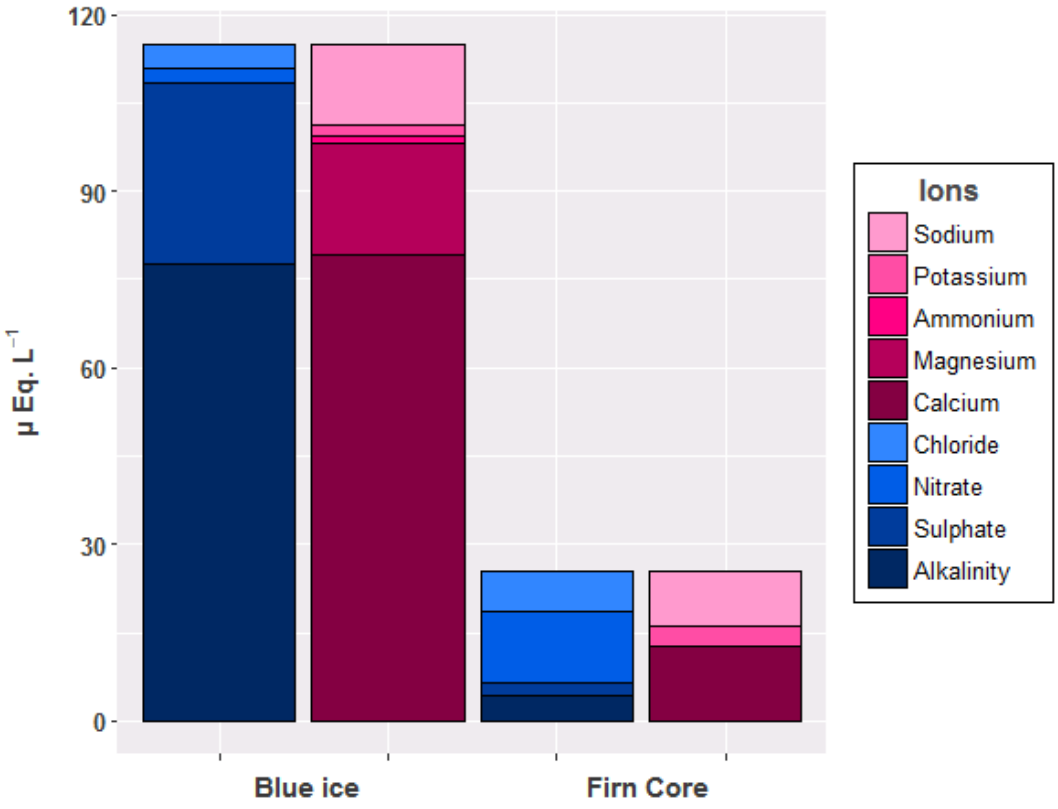

Figure 12 – Stacked bar plots comparing the mean ion concentrations of TBIS and local firn. Cations are shown in pink, anions in blue. Alkalinity is the difference in charge balance. Extreme value were excluded with Tukey's Fences.

3.2.1 – Sodium excess

The major ions signature of the blue ice is extremely unusual, and may give some insight into its origin. There is a notable excess of sodium ions relative to chloride in the Marble Hills BIA. The Cl^-/Na^+ molar ratio is only 0.30, relative to a value of around 1.16 for bulk seawater [175]. This indicates that there is either a loss of chloride between aerosol formation and deposition, or an additional source of sodium ions to the blue ice samples. Both processes are known, and either can affect the assumptions of a major ions investigation. An apparent excess in Na^+ may be due to loss of volatile Cl^- as HCl from the sea spray fraction. However, this is a seasonal process – peaking in the warmer summer months – and is generally balanced by the precipitation of Na^+ as mirabilite ($NaSO_4$) during the polar winter [176]. Given that the volume of ice sampled was much greater than the annual accumulation across the continent, it is unlikely that any one seasonal process will dominate the mean ionic composition. It therefore follows that some of the Na^+ ions in the blue ice samples had a non-sea spray origin (i.e. other than NaCl or $NaSO_4$ in sea spray aerosols). This is consistent with the findings of Qin et al. (1999), who posited crustal-origin Na^+ as a possible cause of unexpectedly high sodium concentrations in samples from the 1990 ITAE [177].

Terrestrial dust, in which Na^+ may be present as aluminosilicates, is the most likely source of the additional sodium ions. Whilst insoluble in a glacial environment, terrestrial sodium has been found to dissolve entirely when passing through ion chromatography columns [178]. In light of this, it may be more appropriate to assume that chloride, rather than sodium, is sourced almost entirely from sea spray. Prior work suggests that this is a reasonable assumption: the Marble Hills BIA is only 50 km from the Filchner-Ronne Ice Shelf, with no topographical obstacles to inhibit winds carrying marine aerosols inland – this renders it an area likely to have particularly high sea spray input [179]. By accepting this assumption, it is possible to separate the concentrations of major ions into sea spray and other (mostly crustal) fractions (Table 11). Note that due to its inland location, this assumption may not hold for the firn core: the sea spray fraction is likely a slight overestimate.

It is clear that sea spray only accounts for a small proportion of the total ion budget (5.9%) of the TBIS. This is not expected for englacial or supraglacial samples from Horseshoe Valley: the delivery of marine aerosols is particularly great around the edge of the Filchner-Ronne Ice Shelf, and so sea spray should be the dominant source of ions [179]. This is not strictly diagnostic of a subglacial origin, as it could potentially be explained by an unusually strong terrestrial input due to erosive winds along the southern side of Horseshoe Valley glacier. However, it is consistent with the release of Na^+ by subglacial weathering, and supports the hypothesis that the TBIS have undergone some kind of subglacial melting and refreezing process, as could be inferred from the water isotope observations.

3.2.2 – Balancing the ionic budget

It is apparent that the ionic budget for the Marble Hills BIA is imbalanced with respect to anions and cations (Figure 12, Table 11). This cation excess is almost entirely due to the large quantity of calcium present in the samples. When taking into account measurements of Na^+, K^+, Mg^{2+}, Ca^{2+}, NH_4^+, F^-, Cl^-, NO_2^-, SO_4^{2-}, NO_3^- and PO_4^{3-}, the imbalance between cations and anions (ΔC) is 77.7 μ eq. L^{-1}, which represents more than 50% of the total ionic budget (Σ). This contrasts steeply with past studies of englacial ice, for which the budget was balanced to within 10% ($\Delta C < \Sigma/10$) based solely upon measurements of the same major ions [180, 181]. Such an imbalance would typically result from the absence of a major anion from the dataset.

Table 11 – Antarctic major ion concentrations, separated by origin. Sea spray fractions were calculated according to the measured chloride concentration and the bulk seawater composition described in Pilson, 2012 [175]. This is predicated on the assumption that chloride ions originated only in marine aerosols.

	Marble Hills BIA		**Ellsworth Firn Core**	
	Sea spray / μ eq. L^{-1}	Other / μ eq. L^{-1}	Sea spray / μ eq. L^{-1}	Other / μ eq. L^{-1}
Ca^{2+}	0.2	78.9	0.1	12.7
Mg^{2+}	0.8	18.4	< LoQ	< LoQ
Na^+	3.5	10.2	5.8	3.5
K^+	0.1	1.6	0.1	3.1
NH_4^+	0.0	1.2	< LoD	< LoD
Cations	4.5	110.3	6.0	19.3
SO_4^{2-}	0.4	30.4	0.3	1.9
Cl^-	4.1	0.0	6.7	0
NO_3^-	0.0	2.3	0.0	12.0
F^-	< LoQ	< LoQ	< LoD	< LoD
NO_2^-	< LoD	< LoD	< LoD	< LoD
PO_4^{3-}	< LoD	< LoD	< LoD	< LoD
Anions	4.5	32.6	7.0	13.9

This unmeasured species is likely to be the bicarbonate anion. Whilst concentrations are typically negligible in Antarctic snow, calcium carbonate is the primary component of Cambrian limestone, the dominant rock type of the Marble Hills. Erosion of these nunataks could potentially account for both the high concentration of Ca^{2+} observed in the ice, as well as the hypothetical 75 μ eq. L^{-1} of CO_3^{2-} required to balance the ionic budget. This is the neatest explanation for the unusual major ions signature. It is not, however a complete explanation: it does not cover *how* the additional calcium carbonate (and other mineral ions) were incorporated into the terminal blue ice. Understanding the mechanism by which this occurs is inherently linked to the history – and by extent, the scientific usefulness – of the ice.

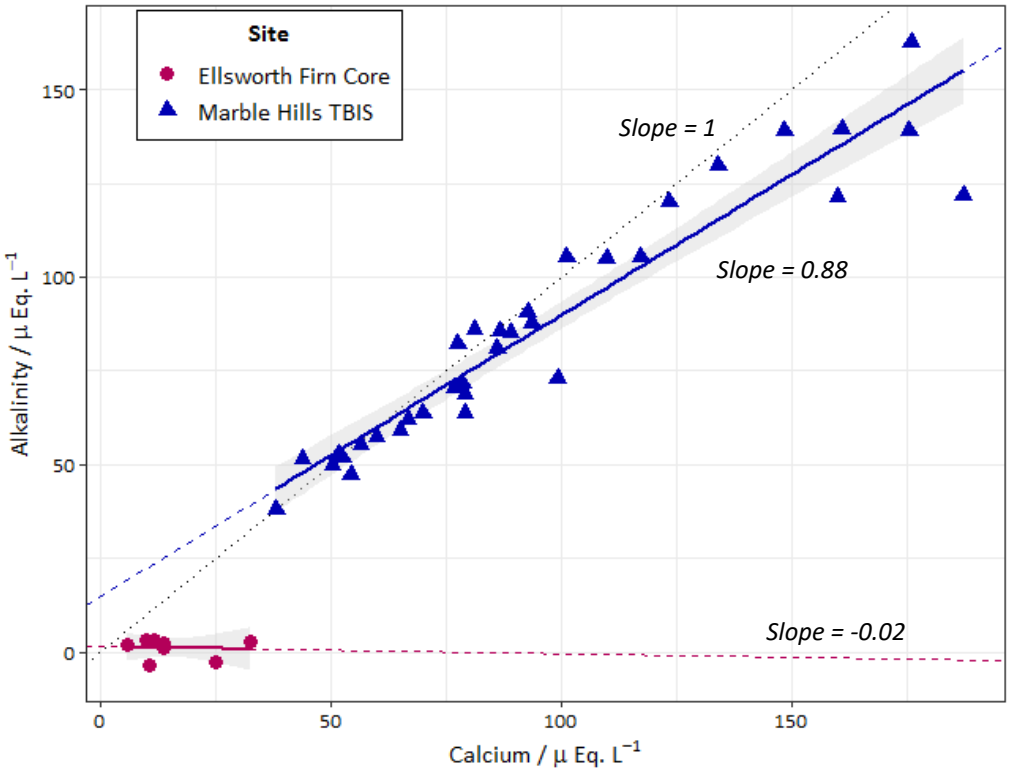

Figure 13 – Plot of alkalinity against Ca^{2+} for the Antarctic samples. The TBIS have a slope close to 1, which would be expected for a system dominated by dissolution of calcium carbonate. In contrast, the lack of correlation between calcium and alkalinity in the Ellsworth firn core effectively rules out calcium carbonate as a major component of continental dust.

3.2.3 – Origins of the TBIS

The question of how the ice acquired these extra nutrients can be broken down into two options: this process took place either before the ice had resurfaced in the blue ice area, or afterwards. The null hypothesis in this case is latter – that the ionic composition is not representative of the blue ice area, but arises only after the ice was brought to the surface. This was the argument employed by Qin et al. to explain the spike in Ca^{2+} concentration found at Site 39 (downwind of the Patriot Hills) on the International Trans-Antarctica Expedition [177]. To elaborate on this theory, air in contact with the peaks of the Independence Hills is cooled and densifies. This dense air sinks, and then warms adiabatically as it rushes down the side of the nunataks. This adds to the pressure gradient, drawing more cool air down behind it and thus generating katabatic wind. These strong winds erode the bare rock beneath them, producing mineral aerosols that are subsequently deposited onto the surface of the firn in the valley below (see Figure 14). This is a convincing hypothesis for the snowpack samples collected by Qin's expedition. However, the same argument is unlikely to hold true for a BIA.

Regions of blue ice are characterised by upwards flow and negative SMB. This means, at least hypothetically, that surface deposition should not be a viable mechanism for the delivery of nutrients. Katabatic winds are responsible for the sublimation of ice from the surface; the same winds are unlikely to be depositing mineral aerosols, any air moving fast enough to erode solid rock is also likely to destabilise the surface of the BIA. Of course, a negative SMB does not require constant erosion, just net removal of mass.

Nevertheless, even if the wind were to slow down enough to deposit nutrients without subliming the ice, it would still only affect the uppermost surface of the BIA. Given that:

1. The methodology employed by this study involved the removal of a significant band of surface ice, both during sampling and back at the Low Temperature Experimental Facility in Bristol, UK;
2. Calcium concentrations were not greatest for the shallowest samples, as would be expected from surface deposition (see Appendix 5 for plots of calcium vs depth).
3. The thirty-six samples were all far denser than could be achieved via a few seasons of compression of nutrient-rich snow, and therefore must be deep glacial ice that has been forced back up to the surface;

We can be certain that the samples that were measured by ion chromatography had not been exposed to these calcium-carrying katabatic winds. We can therefore assume that ice from the terminus of the Marble Hills BIA is enriched in calcium carbonate *before* it resurfaces.

Having established this, we are now confronted by another binary problem: did the ice acquire its distinctive major ions signature whilst below the surface, or was it already enriched before it was first compressed into ice? Both of these hypotheses have plausible mechanisms. In the case of the former, ice is drawn into the BIA from the bottom of Horseshoe Valley Glacier, where it has acquired dissolved crustal species via dissolution within the subglacial environment (Figure 15). In the alternative case, the ice flowing into the BIA does not need to be subglacial: the snowpack higher up the valley already has a calcium-rich ion signature (presumably deposited by non-subliming winds) before it is compressed into englacial ice. This dense, enriched ice travels along the periphery of Horseshoe Valley Glacier, and is drawn into the blue ice area as it nears the Marble Hills (Figure 16).

Neither of these mechanisms are inherently flawed, and so we cannot exclude either without further analytical data. It might be theorised that the subglacial hypothesis (Figure 15) is more likely to lead to the such high concentrations of calcium than the prior-acquisition hypothesis (Figure 16) because subglacial meltwaters tend to be more concentrated than firn samples. Unfortunately, at present there are no ion chromatography studies on the firn, englacial ice or subglacial meltwaters of Horseshoe Valley Glacier in the literature. Without these data, it is not possible to definitively establish the history of the BIA samples through analysis of major ions alone. We must therefore consider species that are not found in the nunataks of Horseshoe Valley but may be generated or stored in the subglacial environment.

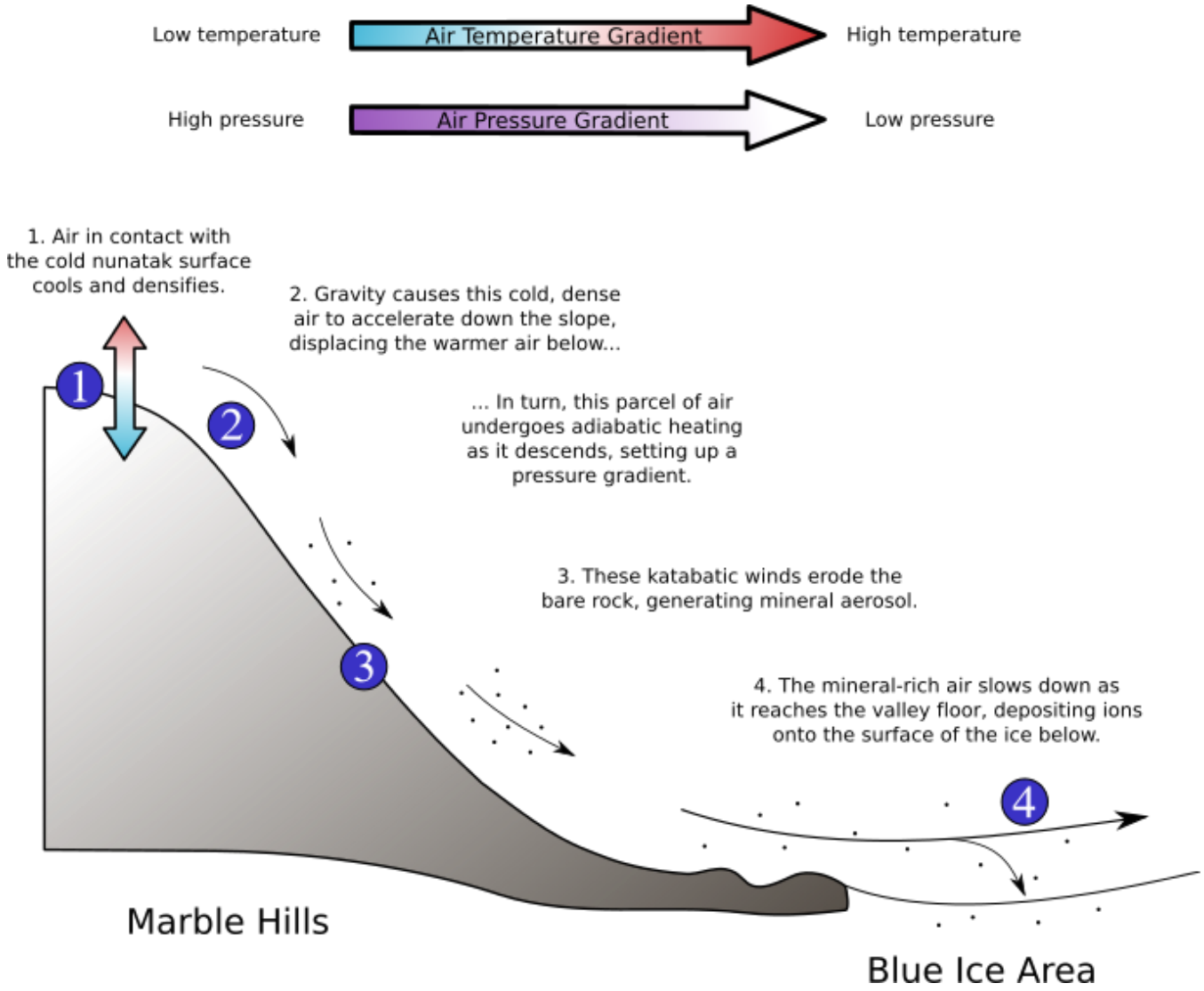

Figure 14 – Schematic for the acquisition of minerals via surface deposition. In this (hypothetical) process, the katabatic winds descending the north-eastern slopes of the Marble Hills wear away at the bare limestone, creating mineral aerosol. These are then deposited on the surface of Horseshoe Valley.

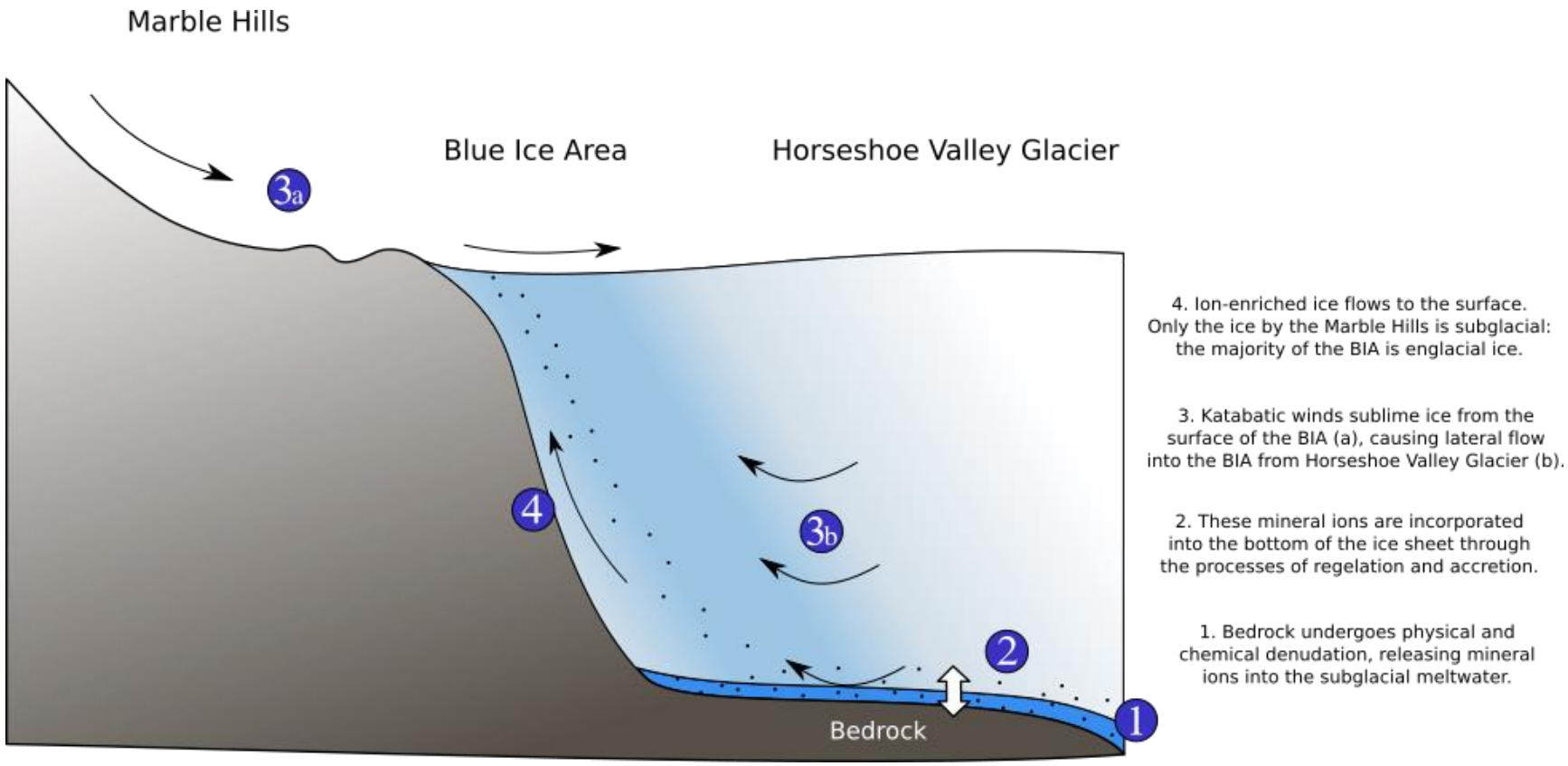

Figure 15 – Schematic for the acquisition of minerals via the subglacial bed. In this (hypothetical) process, Horseshoe Valley Glacier undergoes pressure-induced melting and refreezing at the bed, causing nutrient-rich meltwaters to become mixed in with subglacial ice; simple accretion of meltwaters to the glacier may also occur in places. Some of this enriched subglacial ice is then drawn to the surface by the upwards flow associated with blue ice areas.

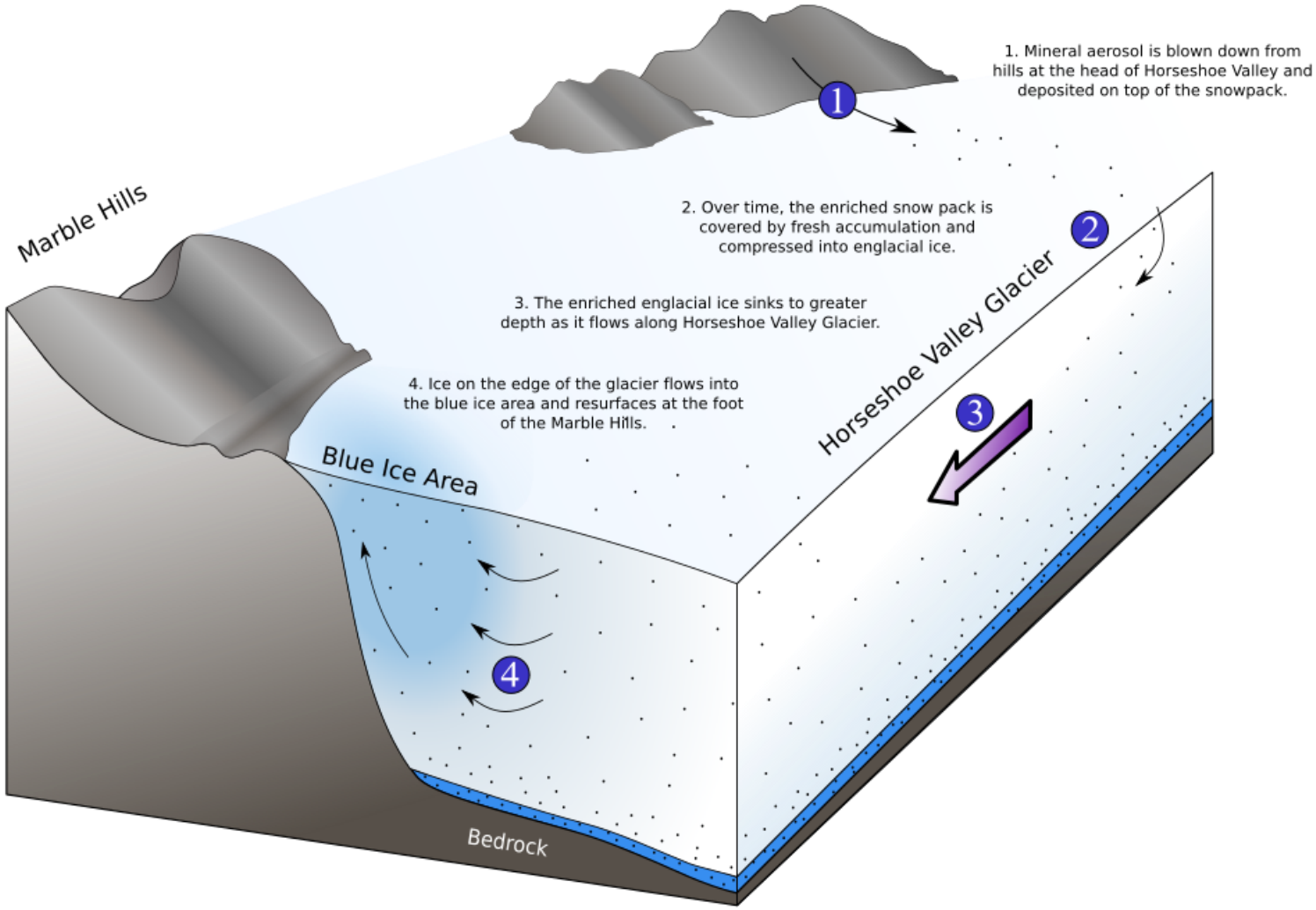

Figure 16 – Schematic for the acquisition of minerals) upstream of a BIA. In this (hypothetical) process, mineral ions are deposited in the snowpack at the head of Horseshoe Valley. This results in the delivery of enriched englacial ice directly to the Marble Hills BIA.

3.2.4 – Oxidation of sulphide

Sulphate ions are typically derived from two sources: atmospheric pollution or the oxidation of sulphide minerals. Given the remoteness of the sampling site, atmospheric inputs are expected to be minimal; this is supported by the low concentrations observed in regional firn (Table 12). In contrast, SO_4^{2-} is an order of magnitude more abundant within the TBIS. These ions cannot arise from erosion of the nunataks (Figure 16), as sulphur is only present in reduced forms (e.g. pyrite). However, at the subglacial bed, this sulphide can undergo a series of reversible reactions to form sulphuric acid. H_2SO_4 is a strong acid, and so tends to donate protons to other oxidised species – further weathering the bedrock and trapping SO_4^{2-} in its oxidised state. This therefore supports the subglacial acquisition hypothesis illustrated (Figure 15).

Table 12 – Comparison of sulphate concentrations in the Ellsworth region. Significantly higher values are observed in the TBIS, indicative of subglacial sulphide oxidation. Note that whilst the TBIS samples have a greater standard deviation, their *relative standard deviation* is actually lower than the other samples.

Dataset	n	SO_4^{2-} / μ eq. L^{-1}	σ / μ eq. L^{-1}	Source
Marble Hills TBIS	32	30.8	9.7	This thesis
Ellsworth Firn Core	8	2.2	1.2	This thesis
1990 ITAE*	7	0.8	0.5	Qin (1999), [177]

*Only including the seven closest samples to the Marble Hills BIA.

3.2.5 – Spatial distribution of ions

The TBIS data underwent multivariate analysis of covariance was used to compare relationships between ion concentrations, depth, distance downstream and proximity to the nunatak (Appendix 5). No significant spatial relationships were observed for the majority of the ions. However, there were significant results for Ca^{2+} ($p_y = 0.0186$, $p_z = 0.0005$, $p_{y*z} = 0.0084$), SO_4^{2-} ($p_z = 0.0173$, $p_{y*z} = 0.0488$) and Cl^- ($p_{y*z} = 0.0462$). The lack of any correlation with the x-axis (towards the foot of the nunataks) seems reasonable. The modelled direction of travel in other BIAs has a significant horizontal component along this axis (i.e. parallel with katabatic winds) [138]. Each sample likely constitutes a number of years of accumulation (due to low snowfall in the valley and extreme compression of annual layers). These multi-year samples are more likely to have a common mean than if annual resolution was available. Under the assumption that any multi-year trends will take place slowly, a block of the size used in this study will not be able to show any appreciable correlation in the direction of travel.

In contrast, the relationships with the y*z interaction (effectively a vector with y and z components) indicates that some flow path difference may introduce some systematic variation into the measured concentrations of Ca^{2+}, SO_4^{2-} and Cl^- . In the case of Cl^-, the lack of significant reaction with the y- or z-axes alone suggests that these axes have opposing effects on Cl^- concentration. These interactions will not however be explored further in this thesis: with such a small variation in x, y and z values, it is unlikely that the spatial distribution of ions within the original block could be upscaled across the whole BIA, let alone used to investigate the origin of TBIS.

3.3 – Dissolved organic carbon

3.3.1 – Representative values

The origin and history of a riverine or glacial sample often influences the concentration and/or properties of dissolved organic carbon (DOC) in the sample. Organic carbon may be incorporated into a glacier during its formation, as it overruns vegetation and soil. Alternatively, it may be fixed from inorganic carbon by microbial communities living within snowpack, supraglacial streams or cryoconite holes, or carried by the wind as biogenic aerosol. Recent work suggests that windblown marine sources are responsible for the majority of organic carbon found in snowpack around the Antarctic coast, although the trend drops off beyond 20 km [182]. Given that the Marble Hills BIA is located more than 50 km from the Filchner-Ronne Ice Shelf – and is much further from open ocean – it can be assumed that it does not receive the high concentrations of organic carbon associated with coastal areas.

Experimentally, DOC concentrations are usually assumed to be equivalent to the non-purgeable organic carbon (NPOC) in an aqueous sample. This is the carbon left in a sample that has undergone both filtration and sparging; importantly, it is also a measure of the bioavailable carbon in basal and supraglacial environments. At the time of writing, there have only been a limited number of studies measuring NPOC concentration on the Antarctic continent. None of these are in the vicinity of the Marble Hills; we can however use them as ball park figures for the DOC content in different types of Antarctic sample. Christner et al. (2006, [183]) analysed concentrations of DOC in accretion ice from the Vostok ice core – the only measurements of this kind – finding average values of 65 μmol L^{-1} and 35 μmol L^{-1} in Type I and II ice respectively. It is commonly accepted that the hydrological systems underneath the AIS are largely interconnected (e.g. [99]), and so it is reasonable to assume that accretion ice – formed by the freezing of subglacial meltwaters to the base of the ice sheets – will generally be the same order of magnitude across the continent. In fact, concentrations of subglacial DOC are arguably more likely to be consistent across the continent because most subglacial carbon is likely derived from prehistoric marine sediments and vegetation – both of which were previously widespread over the current continent. If the blue ice samples are indeed of subglacial origin then it seems likely that the water isotope signature is the result of meltwater freezing to the bottom of the ice sheet; we would therefore expect to observe a DOC concentration of the same order of magnitude as that of the Vostok accretion ice. In other words, DOC concentrations in the region of 15-85 μmol L^{-1} would support the subglacial origin hypothesis.

Legrand et al. (2013, [184]) conducted a study of organic carbon across several different sites in Antarctica, finding typical values for DOC in englacial ice ranging from 0.4 to 1.8 μmol L^{-1} (Table 13). Similarly low concentrations of DOC were found in surface snow. These samples were again taken from East Antarctica, so should not be treated as perfectly representative values for Horseshoe Valley. However, they do illustrate one important generalisation: the DOC content of snow and ice that has not interacted with the subglacial environment tends be an order of magnitude less than that which has been observed in accretion ice. This is consistent with studies conducted all over the cryosphere, which generally find little DOC in supraglacial samples, but much higher concentrations in basal ice and streams derived from subglacial meltwaters [30,

59]. Consequently, we can expect that if the Marble Hills blue ice samples have not been exposed to the subglacial environment, they will contain 0-8 µmol L^{-1} of DOC.

3.3.2 – Results of NPOC analysis

The DOC content of the blue ice samples was measured using a Shimadzu TOC-L CPH/CPN instrument (see section 2.5). These results are summarised in Table 13, along with comparable measurements from other Antarctic samples.

Table 13 – Mean concentrations of DOC measured in a variety of Antarctic samples. The value given for the Marble Hills BIA is after applying Tukey Fences (prior values: $\bar{x}$ = 398 ± 284 ppb, n = 36). Other values were taken from their corresponding papers and averaged or converted to ppb as required.

Location	Type	[DOC] / µmol L^{-1}	σ / µmol L^{-1}	n	Presented in
Marble Hills BIA	Terminal blue ice	23.7	6.0	30	This thesis
Vostok Station	Accretion ice I	65	-	18	Christner et al., 2006
Vostok Station	Accretion ice II	35	-	2	Christner et al., 2006
East Antarctica*	Englacial ice	0.7	0.5	61	Legrand et al., 2013
Concordia Station	Surface snow	1.8	-	2	Legrand et al., 2013

*Mean value of ice core samples from Vostok, Dome C, D-47 and Caroline stations.

The samples from the Marble Hills BIA contain slightly less DOC than the Vostok accretion ice, however the measurements are undoubtedly the same order of magnitude. The average concentration for englacial ice is, in comparison, less than thirty times that of the blue ice. This suggests that the blue ice may have interacted with the subglacial environment, which is consistent with the subglacial-acquisition hypothesis in Figure 15.

3.3.3 – Spatial distribution of DOC

Multivariate analysis of covariance was used to assess the distribution of DOC across the original block from which the TBIS were sectioned (Appendix 5). No significant spatial relationships were found.

3.4 – Discussion

3.4.1 – The origin of the ice

The glaciochemical analysis appears to paint a clear picture of the terminal blue ice samples (TBIS). The best explanation for the elevated concentrations of Ca^{2+}, SO_4^{2-} and DOC that were observed in each of the thirty-six samples – as well as the high concentrations of debris collected during filtration (often more than 2g per 500 ml sample) – is that the ice has previously undergone some kind of interaction with the subglacial environment. This is supported by the relationship between δ^2H and δ^{18}O, which has a slope of 5.6 – well below that which would be expected for meteoric ice. This slope is consistent with both the theoretical and the observed values for ice that has undergone pressure-induced regelation in the basal layer. This raises a novel hypothesis: that TBIS may contain traces of subglacial meltwater and sediment, acquired through some kind of subglacial regelation or accretion process. If this hypothesis proves to be true, then it would have enormous implications for the study of the Antarctic subglacial environment.

It should be noted that this subglacial process is likely distinct from Weertman regelation, as has been previously studied in small valley glaciers. In such glaciers, sufficient pressure to induce regelation is only achieved as the ice travels over small striations in the bedrock, which results in the formation of thin laminae of regelated ice [166]. In contrast, Antarctic basal ice is under much greater pressure, and travels relatively slowly along a much greater flow path. All of this could feasibly result in the formation of thicker layers of isotopically enriched ice. Unfortunately, it would be extremely difficult to investigate this with BIAs: even if this Antarctic regelation did impose a distinct substructure within the basal ice, this ice would surely have metamorphosed into a more continuous form by the time it had travelled to the surface. Indeed, this would potentially explain the appearance of the TBIS, which was fairly homogeneous, with no obvious substructure other than some sparse bands of fine debris and a surprising density of trapped air bubbles (Figure 6). Nevertheless, it is important to consider the possibility of alternative explanations for the chemical and physical properties of TBIS. To do so, we need to revisit what is known about flow in regions of blue ice.

The flow paths of a number of different BIAs have been modelled by glaciologists. Some regions, such as the Allan Hills BIA, are not believed to come in contact with the subglacial bed [138]. The oldest glacial ice in the Allan Hills is projected to sink down to within 200m of the bed, before flowing back up to the terminus of the blue ice area (Figure 17). In contrast, models of the Scharffenbergbotnen BIA indicate that a good deal of ice is dragged along the subglacial bed before resurfacing [138]. This ice is again the oldest and deepest, and subsequently resurfaces at the furthest end of the BIA. The main difference between these two cases is the topography of the underlying bedrock. In the Allan Hills, the bedrock is smooth, and never comes within 500m of the surface; the bedrock in the Scharffenbergbotnen BIA rises steeply up to within 50m of the surface, before dropping down and then rising again. This forces the flow of ice to interact with the subglacial bed in a way that is not intuitive for an open BIA such as at the Allan Hills. The situation at the foot of the Marble Hills, a closed BIA, is much more similar to that of the Scharffenbergbotnen BIA. In this case, flow into the area is perpendicular to Horseshoe Valley Glacier, forcing ice to flow towards steeply rising topography. Unlike at Scharffenbergbotnen, this topography actually breaks the surface, giving rise to the Marble Hills.

Given that the BIA terminus falls so close to the foot of the nunatak, the ice reaching the surface would have to have an extremely shallow path in order to not come in contact with the rising bedrock.

It is important to note that not all of the ice at the surface of the Scharffenbergbotnen BIA has interacted with the subglacial environment, only that which originated at the greatest depth. Likewise, it is expected that ice further from the terminus of the Mable Hills BIA should be englacial in character. This provides an opportunity to test the findings of the water isotope analysis: if the isotopic signature truly does arise from subglacial regelation, then it should only be present at the terminus. At present, there are no data available for samples taken at the Horseshoe Valley Glacier side of the Marble Hills BIA. Fortunately, data are available from Site Bit-58, a shallow ice core from the Allan Hills BIA analysed by Higgins et al. (2015, [185], supplementary information). As mentioned above, flow models for this BIA indicate that all of the blue ice found on the surface of this region should be englacial. It therefore makes an excellent control for our Marble Hills study.

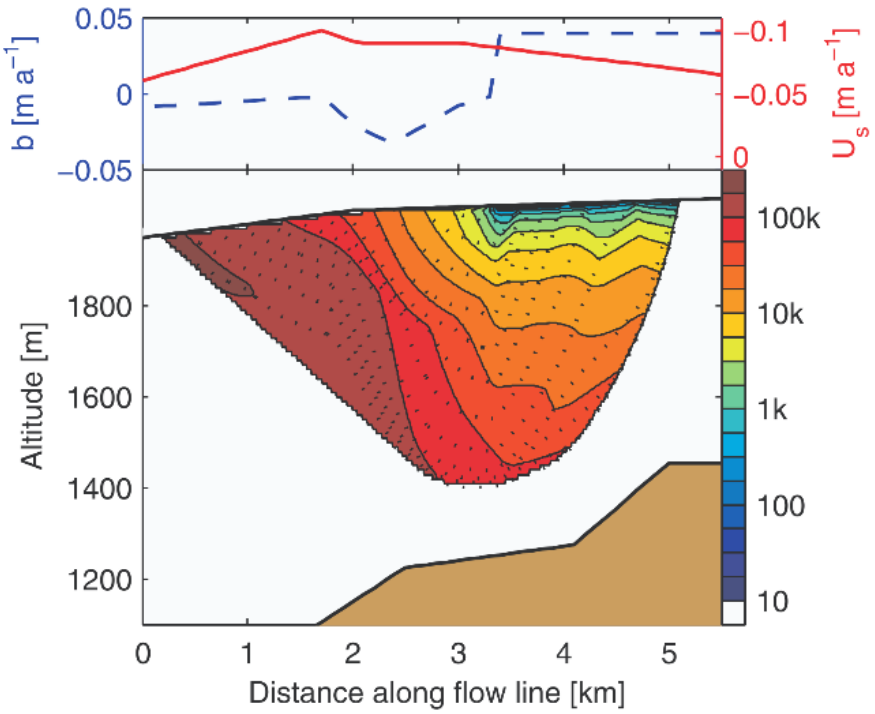

Figure 17 – Modelled flow of the Allan Hills BIA, reproduced from Grinsted et al., 2003 [138]. The upper section denotes surface mass balance (blue) and surface velocity (red). The lower section depicts ice of similar age along the BIA, illustrating a flow path that sinks towards the bed but never reaches the subglacial environment.

It might not be immediately apparent why this additional control is necessary. The δ^2H / δ^{18}O relationship in Equation 9 has already been compared with two LMWLs (Equations 7 and 8), so we can be confident that the ice is not meteoric: the findings have been validated. However, since this is the first time that the relationship between δ^2H and δ^{18}O has been used to indicate a subglacial origin in BIAs, we must use an additional control to validate the technique as well. Put another way, we need to consider that some hitherto unknown fractionation process occurs within BIAs. If samples from the Allan Hills BIA – or indeed any instance of englacial blue ice – are found to share the distinctive δ^2H / δ^{18}O relationship observed at the foot

of the Marble Hills, then this should call into question the regelation hypothesis. On the other hand, if ice from the Allan Hills BIA is found to be meteoric, then this would not only support the hypothesis that ice from the terminus of the Marble Hills BIA is subglacial in origin: it would also support the use of δ^2H / δ^{18}O slopes as evidence for regelation in other regions of blue ice.

Figure 18 displays a plot of δ^2H against δ^{18}O for the Bit-58 isotope data collected by Higgins et al. [185]. Parametric linear regression found a strong correlation between the two variables:

$$\delta 2H = 8.3973 \times \delta 18O - 8.6289 \text{ ‰} \qquad \text{Equation 14}$$

$$R^2 = 0.9656$$

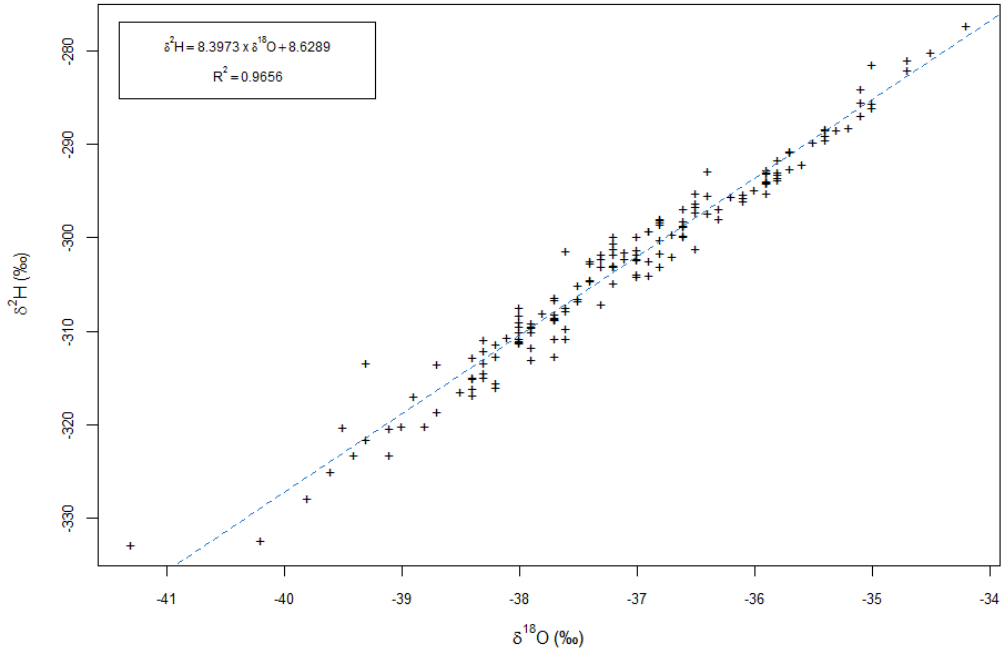

Figure 18 – Plot of δ^2H vs δ^{18}O for the BIT-58 ice core from the Allan Hills BIA. The original data were collected by Higgins et al. (2015) and presented as supplementary information [185]. Both variables passed the Shapiro-Wilks test for normality and so can be predicted with a parametric linear model.

A meteoric relationship is observed for the BIT-58 ice core (slope = 8.3973). Given the strength of the correlation the and size of the dataset (R^2 = 0.9656, n = 157), we can be confident that ice in the Allan Hills BIA has not experienced any significant fractionation since being formed from meteoric precipitation. In fact, the relationship is strikingly close to the Global Meteoric Water Line (Equation 6). There are only two differences between the Allan Hills BIA and the Marble Hills BIA: their locations (on opposite ends of the Trans-Antarctic Mountains) and their expected flow paths. If location were behind the differences between Equations 9 and 10, then this would have likewise affected the LMWLs for the Ellsworth firn core and the International Trans-Antarctic Expedition; we have already seen that this is not the case. Differences in flow path are therefore, at present, the only viable explanations for this variation in water isotope signature. When coupled with supporting evidence from ion chromatography and DOC analysis, it seems increasingly likely that ice at the terminus of the Marble Hills BIA has indeed been influenced by the subglacial environment.

3.4.2 – Subglacial processes

If we accept the evidence that the Marble Hills TBIS have undergone subglacial regelation, it is possible to identify the dominant processes taking place at the bed of Horseshoe Valley Glacier. In section 3.2, high levels of Ca^{2+}, SO_4^{2-} and alkalinity (most likely HCO_3^-) were observed. Given the Cambrian limestone bedrock underneath the BIA, the most probable source of these ions is the dissolution of calcite coupled with the oxidation of pyrite. This hypothesis is easily tested by plotting Ca^{2+} against SO_4^{2-} (Figure 19) and SO_4^{2-} against the S-ratio (Figure 20), which can indicate the stoichiometry of the dominant subglacial processes.

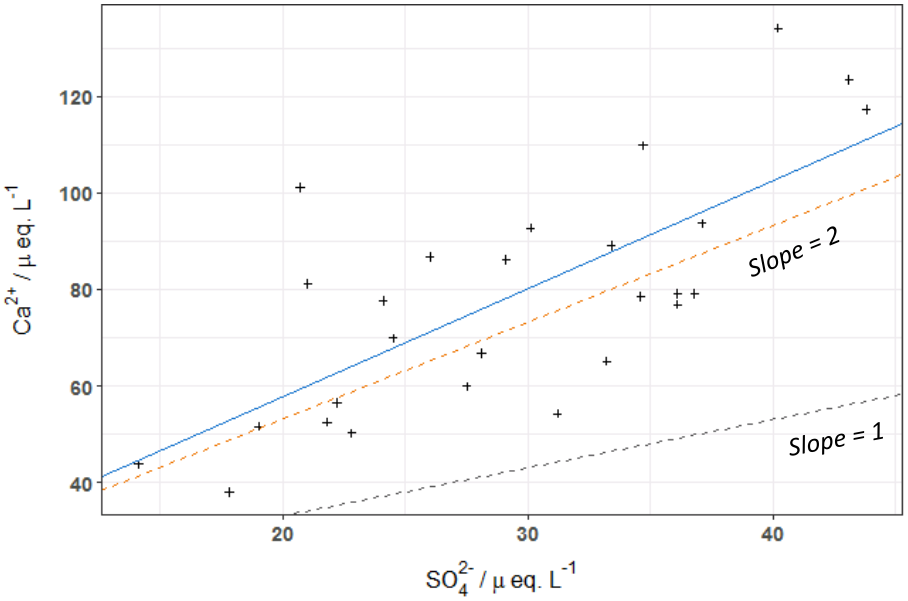

Figure 19 – Plot of Ca^{2+} against SO_4^{2-} for the Marble Hills TBIS. These data have a slope of 2.2 – slightly above the stoichiometry of coupled calcite dissolution and pyrite oxidation.

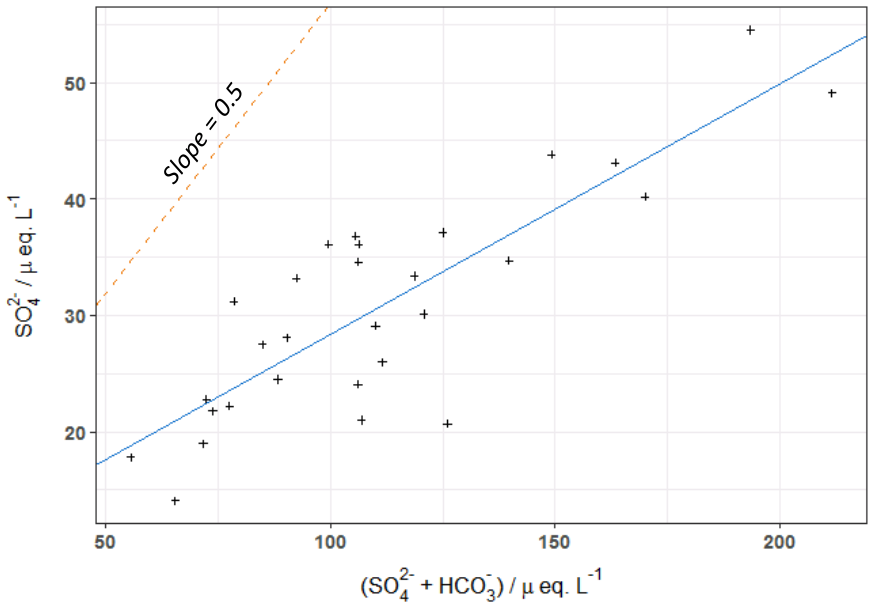

Figure 20 – Plot of the S-ratio for the Marble Hills TBIS. The data have a slope of 0.22, which suggests that additional $CaCO_3$ dissolution takes place in addition to the pyrite-coupled reaction.

The simplified equation for coupled calcite dissolution and pyrite oxidation is as follows:

$$4FeS_2 + 16CaCO_3 + 15O_2 + 14H_2O \rightarrow 16Ca^{2+} + 16HCO_3^- + 8SO_4^{2-} + 4Fe(OH)_3$$

Equation 15

The stoichiometry indicates that the expected Ca^{2+}/SO_4^{2-} ratio is 2 for this process. In comparison, the release of Ca^{2+} and SO_4^{2-} via the dissolution of gypsum would correspond with a slope of 1. The actual slope observed in Figure 19 is 2.2, supporting the hypothesis that coupled calcite dissolution and pyrite oxidation are the dominant chemical processes underneath Horseshoe Valley Glacier. The slightly greater slope suggests the existence of additional processes that release Ca^{2+} but no SO_4^{2-}; this is also observable in the S-ratio, which has a slope (0.22) slightly below the theoretical (0.33). Given that the Ca^{2+} to alkalinity ratio is 1:1 (Figure 13), this process is probably calcite dissolution coupled with a different redox reaction.

Whilst this chapter has focused mostly on the origin of the TBIS, there is the potential for later analyses to further pinpoint dominant biogeochemical processes under the ice. Firstly, a surprising mass of debris was collected during filtration of the samples; this has been retained and frozen in a sterile manner. Future analyses of sediment-bound nutrients (e.g. colloidal iron) may give further insight into the chemical weathering of the bedrock and the subsequent nutrient inputs into the SO. Furthermore, the samples were observed to contain a great number of small air bubbles. TBIS from the nearby Patriot Hills have been saved for the chromatographic measurement of trapped gases: this can be used to constrain our understanding of subglacial conditions (e.g. level of anoxia) and may also capture metabolic by-products for respiring cells.

3.4.3 – Summary

In this chapter, we have discussed the first glaciochemical investigation of terminal blue ice from a closed BIA. The overwhelming results of the findings present a new hypothesis: that ice from BIAs may have undergone regelation at the bed of the ice sheet. This process would likely compromise the very oldest ice in such areas for paleoclimatic investigations; it would also open up the potential to study the chemical and the biological conditions of the subglacial environment. At present, it is unclear as to the extent to which such TBIS could be used to investigate the Antarctic bed. However, given the distribution and number of potential samples sites across the continent, there is promise that TBIS could provide biogeochemical data for many of the hydrological systems under the ice. Consequently, further work is required to identify additional regions of blue ice with similar properties to those of the Marble Hills BIA.

Chapter 4 – What can we learn from calved Patagonian icebergs?

Steffen Glacier is the southernmost outlet glacier of the North Patagonian Icefield (NPI), and one of the longest. Like the majority of Patagonian glaciers, Steffen is a calving glacier; it emerges from the Andes and terminates in Lago Steffen, an elongated lagoon around 5 km long and 2 km wide. Water from Lago Steffen feeds the Rio Huemules, which flows into the Baker–Pascua Estuary via Steffen Fjord before draining into the Pacific Ocean at the southern side of the Gulf of Penas (Figure 21).

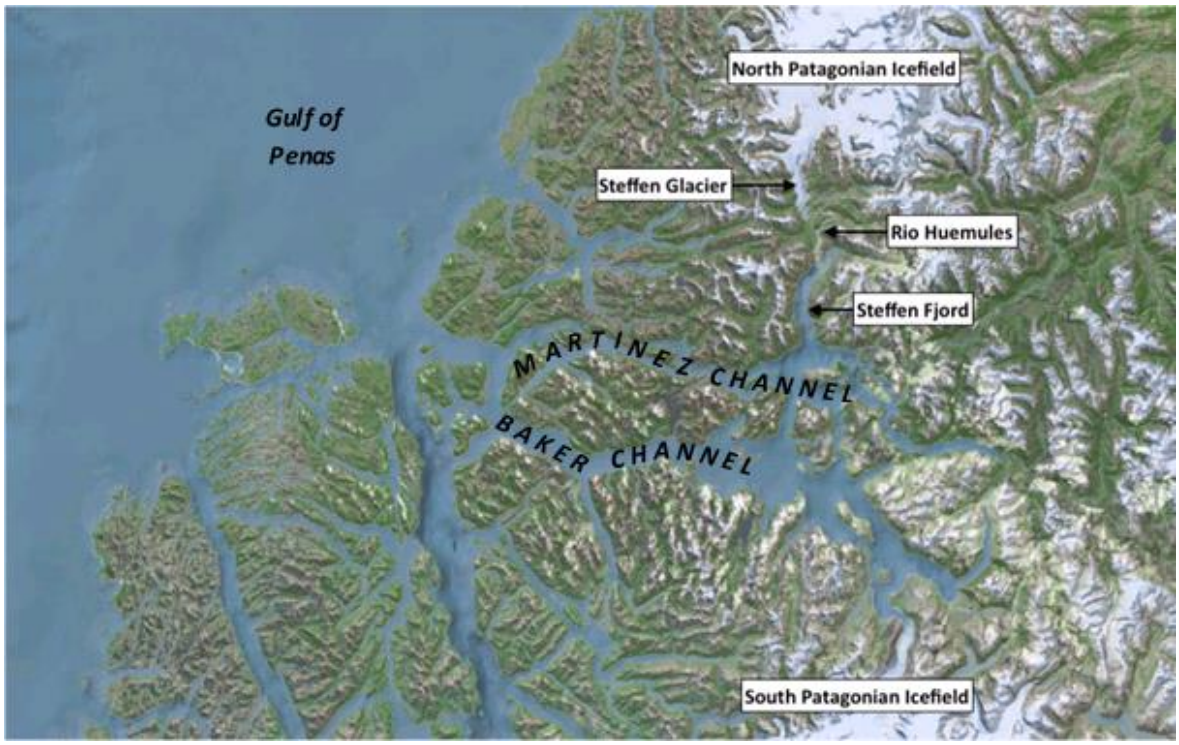

Figure 21 – ArcGIS map of the Baker-Martinez fjord complex. Includes raster data sourced from Esri, USGS, NASA, Google and the GIS User community.

The Rio Huemules is believed to be a significant source of glacial nutrients and contaminants to the fjord ecosystem. However, due to its situation within the Wet Andes, Steffen Glacier is extremely difficult to directly sample on foot. Extreme topography inhibits approach from the west, north and east; thick vegetation dominates the lower hills to the south east (and indeed all low-lying ground in the region). Approach by lake is practically impossible, as calved ice dams Lago Steffen near its midpoint. This inaccessibility means that direct analysis of glacial composition is not a realistic goal for most research expeditions, which in turn hinders any investigation into the impact of melt from Steffen Glacier on water quality in the Rio Huemules and the Baker-Martinez fjord complex.

This chapter explores the use of iceberg sampling as an alternative to collecting ice directly from inaccessible glaciers, with particular focus on the impact of Steffen Glacier on river chemistry. To do this, it presents glaciochemical data from icebergs in Lago Steffen. These data are then used to predict the composition of ice on the mother glacier and how this may affect the Rio Huemules. Finally, this glacial input is contrasted with data from the non-glacial Rio Quince, a humic river that runs from a non-glaciated valley

southwest of Lago Steffen and joins the Rio Huemules around 2 km from Steffen fjord. In the conclusion, it is discussed whether or not these iceberg samples have a place in the modern research environment in instances where direct sampling is impractical.

4.1 – Dissolved organic carbon

Dissolved organic carbon (DOC) accumulates within mountain glaciers through two main processes: by dry or wet deposition and *in situ* carbon fixation. Deposition can be sourced either from terrestrial sources (e.g. vegetation overridden by glacial advance) or anthropogenic sources (e.g. incomplete combustion of fossil fuels), while biological carbon-fixation is driven by autotrophic microbial activity (RuBisCO-producing cells) found above and underneath the ice. Due to the typical flow path of alpine glaciers (Figure 2), ice arriving at the glacial terminus will be of varied ages and depths. The majority of samples in this study are likely to consist of englacial ice, simply because that is the largest component of a glacial cross-section (rotation of icebergs may expose a small number of subglacial samples, which may appear chemically distinct from the others). Given that the englacial zone consists of compressed firn from the glacial surface, sources of organic matter to the supraglacial environment are likely to also affect the concentration of DOC in englacial ice. In contrast, subglacial activities are unlikely to have much bearing on the DOC content of the englacial ice above. Consequently, the most important sources of DOC in iceberg samples are likely to be those which affect the surface: atmospheric deposition, local wind blow of plant matter and metabolism within cryoconite holes.

DOC in Patagonian icebergs was isolated through sequential removal of the inorganic fraction (via sparging), followed by oxidation. Evolved $CO2_{(g)}$ was then measured via infrared spectroscopy (Shimadzu TOC-L CPH/CPN) to give a mean DOC concentration of 6.9 ± 2.6 μmol L^{-1}. The spread of DOC concentrations was variable both between icebergs and between samples from the same iceberg (Figure 22). The results are discussed in section 4.5.

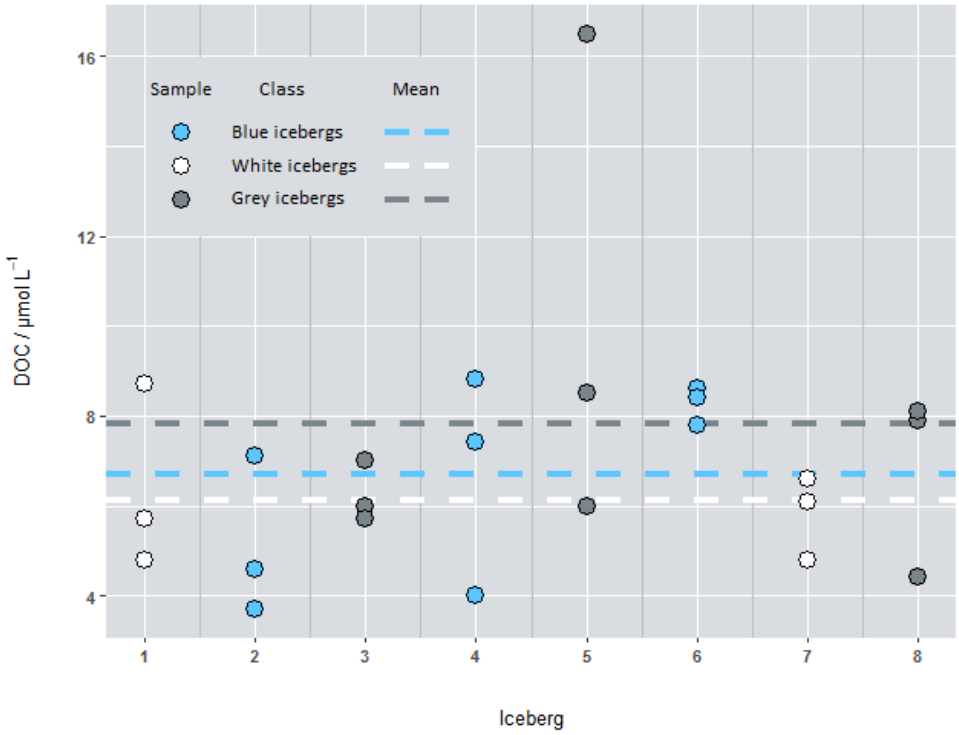

Figure 22 – Observed DOC content in Lago Steffen calved icebergs. Values presented include the arithmetic means of icebergs that were categorised as "White", "Grey" or "Blue".

4.2 – Major ions

Concentrations of Na^+, K^+, Mg^{2+}, Ca^{2+}, NH_4^+, F^-, Cl^-, NO_2^-, SO_4^{2-}, NO_3^- and PO_4^{3-} were determined by ion chromatography (Dionex ICS-5000). Table 14 presents the results of these analyses in units of micro-equivalents per litre (µ eq. L^{-1}). These are compared with the compositions of local freshwater (Table 15).

Table 14 – Measurements of major ions within calved icebergs from Lago Steffen . Values presented include the arithmetic means of icebergs that were categorised as "White" (n=6), "Grey" (n=9) or "Blue" (n=9). Alkalinity is calculated as the sum total of all major cations minus all major anions. The low Cl–/Na+ ratio is indicative of limited marine aerosol influence, Cl– loss from snowpack, or preferential exclusion of Cl– during ice formation.

Class	Concentration / µ eq. L^{-1}											
	Na^+	NH_4^+	K^+	Mg^2	Ca^{2+}	F^-	Cl^-	SO_4^{2-}	PO_4^{3-}	NO_x	Alk	Cl^-/Na^+
W	10.9	*	1.1	*	1.1	1.1	0.5	0.4	*	*	11.0	0.05
G	10.8	*	1.3	*	1.5	*	0.7	1.2	*	*	11.8	0.07
B	17.3	1.1	1.6	*	*	2.3	0.5	0.6	*	*	16.6	0.03
All	13.2	0.9	1.4	*	1.1	1.5	0.6	0.8	*	*	13.7	0.04

*Detectable, but below the Limit of Quantification.

Table 15 – Comparison of major ions within freshwater bodies local to Steffen Glacier. Measurements for precipitation, the Rio Quince, the glacial tributary and the Rio Huemules reproduced courtesy of Hawkings et al. (currently unpublished data). Alkalinity is again calculated as the sum total of all major cations minus all major anions. Note that the precipitation samples appeared to belong to two distinct groups based upon the concentration of Cl^- (presumably depending on the wind direction). However, there were too few samples available to verify this statistically, so only the mean has been presented. * Detectable, but below the Limit of Quantification. ** Restricted to sampling on the same day as those for Sites B and C.

Sample	Source	Concentration / μ eq. L^{-1}								
		Na^+	K^+	Mg^2	Ca^{2+}	F^-	Cl^-	SO_4^{2-}	Alk.	Cl^-/Na^+
Icebergs	Glacial	13.2	1.4	*	1.1	1.5	0.6	0.8	13.7	0.05
Precipitation	Non-glacial	14.5	1.5	5.5	8.4	*	19.8	4.0	6.0	1.37
R. Quince	Non-glacial	35.7	7.4	16.5	63.9	2.6	32.8	10.1	78.0	0.92
Tributary	Semi-glacial	19.8	7.1	16.5	104.5	3.2	15.5	13.9	115.4	0.78
R. Huemules	Semi-glacial									
Site A **		20.4	7.0	11.4	44.1	1.6	15.0	10.4	55.9	0.74
Site B		20.5	7.0	10.9	48.7	1.8	15.0	10.4	59.8	0.73
Site C		28.4	8.1	17.2	72.0	2.1	18.4	11.4	93.8	0.65
LOQ		1.3	0.5	1.3	0.9	1.0	0.3	0.1	-	-

The results of the ion chromatography analysis of iceberg samples are comparable with firn and snow samples taken from elsewhere in Patagonia [186], the Andes [187] and the Alps [188].

4.2.1 – Post-depositional processes

The ratio between chloride and sodium ions in Steffen icebergs is extremely low: only 0.05, as opposed to a bulk seawater value of 1.16. Although this is an unusual finding, these data do not appear to be anomalous. For one, similar low Cl^-/Na^+ ratios have previously been observed in Tyndall Glacier and the central Southern Patagonian Icefield (SPI) [186, 189]. Moreover, none of the other samples or blanks measured at the same time as the iceberg samples gave unexpected results. This suggests that there is either a major source of non-sea salt sodium to the NPI, significant removal of marine chloride from precipitation/firn/ice, or some combination of the two. Observations of local precipitation can narrow down the possibilities:

1. The Cl^-/Na^+ ratio of local precipitation is significantly different to that of the ice (and close to the bulk seawater value). This suggests that any chloride loss / sodium enrichment is taking place after precipitation: ruling out processes such as the loss of $HCl_{(g)}$ from marine aerosol.

2. The iceberg samples are not enriched in crustal species (e.g. Na^+, K^+, Mg^{2+}, Ca^{2+}) relative to precipitation, which indicates that the low Cl^-/Na^+ ratio of englacial ice is not due to the deposition of terrestrial dust (adding Na^+ to the firn).
3. The measured concentration of Cl^- ions in precipitation is nearly five times greater than that of the iceberg samples, consistent with the post-depositional loss of Cl^-.

Two post-depositional processes are known to reduce the chloride concentration of the glacial surface. The first possibility is the loss of major ions through elution. This would occur if the surface of the snowpack melted and drained vertically down through hydrological channels in the ice, eventually reaching the water table and being lost from the icefield. Ions in snow tend to be located on the outer surfaces of snow grains and thus, are lost preferentially during snowpack melt. Meltwater can therefore remove nutrients from surface firn as it passes through. Previously, elution within a Norwegian ice cap has been shown to reduce the concentration of major ions within the englacial zone by an order of magnitude relative to precipitation [190]. This would also explain the low concentrations of SO_4^{2-} and Ca^{2+}, which tend to be very sensitive to elution. Most studies of the elution sequence find that elution of chloride is less efficient than that of sodium (e.g. [191, 192]), which could not explain a low Cl^-/Na^+ ratio. Nevertheless, this explanation was given by two previous studies of Cl^-/Na^+ ratios in Patagonian ice [186, 189], so there is some support for the notion that chloride is preferentially eluted over sodium in the region – perhaps because in such a remote region, there is a scarcity of the more mobile anions (SO_4^{2-} and NO_3^-), which are emitted by large human settlements.

The second possible process, dechlorination, involves the loss of hydrogen chloride gas via the reaction:

$$Cl^-_{(s)} + H^+_{(s)} \rightarrow HCl_{(g)}$$

wherein the chloride ions are provided by an ionic lattice (usually $NaCl_{(s)}$) and the protons are derived from inorganic acids (H_2SO_4 or HNO_3). This is a process that has been observed in many Antarctic ice cores but – to the best of my knowledge – has not yet been discussed in the context of temperate glaciers. If dechlorination is indeed happening within the NPI, then it seems likely that it is also the cause of the low Cl^-/Na^+ ratio of englacial ice in the Southern Patagonian Icefield.

It is important to note that the rationale above relies upon one crucial assumption: that the precipitation collected during the 2017 fieldwork season was representative of the precipitation from which the icebergs were formed. This may not be the case. For one, the NPI is the remnant of the Patagonian Ice Sheet that existed during the last glacial period (~ 115,000 – 11,700 y.a.) – meaning that the ice in Steffen Glacier could conceivably be thousands of years old. If local weather systems have changed in that time, then the Cl^-/Na^+ ratio of modern precipitation may not be representative of that which now forms the modern-day glacier.

In addition to this, the available precipitation samples were collected intermittently over a fifty-day period. This may not be representative of the contemporary annual precipitation around the NPI, as the abundances of tropospheric aerosols (which are trapped in precipitation) are known to have seasonal variation [193]. This seasonal pattern is often preserved well enough that fluctuations in ion concentrations

have been used to date ice cores both in Patagonia and worldwide (e.g. [194, 195]). It is therefore probable that the precipitation samples in 4.2 contain higher concentrations of ions from terrestrial sources (such as Ca^{2+}) than was present in the annual precipitation over the NPI, even before any elution took place.

Lastly, the difference in altitude between snowfall on the NPI and rain around Lago Steffen may affect its chemical composition. Nonetheless, the low Cl^{-}/Na^{+} ratio is a very interesting observation, and one which demonstrates the idea that iceberg samples could play an important role in pilot studies: as a low-cost approach to narrowing down which glaciers/nutrients are worth including in a larger investigation.

4.2.3 – K^{+}/Na^{+} ratio of iceberg samples

The K^{+}/Na^{+} ratio was 0.11. This is significantly higher than that of bulk seawater (0.023), and is of the same order of magnitude as the high K^{+}/Na^{+} ratio observed by Aristarain & Delmas (1993) in the nearby SPI [186]. There is no community consensus on whether more K^{+} or Na^{+} will be removed by elution, with different studies finding that K^{+} ions are more [191], less [196], or approximately as [192] mobile as Na^{+}. Considering this lack of agreement, it is unlikely that the difference in mobilities within the snowpack is significant enough to drive a fivefold change in the K^{+}/Na^{+} ratio. Given that precipitation at Site A has a similar ratio (0.10), it seems likely that there is a large amount of K^{+}-rich dust in the region, which is a major source of cloud-condensation nuclei (hence elevating K^{+} concentration in both rain and ice). However, unless the effect of elution is reliably assessed, it is impossible to make any such conclusions with certainty.

4.2.4 – Downstream variation in ionic composition

One potential use of calved icebergs is as a means for monitoring glacial input into river and fjord systems. Whilst water isotopes are a more reliable tracer of glacial input, any significant impact on biological activity is likely to arise from the contribution of bioavailable nutrients such as potassium, phosphorous and nitrate. The concentrations of major ions were therefore also measured at three downstream sites on the Rio Huemules, as well as in a nearby non-glacial river (the Rio Quince). This was designed to give context to the observations of major ions in Steffen Glacier.

Every single measured ion – to varying extents – was found to be more abundant in the non-glacial river than they were in either glacial ice or in precipitation. Calcium and carbonate (indicated by alkalinity) were particularly enriched in non-glacial freshwater. This is because most water entering the Rio Quince has undergone prolonged water-rock interactions since falling as precipitation, picking up nutrients from the beds of streams or from within aquifers. This is also why the composition of the Rio Huemules changes as it acquires nutrient-rich water. As the Rio Huemules travels further from Lago Steffen and the NPI, the majority of freshwater inputs to the river arise from rocky mountain streams or from subterranean drainage; this is consistent with the water isotope analyses in section 4.3.2, which indicate that the relative non-glacial input into the Rio Huemules increases with distance downstream. These sources of non-glacial freshwater are more enriched than the Rio Huemules, and lead to a gradual increase in the concentration of major ions. The impact of glacial input into the Rio Huemules is discussed further in section 4.5.

4.3 – Water isotope analysis

The δ^2H, δ^{18}O and δ^{17}O values of iceberg samples were determined by off-axis integrated cavity output spectroscopy (Los Gatos Research T-LWIA 45-EP). These delta values are presented in Table 16. If these data are representative of the whole calving front, then a number of inferences can be made about the isotopic composition of Steffen Glacier and the NPI.

Table 16 – Stable isotopes of water in samples of icebergs from Lago Steffen, Chile. Three samples were taken from each of the eight icebergs, which were loosely classified as "White", "Blue" or "Grey" according to their physical appearance and density.

	Delta values / ‰					
	δ^2H		**δ^{18}O**		**δ^{17}O**	
SG1	-95.7	±0.2	-13.1	±0.2	-7.00	±0.06
SG2	-86.2	±0.2	-12.0	±0.2	-6.30	±0.05
SG3	-79.70	±0.02	-11.30	±0.01	-5.99	±0.05
SG4	-96.7	±0.2	-13.33	±0.05	-7.08	±0.04
SG5	-96.3	±0.3	-13.2	±0.1	-7.0	±0.1
SG6	-99.8	±0.2	-13.89	±0.03	-7.2	±0.1
SG7	-94.6	±0.2	-13.32	±0.03	-6.9	±0.1
SG8	-94.9	±0.2	-13.2	±0.1	-6.90	±0.09
SG9	-90.4	±0.1	-12.62	±0.04	-6.61	±0.07
SG10	-94.4	±0.1	-13.34	±0.02	-6.93	±0.05
SG11	-111.7	±0.3	-15.16	±0.05	-7.88	±0.05
SG12	-88.4	±0.1	-12.35	±0.06	-6.50	±0.05
SG13	-82.40	±0.09	-11.3	±0.1	-5.96	±0.07
SG14	-71.17	±0.05	-9.77	±0.04	-4.99	±0.03
SG15	-72.9	±0.2	-9.95	±0.2	-5.22	±0.03
SG16	-91.54	±0.09	-13.1	±0.2	-6.842	±0.007
SG17	-108.92	±0.05	-15.0	±0.2	-7.96	±0.01
SG18	-103.4	±0.1	-14.5	±0.1	-7.57	±0.03
SG19	-103.69	±0.06	-14.44	±0.06	-7.57	±0.05
SG20	-101.30	±0.07	-14.099	±0.003	-7.39	±0.06
SG21	-106.66	±0.03	-14.76	±0.04	-7.70	±0.03
SG22	-91.1	±0.2	-12.7	±0.1	-6.70	±0.05
SG23	-88.1	±0.2	-12.3	±0.1	-6.42	±0.02
SG24	-85.72	±0.06	-12.0	±0.1	-6.24	±0.05
Blue	-99	±8	-14	±1	-7.2	±0.5
White	-96	±20	-13	±3	-7	±1
Grey	-86	±9	-12	±1	-6.2	±0.7
Total	**-93**	**±13**	**-13**	**±2**	**-6.8**	**±0.9**

4.3.1 – Are the calved icebergs composed of meteoric ice?

As in the last chapter, the relationship between δ^2H and $\delta^{18}O$ can indicate the history of water molecules in the iceberg samples. These variables are plotted against each other in Figure 23. The two datasets are normally distributed (see Appendix 6) and an ordinary least squares linear regression finds the following relationship:

$$\delta^2H = 7.226 \times \delta^{18}O - 0.424 \text{ ‰} \qquad \text{Equation 16}$$

$$R^2 = 0.9873$$

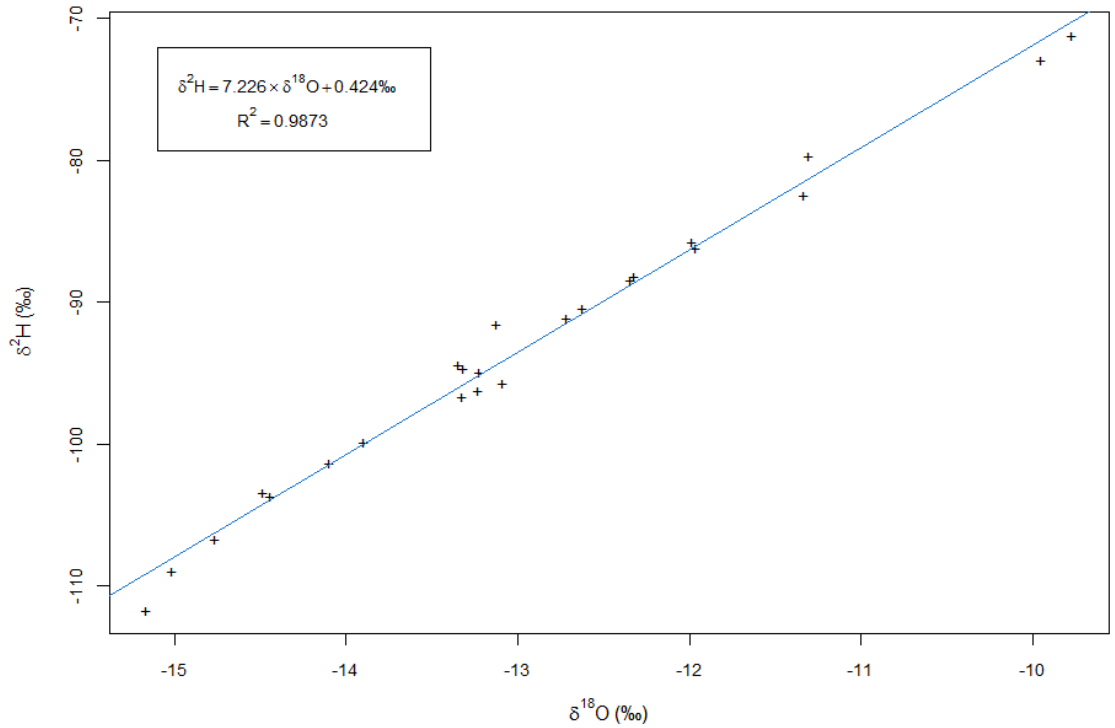

Figure 23 – Scatter plot of the δ^2H and $\delta^{18}O$ values observed in icebergs from Lago Steffen, Chilean Patagonia. The trend (blue) was calculated via ordinary least squares linear regression.

The relationship in Figure 23 is slightly (but significantly) distinct from the GMWL. However – unlike in the Marble Hills TBIS – there is no obvious regelation signature. So what process is responsible for this isotopic signature? The simplest explanation is that the relationship represents the LMWL: an isotopic fingerprint shared by all meteoric water within a locality. LMWLs often differ slightly from the GMWL because of local variation in the fractionation of water across the world's oceans. Nevertheless, it should be noted that very few LMWL in the existing literature have a gradient of less than 7.9. In order to establish whether or not local atmospheric processes are sufficient to create this peculiar relationship, the iceberg data can be compared with local meteoric water from the Rio Quince, a nearby non-glacial river. A plot of δ^2H vs $\delta^{18}O$ for these data is displayed in Figure 24. Ordinary least squares linear regression finds the following relationship for the Rio Quince:

$$\delta^2H = 8.0009 \times \delta^{18}O - 9.8032 \text{ ‰} \qquad \text{Equation 17}$$

$$R^2 = 0.9236$$

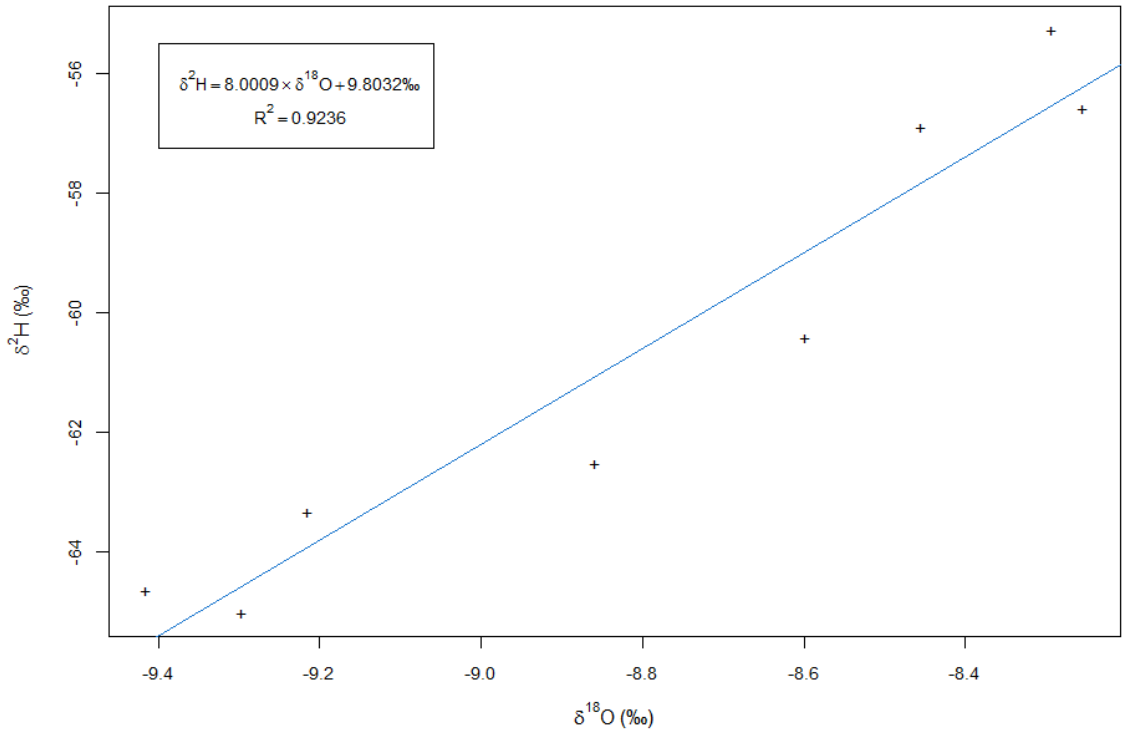

Figure 24 – Scatter plot of the δ^2H and δ^{18}O values observed in the Rio Quince, a non-glacial river in Chilean Patagonia. The trend (blue) was calculated via ordinary least squares linear regression.

Equation 4.2 almost exactly matches the GMWL. It is therefore likely that the LMWL in the region around the Rio Huemules is consistent with the GMWL, which in turn suggests that Equation 4.1 does not arise as from the natural variation within meteoric water, but is caused by a further fractionation process that occurs after precipitation.

It is also unlikely that subglacial regelation is responsible for Steffen Glacier's isotopic fingerprint. It *is* conceivable that a small subset of the samples were taken from regelated basal ice, exposed by the rotation of icebergs in Lago Steffen. Regelated ice is usually associated with a typical range of δ^2H vs δ^{18}O gradients between 4.5 and 6.9 [166]: this would cause the relationship in Figure 23 to lie somewhere in between the δ^2H–δ^{18}O lines of the (meteoric) englacial samples and the (regelated) subglacial samples. However, such a weighted average would have a sizeable spread of data points on either side of the line of best fit. This is not observed: the data fit the line extremely well (R^2 = 0.9873). Consequently, it seems likely that the additional fractionation process affects all of the ice more-or-less equally.

The most likely process behind the relationship in equation 4.1 is partial sublimation of firn from the glacier surface. Heavier isotopes of water sublimate less readily than common $H_2{}^{16}O$, causing meteoric firn to become slightly enriched in terms of heavy isotopes. This means that partial sublimation can cause the δD vs δ^{18}O gradient of snow and firn to fall significantly below the GMWL [197]. Given that glacial ice is formed when firn is compressed by the weight of fresh accumulation, the isotopic signature of supraglacial firn can be preserved within the englacial zone – and is therefore observed in calved icebergs. There are few field observations of these phenomenon in englacial ice, however fractionation of the surface via partial

sublimation is not a new idea. Grabczak et al. (1983) observed a similar relationship in Broggi Glacier (Peruvian Andes), which they attributed to the same process [198]:

$$\delta^2H = (7.3 \pm 0.2) \times \delta^{18}O + (1 \pm 3)\ ‰ \qquad \text{Equation 18}$$

The similarity between equations 4.1 and 4.3 is consistent with the high humidity levels (a major factor controlling the rate of sublimation) reported for both regions.

4.3.2 – Spatial variation in glacial input

Table 17 – Mean values of δ^2H, $\delta^{18}O$ and $\delta^{17}O$ in water bodies local to Steffen Glacier during the austral summer of 2017. The "# Samples" column indicates the number of discrete samples of water/ice were collected from each location across the summer, while the "# Injections" column indicates the total number of measured injections (Los Gatos T-LWIA 45-EP) make up each average. The uncertainty given is the standard deviation of all injections from any single source, which was chosen to take into account both experimental error and temporal fluctuations in true value.

Sample	Source	δ^2H / ‰	$\delta^{18}O$ / ‰	$\delta^{17}O$ / ‰	# Samples	# Injections
Icebergs	Glacial	-93 ±13	-13 ±2	-6.8 ±0.9	24	407
Tributary	Semi-glacial	-83.1 ±0.9	-11.4 ±0.2	-6.08 ±0.09	14	120
Lago Steffen	Semi-glacial	-82.5 ±0.5	-11.7 ±0.1	-6.14 ±0.04	6	39
R. Quince	Non-glacial	-61 ±4	-8.8 ±0.4	-4.7 ±0.2	16	135
R. Huemules	Semi-glacial					
Site A		-83.0 ±0.6	-11.8 ±0.3	-6.2 ±0.5	53	825
Site B		-83.1 ±0.3	-11.77 ±0.10	-6.20 ±0.05	7	123
Site C		-81.8 ±0.7	-11.5 ±0.2	-6.06 ±0.07	8	136

Given the differences in water isotope signature observed between icebergs and the Rio Quince, it should be possible to use a simple two-component model to follow the changing magnitude of glacial input along the length of the Rio Huemules, in which the end members are the mean glacial and non-glacial inputs (icebergs and Rio Quince, respectively). Table 17 displays the values of δ^2H, $\delta^{18}O$ and $\delta^{17}O$ for a number of locations between the NPI and Steffen fjord. The primary headwaters of the Rio Huemules begin at Lago Steffen; however these are soon joined by a tributary river from Laguna Los Huemules. Both of these lakes are subject to glacial influence from the ice field to the north: measurements of stable isotopes indicate that water in Lago Steffen and the small glacial tributary are far more depleted in terms of heavy isotopes than the Rio Quince. Conversely, they are still less depleted than the average iceberg from Steffen Glacier, suggesting groundwater/stream sources in addition to glacial melt.

It is worth noting that although subglacial meltwater may have a different water isotope signature to that of englacial ice, the iceberg samples should be approximately representative of the long-term glacial inputs into the Rio Huemules. This is because the removal of heavier isotopes from meltwater occurs with a

corresponding enrichment of basal ice [166]. As both of these ultimately feed into Lago Steffen, their overall contribution towards the water isotope signature of the Rio Huemules is that of their common ancestor: englacial ice.

The data for the glacial tributary, Lago Steffen and the Rio Huemules all lie at intermediate values between the glacial and non-glacial sources. The position at which they lie – slightly closer to the glacial end-member – indicates that the magnitude of the glacial input is slightly stronger than that from non-glacial sources. Assuming that:

1. The Rio Quince can constitute the end-member for local non-glacial freshwater;
2. The mean delta value of Lago Steffen icebergs constitutes a representative glacial end-member;

then we should be able to estimate the relative size of the glacial input into the freshwater systems downstream of Steffen Glacier. This simplistic model may have a useful application in the remote monitoring of glacial flux. A change in the isotopic signature of the Rio Huemules could be driven by a change in the flux of non-glacial or glacial water into the system, or a shift in the end-members. Provided that the average isotopic composition of glacial inputs remains relatively stable, then regular monitoring of the water isotope signature of the two rivers (Huemules and Quince) should give an estimate of the percentage of the glacial component of meltwater at a downstream sampling site on the Rio Huemules. Combined with flux measurements from the same site, this could be used to monitor glacial flux – and therefore the rate of glacial melt – from a remote downstream location. Given that these monitoring sites are more accessible than Steffen Glacier, this opens the possibility of identifying seasonal and annual trends in glacial melt through a simple monitoring network with high temporal resolution.

The mathematical principle behind this theory is quite straightforward. A given isotopic ratio in any of these locations is the weighted average of the isotopic ratios of the glacial and non-glacial sources:

$$R_{SAM} = \frac{xR_{GLA} + yR_{NON}}{x + y} \qquad \text{Equation 19}$$

where x and y are the relative magnitudes of the glacial and non-glacial inputs, respectively. In Appendix 7, this is combined with the two simultaneous equations:

$$x + y = 1 \qquad \text{Equation 20}$$

$$R = \left(\frac{\delta}{1000} + 1\right) \times R_{STD} \qquad \text{Equation 21}$$

to show that:

$$x = \frac{\delta_{SAM} - \delta_{NON}}{\delta_{GLA} - \delta_{NON}} \qquad \text{Equation 22}$$

and

$$y = \frac{\delta_{SAM} - \delta_{GLA}}{\delta_{NON} - \delta_{GLA}} \qquad \text{Equation 23}$$

These two equations were used to estimate the glacial and non-glacial contributions to different freshwater sites across the sampling period (Table 18). The different sets of ratios calculated from the δ^2H,

$\delta^{18}O$ and $\delta^{17}O$ data vary by as much as ±0.03 either side of the average. Given that there is no consistent trend in these deviations – none of the isotopes are consistently predicting the highest or lowest glacial input – it can be assumed that the differences arise from temporal fluctuations and experimental uncertainty. Temporal fluctuations are particularly likely to affect the results of this analysis: if this method is repeated to include all fifty-three samples taken from Site A – as opposed to those which correspond with sampling at the other sites along the Rio Huemules – then the estimated glacial input falls from 74.3% to just 70.9%. This is because water isotope composition varies on both a daily and an hourly basis.

The proportion of glacial input to the Rio Huemules at Site A is almost three-quarters; this falls significantly at Sites B and C, which are situated further downstream. This is consistent with the increasing concentrations in Ca^{2+} and alkalinity (potentially carbonate ions) observed in section 4.2. The impact of glacially-derived species will therefore be more pronounced in biological communities in the upper Rio Huemules. Note that this does not mean that any climate-induced changes in glacial discharge will be limited to the upper river: upstream changes in the chemistry and ecology of the Rio Huemules are likely to have cascading effects downstream [31]. Once the average annual glacial and non-glacial water isotope signatures have been determined, this simple model could be used to monitor glacial discharge from Steffen Glacier from a more easily accessible downstream site. If combined with reliable research into the biology and chemistry of the Rio Huemules / Steffen fjord, this would enable researchers and national organisations to predict regional water quality and ecosystem change.

Table 18 – Estimated glacial/non-glacial input into freshwater local to Steffen Glacier: Lago Steffen, the Rio Huemules, and the Huemules glacial tributary (which is largely influenced by Laguna Los Huemules). Estimates were calculated by substituting the delta values from Table 17 into equations 4.10a and 4.10b, based on the assumption that a) the Steffen icebergs were representative of a purely glacial source (δ_{GLA}) and b) the Rio Quince is representative of a purely non-glacial source (δ_{NON}). Note that this means that the ratios calculated for these two sources are 1:0 and 0:1 by definition.

Sample	**Source**	**Estimated ratios of glacial : non-glacial inputs**			**Glacial input**	**Non-glacial input**
		(from δ^2H)	**(from $\delta^{18}O$)**	**(from $\delta^{17}O$)**		
Icebergs	Glacial	1 : 0	1 : 0	1 : 0	100 %	0 %
R. Quince	Non-glacial	0 : 1	0 : 1	0 : 1	0 %	100 %
Tributary	Semi-glacial	0.692 : 0.308	0.630 : 0.370	0.665 : 0.335	66.2 %	33.8 %
Lago Steffen	Semi-glacial	0.673 : 0.327	0.705 : 0.295	0.693 : 0.307	69.0 %	31.0 %
R. Huemules	Semi-glacial					
Site A *		0.690 : 0.310	0.745 : 0.255	0.794 : 0.206	74.3 %	25.7 %
Site B		0.691 : 0.309	0.717 : 0.283	0.724 : 0.276	71.1 %	28.9 %
Site C		0.652 : 0.348	0.651 : 0.349	0.657 : 0.343	65.4 %	34.6 %

**Restricted to samples taken on the same day as those for Site B and C.*

4.4 – Heterogeneity of icebergs

Glacial ice is not homogenous. Longitudinal streaks and differently coloured areas of ice can be observed in virtually any photograph of an alpine glacier. This variation in physical appearance is due to the different flow paths that ice can take along the glacier. For instance, some of the older/deeper ice may undergo a greater level of compression as it travels along the glacier, while ice flowing along the lateral and basal edges is more likely to acquire sediment from weathered rock. As well as affecting the physical characteristics, these different flow paths are likely to have some bearing on the chemical composition of ice arriving at the terminus of a glacier. It follows that the icebergs formed at the calving front of a lake-terminating glacier will also have differing physical and chemical characteristics. Consequently, one of the biggest challenges in iceberg sampling was how to get a representative picture of the glacier without needing to collect an impractically large number of samples.

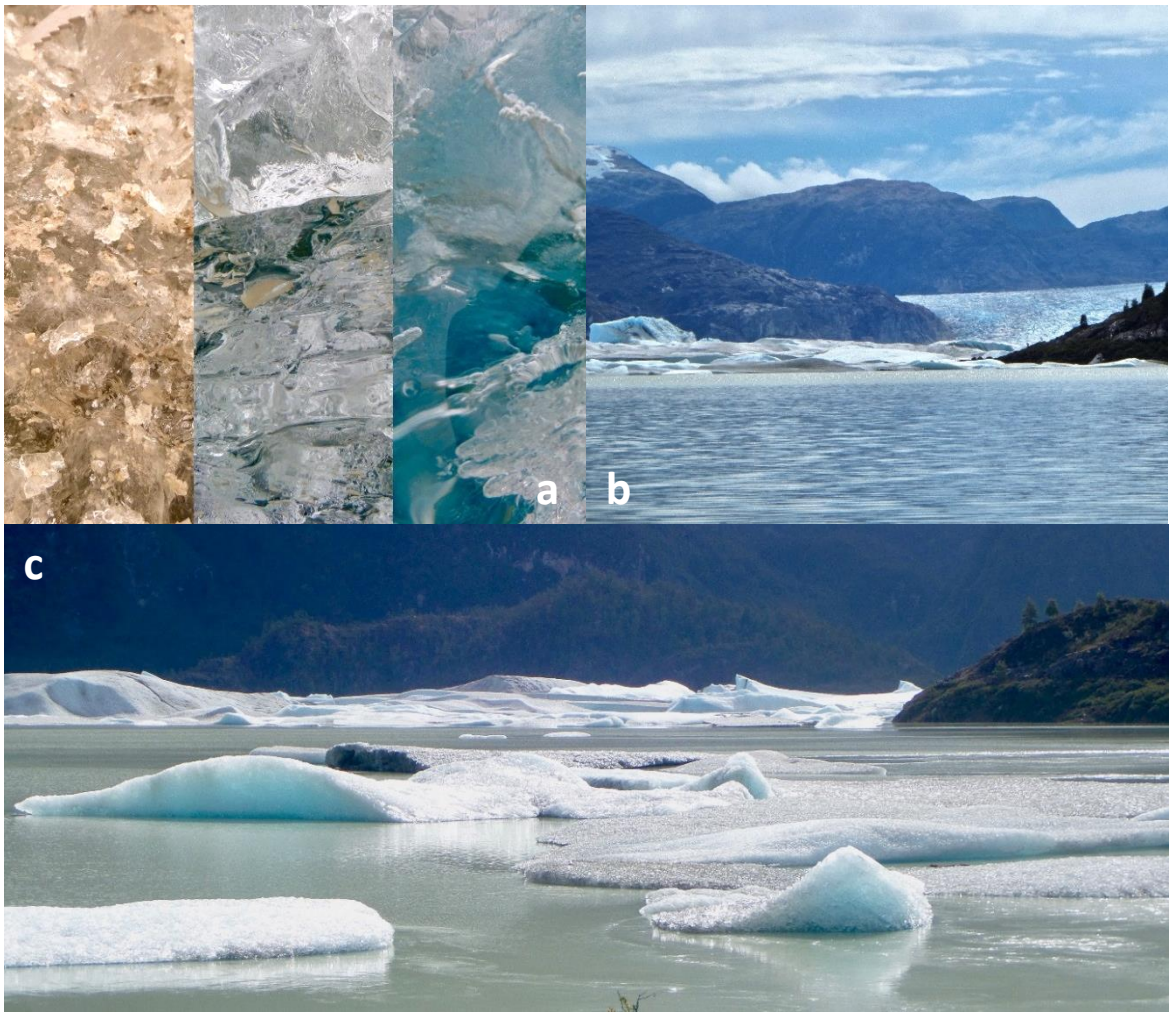

Figure 25 – Images of icebergs in Lago Steffen (handheld Samsung WB200F camera, February 2017); a) side-by-side comparison of grey, white and blue icebergs (left-right); b) photograph from the southern end of Lago Steffen depicting Steffen Glacier (middle right), the mountains and vegetation that inhibit approach via land, and the bottleneck in the middle of Lago Steffen where accumulated icebergs hinder approach by water; c) photograph of the southern end of Lago Steffen, from where nine blue, nine grey and six white iceberg samples were collected.

In order to simplify this problem, the icebergs present in Lago Steffen were loosely classified as either "white", "blue" or "grey" (Figure 25). The purpose of these classes was to examine whether or not icebergs with particular physical characteristics corresponded with certain chemical differences. If icebergs can be subdivided into distinct classes for which the average chemical composition can be consistently calculated, then the average of these different classes of ice – weighted according to the relative abundance of each type of ice at the calving front – should give a more reliable estimate of the average glacial contribution than a simplistic random sampling exercise.

For instance, if 40% of the icebergs that calve from a particular glacier happen to be blue – and blue icebergs are associated with more depleted delta values for δ^{2}H, δ^{18}O and δ^{17}O – then the sampling protocol should ensure that 40% of the samples are from blue icebergs. Alternatively, researchers could calculate representative values for blue icebergs, and then weight their estimate of average glacial composition so that 40% of the input is based on the composition of blue icebergs. Ideally, the relative abundance of each classification of iceberg should be calculated from aerial images of the calving front, as might be easily achieved with drone technology. However, for the small pilot study carried out in this chapter, the frequencies of each iceberg type were estimated from the icebergs present in the (accessible) southern end of Lago Steffen, 3 km downstream from Lago Steffen. The approximate ratio of white, blue and grey ice in this region was 2:3:3.

4.4.1 – Suspended debris

The most obvious sign of heterogeneity when sampling icebergs was the variable size and abundance of sediment deposits dispersed throughout the icebergs. Predictably, the six greatest quantities of debris were observed within the grey iceberg population (Figure 26). However, the concentration of sediment could be surprisingly variable between different samples within the same iceberg. Note also that iceberg 8 (grey) contained relatively little sediment, comparable with that of icebergs 1 (white) and 4 (blue).

As the data are not normally distributed, the Kruskal-Wallace test was used to evaluate whether or not the aggregated data arises from the same distribution (see Appendix 6). This null hypothesis was rejected (χ^2 = 21.294, df = 7, p = 0.003358), and so a post-hoc Dunn test was employed to make pairwise comparisons between the three groups. This analysis found that sediment observations in grey icebergs were stochastically dominant over both the blue and white groups ($p_{Grey\text{-}Blue}$ = 0.0001; $p_{Grey\text{-}White}$ = 0.0093). Conversely, no significant difference was found for the white-blue pairing ($p_{White\text{-}Blue}$ = 0.1851).

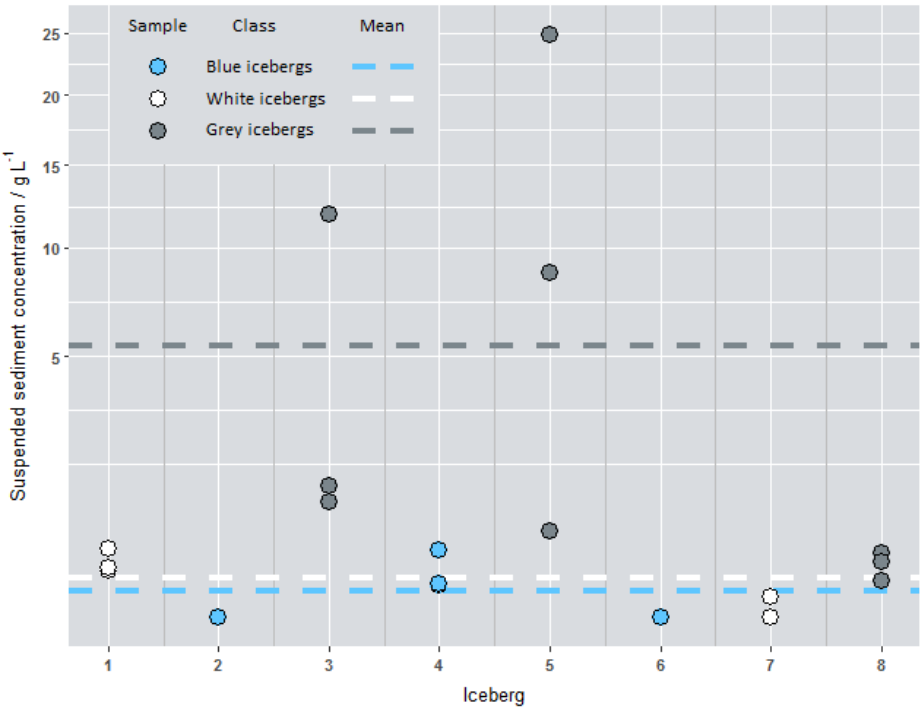

Figure 26 – Scatterplot of debris in Lago Steffen icebergs. Note that the y-axis has been plotted on the square root scale in order to increase the visibility of samples with less than 1 g L^{-1} of sediment.

4.4.2 – Water isotopes

The data in Table 16 indicate that calved icebergs are quite variable in terms of isotopic composition. This is evident in the high standard deviation that arises when all icebergs are treated as a single sample; the coefficient of variation (or Relative Standard Deviation, RSD) is respectively 13.5%, 13.5% and 13.2% for δ^2H, δ^{18}O and δ^{17}O. While the RSD is lower when the blue and grey iceberg classes are considered separately (generally in the region of 7-10%), it is higher for the white iceberg class. Theoretically, this may suggest that further subdivision of this class may be possible. However, as the smallest population, a higher RSD would be expected for the white icebergs if all else were equal. Further sampling of white icebergs should therefore be conducted to ascertain whether or not the RSD remains above 10%.

One-way ANOVA was used to compare the population means (Appendix 6). This analysis found that for each isotope, the null hypothesis was rejected (p (δ^2H) = 0.0133; p (δ^{18}O) = 0.0115; p (δ^{17}O) = 0.00854); this indicates that the iceberg samples do indeed belong to populations with different means. In all three cases, Tukey's HSD found that the grey and blue icebergs belonged to significantly different populations (p (δ^2H) = 0.0120023; p (δ^{18}O) = 0.0103262; p (δ^{17}O) = 0.0082437), whereas the blue-white and grey-white pairings did not differ significantly from each other. These results are illustrated in Figure 27. The contrast between the two most common classes of iceberg in Lago Steffen – blue and grey – indicates that classification of icebergs is a worthwhile practice for the estimation of glacial composition via iceberg sampling.

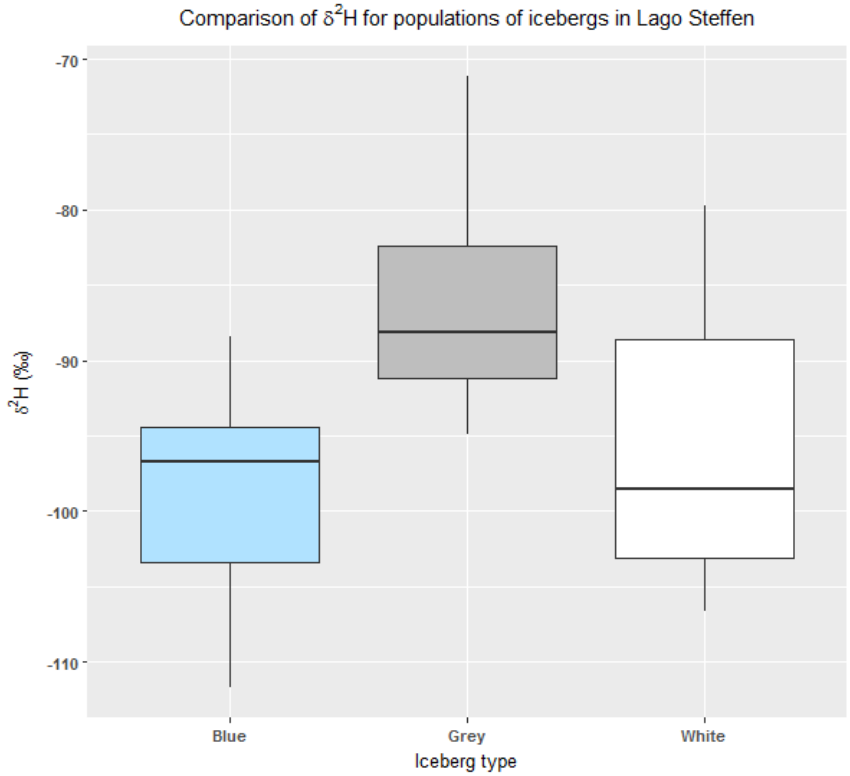

Figure 27 – Boxplots of the δ^2H values observed in blue, grey and white icebergs. Post-hoc application of Tukey's HSD reveals that the blue and grey populations are significantly different. Similar plots for the δ^{18}O and δ^{17}O data are available in Appendix 6.

4.4.3 – Dissolved Organic Carbon

Figure 28 juxtaposes boxplots for the measurement of DOC in blue, grey and white icebergs. Unlike the water isotope analyses, there is a significant amount of overlap between all three populations. The Kruskal-Wallis test confirms this assessment ($p = 0.3768$, see Appendix 6). These findings indicate that the concentration of DOC within terminal ice is *not* dependent on the path taken down the glacier. This suggests that the majority of DOC observed originated on the surface of the NPI (or the Steffen Glacier accumulation zone) – and was then compressed into englacial ice – rather than being picked up from the base and sides of the glacier itself.

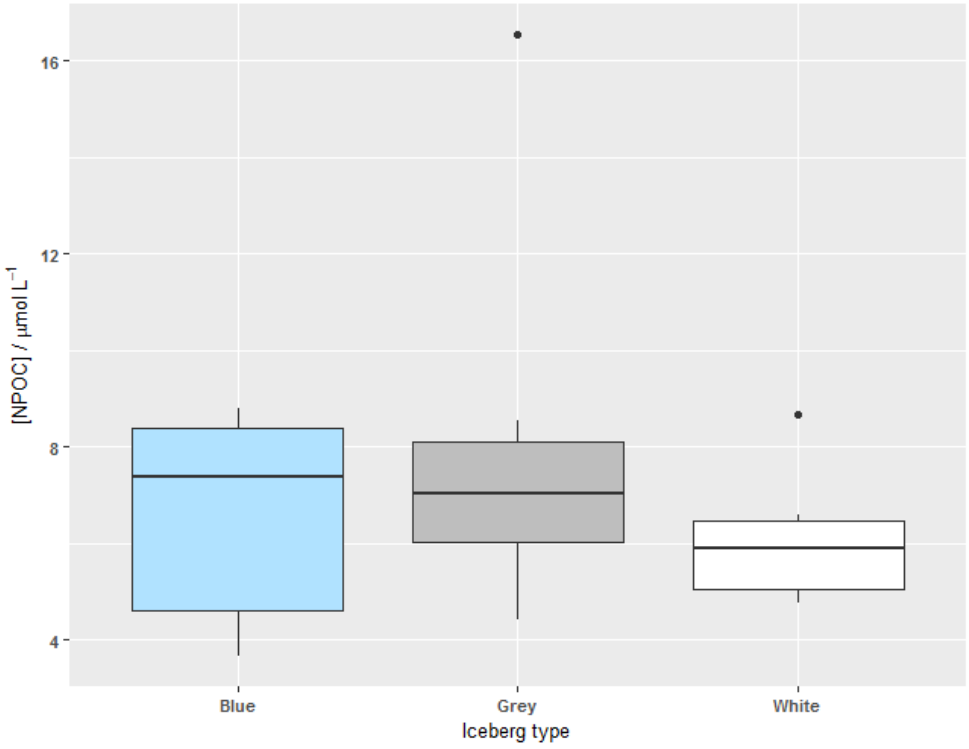

Figure 28 – Boxplots of the DOC concentrations observed in blue, grey and white icebergs. One-way ANOVA confirms that these populations are not significantly different from each other.

4.4.4 – Major ions

As with DOC, no significant relationship was found between the classification of icebergs and the concentration of any dissolved ion (see Appendix 6). Again, this indicates that the distribution of dissolved ions throughout the englacial region is independent of the flow path, and therefore has likely remained consistent since the compression of supraglacial firn into glacial ice.

4.5 – Discussion

4.5.1 – What can we learn about Steffen Glacier from calved iceberg samples?

The glaciochemical analysis of icebergs in Lago Steffen paint a fairly logical picture of the glacier, including a couple of post-depositional processes that have not previously been documented in the NPI. In some cases, these processes limit what we can learn about the history of the ice.

Source of organic matter

Given that the observed DOC concentrations were similar for all colours of ice, it is conceivable that the major source of organic matter is derived from supraglacial sources which are trapped underneath precipitation. Macroscopic leaf debris was observed in some melted iceberg samples, which indicates a ready supply of reduced carbon that may be broken down by primary consumers.

Figure 29 – Photograph of organic matter suspended in a melted iceberg sample. Taken on a handheld Samsung WB200F camera (February 2017, NPI).

Conversely, the relatively low DOC content suggests that this is a less significant process than has been found on the surface of glaciers in the Northern Hemisphere. This would not be surprising: soluble nitrate concentrations were below the limit of quantification, which would likely restrict cell proliferation within the supraglacial and englacial environments. Furthermore, the steep topography constraining ice within the NPI and Steffen Glacier (as opposed to the relatively flat Greenland Ice Sheet) reduces the period for which direct sunlight can reach photosynthesising cells, and may limit the formation of cryoconite holes. Advanced techniques such as spectrofluorescence microscopy may be able to shed more light on the source of the DOC, and whether or not the most soluble fractions have been removed by elution.

Post-depositional processes

The unusual $\delta^{2}H$-$\delta^{18}O$ slope is consistent with slow sublimation of snow and firn from the surface of the NPI under conditions of high relative humidity. Whilst significant sublimation has been known to concentrate ions within ice, the major ion content of Steffen Glacier is very low. This is likely due to elution of ions in surface melt during the summer months, removing species that are less soluble in snowpack than they are in water. As a result, the main supply of glacial nutrients to the Rio Huemules is likely to be in the form of suspended sediments, which are less bioavailable than dissolved ions, but are also less susceptible to leaching.

Anthropogenic inputs

Ordinarily, the low concentrations of DOC, SO_4^{2-} and NO_x species observed in the Steffen icebergs would indicate that there is very little long-range transport of anthropogenic material to the ice. This would be consistent with the extreme remoteness of the NPI. However, post-depositional processes may have altered the composition of the ice, making it an unreliable record of air-ice inputs. For instance, the mean concentration of SO_4^{2-} observed in precipitation was five times greater (4.0 μ eq. L^{-1}) than that which was observed in icebergs samples (0.8 μ eq. L^{-1}). Given that the ice calving into Lago Steffen is likely thousands of years old, this difference in SO_4^{2-} concentration could be due to differences in atmospheric composition or local weather systems. However, the SO_4^{2-} ion is once again known to be susceptible to elution, so unless the concentration of the original precipitation can be reverse-engineered, the analysis of aerosols from Steffen Glacier can only be of limited utility for research.

Deposition of terrestrial dust

Previous studies have shown that Mg^{2+} is relatively unaffected by elution within temperate glaciers [193]. Consistently low measurements of Mg^{2+} in the iceberg samples indicates that there is little deposition of terrestrial dust onto the glacier *relative to the precipitation rate*. Note that the measurable concentration of terrestrial dust will be diluted if precipitation is very high, even if a large volume of dust is deposited onto the NPI each year. Escobar et al. (1992, [199]) estimated that the NPI receives around 6000-7000 mm of precipitation per year – approximately thirty to forty times higher than the Antarctic Ice Sheets, for which estimates of average annual precipitation (1989-2009) range between 164-224 mm per year [200].

Taking this into account, we can infer that the deposition of terrestrial dust onto the NPI is actually significantly greater than was observed in the Ellsworth Firn Core (previous chapter). The concentration of Mg^{2+} in both of these environments was below the LOQ. However, given that the measurements were also above the LOD, we can infer that they are of the same order of magnitude: Mg^{2+} is presumably somewhere within the range of 0.21-1.93 μ eq. L^{-1} in the Ellsworth Firn Core, compared with 0.72-1.27 μ eq. L^{-1} in the Steffen icebergs. Similarly, the concentration of Ca^{2+} (a more abundant crustal ion) in the firn core was only ten times greater than that of the Steffen englacial ice, which is a lot closer than would be expected when taking into account both precipitation rate (up to forty times higher over the NPI) and the removal of Ca^{2+} ions by elution.

4.5.2 – What can we learn about the downstream effects of glacial input?

The water isotope signature of Steffen Glacier is distinct from that of local non-glacial rivers, which enables the estimation of glacial input at any downstream location. Glacial input predictably decreases at downstream sites, and is inversely correlated with the concentration of major ions. Figure 30 shows the relationship between $\delta^{18}O$ (a proxy for glacial input) and the total concentration of major ions studied in the Rio Huemules river system. The almost-perfect exponential relationship arises because sites with less glacial influence (i.e. less dilution of nutrients) tend to receive water that has travelled further along/under the ground, and so are more enriched in terms of major ions than if meltwater and precipitation were mixed in the same ratio. Furthermore, the gradual chemical denudation of glacially-derived sediments may lead to a delayed release of dissolved ions at downstream locations. Put simply, the total concentration of major ions is a function of both the proportion of glacial input at that point, and the level of water-rock interactions (either with streambeds, aquifers or suspended sediment) prior to sampling.

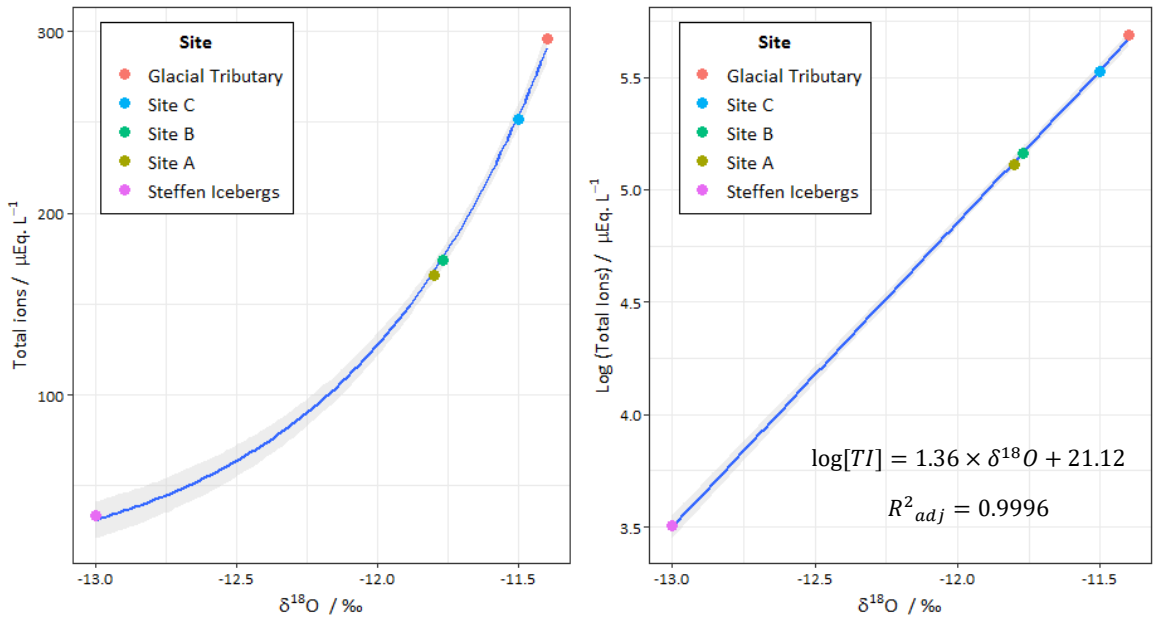

Figure 30 – Plot of total ion concentration vs $\delta^{18}O$ in the Rio Huemules river system. In descending order of glacial influence (L-R), these are: Lago Steffen icebergs, Site A, Site B, Site C, and the glacially-influenced tributary from Laguna Los Huemules. Water in Sites A-C picks up additional ions from the river bed and increasingly nutrient-rich non-glacial inputs as it travels downstream. The glacial tributary, whilst upstream of the other sites, is fed partially by non-glacial streams from the mountains to the south, and acquires nutrients from the lake/river beds before it reaches Lago Steffen. This demonstrates the net diluting effect that the glacial input has on dissolved ions within the Rio Huemules. Note that the total ion concentration is largely dominated by Ca^{2+} and alkalinity – both of which tend to have crustal sources.

Obviously, englacial ice (as represented by calved icebergs) is only one way through which Steffen Glacier influences the Rio Huemules. In particular, subglacial meltwater will be flowing underneath the glacier and into Lago Steffen; this water will presumably contain a greater concentration of dissolved ions than the icebergs. However, it appears that this input is not great enough to significantly increase the concentration of major ions in Lago Steffen: the dissolved ion content of the glacial tributary (sampled before merging with

water from Lago Steffen) is in fact slightly higher than that which was observed a couple of kilometres downstream at Site C. This indicates that flow from Lago Steffen dilutes the glacial tributary, reducing the concentration of dissolved species available to downstream ecosystems. Therefore, even if subglacial meltwater is nutrient-rich, there was insufficient quantity in the 2017 austral summer to for the overall glacial input to the Rio Huemules to match the solute-rich non-glacial inputs.

Note that there are two important exceptions to this rule: Na^+ and Cl^-, the primary sea spray aerosols. Both of these species are slightly *less* abundant in the glacial tributary than they are at Site A, and continue to increase in concentration at Sites B and C. This increase from Sites A-C means that there are still sources of freshwater that are richer in terms of Na^+ and Cl^- than Lago Steffen. Conversely, water from Lago Steffen does not dilute water from the tributary, as seen with other nutrients. This apparent lack of relationship between the magnitude of glacial input and the concentration of sea spray aerosols suggests that there is another factor controlling the concentrations of Na^+ and Cl^-. For example, if altitude affects the distribution of sea spray ions in precipitation, then high-altitude precipitation (feeding both Steffen Glacier and Laguna Los Huemules) would be responsible for the marginally lower Na^+ and Cl^- concentrations in Lago Steffen and the glacially tributary, whereas low-altitude precipitation (which feeds the non-glacial inputs downstream of Lago Steffen) would be responsible for the downstream increase in concentrations.

Lastly, dissolved ions are not the only medium through which Steffen Glacier might enrich or dilute the downstream freshwater system. Due to the high ratio of physical to chemical weathering in glaciated terrain, a significant proportion of the glacially-derived nutrients released into the Rio Huemules may be in the form of fine mineral sediment, rather than soluble ions. These particles may contain sparingly-soluble species such as nanoparticulate iron and sediment-bound phosphorus, which are believed to be sufficiently bioavailable to have a significant impact on biological activity. Moreover, sediment-bound nutrients may undergo chemical denudation once in the river, resulting in a delayed release of glacially-derived nutrients further downstream (contributing to the elevated concentrations at Sites A-C). Previous studies have shown that these partially-soluble nutrients can control primary productivity by delivering rate-limiting nutrients to aquatic systems as ice-rafted debris or suspended sediment [39, 201].

The concentration of debris between (and within) icebergs was extremely variable, with masses of dry sediment ranging from < 0.01 g L^{-1} to almost 25 g L^{-1}. Unsurprisingly, the grey icebergs were by far the most sediment rich, carrying a mean sediment load of 5.43 g L^{-1} – as opposed to 0.12 g L^{-1} and 0.05 g L^{-1} in white and blue icebergs, respectively. Assuming that this is a representative sample, and that the estimated 3:3:2 ratio of grey : blue : white icebergs (Section 4.4) holds for the entire calving front, then the mean concentration of suspended sediment released from melting icebergs along the Rio Huemules is approximately 2 g L^{-1}. In comparison, the mean concentration of suspended sediment observed at Site A over the 2017 austral summer was only 0.09 g L^{-1}, while the winter mean was just 0.06 g L^{-1} (Hawkings et al., unpublished data). Of course, the translation from debris to suspended sediment in the Rio Huemules will not be exact, as some sediment will drop out to the bed. Nonetheless, the fact that the concentration of suspended sediment in Rio Huemules is greatest in the summer – coinciding with the peak melt season for Steffen Glacier – supports the hypothesis that Steffen Glacier is responsible for a significant sediment input

into the river system. Samples of filtered sediment from this investigation have been frozen and retained for future analysis of sediment-bound nutrients (Fe, N, P, Si). This sediment dimension is expected to add value to the study of calved icebergs, however is beyond the scope of this thesis.

Conclusion

Both investigations of easily-accessible deep ice have yielded provocative results. In Chapter 3, the water isotope signature of TBIS was found to be consistent with subglacial regelation; the presence of high concentrations of DOC, calcium carbonate and oxidised sulphate in the samples strongly supports the hypothesis that this ice has been in contact with the subglacial bed. In Chapter 4, the glaciochemical analysis of iceberg samples allowed us to infer two post-depositional processes taking place on the surface of Steffen Glacier/the NPI (sublimation and elution). It was also observed that the concentration of dissolved nutrients in englacial ice was generally low, however the sediment contribution to the Rio Huemules was significant – especially in grey icebergs. Lastly, the clear distinction between water isotope signatures of icebergs and a nearby non-glacial river enabled the construction of a two-component model for glacial input into the Rio Huemules.

These findings illustrate the promising ways in which alternative ice sampling can be used to study glacial environments when direct access is restricted. However, is this enough to endorse terminal blue ice and iceberg sampling as *de facto* modes of investigation that have utility in the wider research context? In order for either of these approaches to be adopted for further research, they must satisfy the following two criteria:

1. The data obtained must be useful;
2. There must be a number of viable sample sites, distributed over several regions of interest.

These points will be considered first for Antarctic TBIS, and then for Patagonian icebergs.

5.1 – Terminal Blue Ice Samples

5.1.1 – Usefulness of data

It may seem strange to ask whether or not our glaciochemical data are useful: we have already established in Chapter 1 that glaciochemical data are fundamental to our understanding of subglacial processes. What does however need to be established is whether or not the glaciochemical data *observed in TBIS* are representative of the subglacial environment. The evidence laid out in this chapter indicates that such terminal blue ice has indeed interacted with subglacial meltwaters, most likely via the processes of regelation and/or accretion. Nonetheless, this does not necessarily mean that it has the same glaciochemical composition as subglacial meltwater, only that their composition has been influenced by meltwater. Without a quantitative understanding of how the compositions of TBIS and subglacial meltwater relate to one another, we may only be able to treat the results of certain analyses qualitatively.

The DOC data from section 3.3 illustrate this point. Whilst the concentration of DOC in TBIS was consistently much higher than that of snowpack and englacial ice, it was still only around half that of Type I accretion ice from the Vostok ice core. The simplest explanation for this is that there is more organic carbon under the central EAIS than there is underneath Horseshoe Valley Glacier. Alternatively, the differences in DOC concentration may be because the ice has undergone different processes prior to sampling. Regelation involves the pressure-induced melting of glacial ice at the bottom of an ice sheet or glacier, followed by

refreezing. Accretion is simply the freezing of subglacial meltwaters to the base of the ice sheet. In practice, this may not be an important distinction, as the final step in both processes is the freezing of subglacial water. Nonetheless, if mixing in the subglacial environment is poor, then subglacial meltwaters should be more dilute in areas where regelation is ongoing, because the melting englacial ice contains very little DOC. In contrast, if subglacial meltwaters flow into an area below the pressure-induced melting point (i.e. where very little regelation is taking place) before freezing onto the base of the ice sheet, then the resulting accretion ice may be more concentrated than regelation ice from the same region. The lower apparent DOC underneath Horseshoe Valley Glacier might therefore be an artefact of the TBIS, rather than a spatial pattern. As it happens, the ionic composition of the TBIS appears no more dilute than that of the Type I accretion. The blue ice is actually considerably richer in Ca^{2+} and Mg^{2+}, while the Type I accretion ice contains two to three times more Na^{+} and Cl^{-}. The fact that Vostok accretion ice is less rich in certain nutrients suggests that these glaciochemical differences may be due to spatial variance rather than an inherent difference between regelated and accreted ice.

Even if TBIS were found to be more dilute than accretion ice, would this necessarily be a problem? Accretion ice is considered to be an extremely useful research tool, even though it must be more dilute than subglacial waters due to the exclusion of solutes that occurs during freezing. Our present understanding of the composition of Subglacial Lake Vostok did not arise from direct measurements of lake water: researchers have only been able to make projections based on the concentration of accretion ice in Borehole 5G. In my opinion, there is no reason that the same approach cannot be applied to glaciochemical data from TBIS. In the long term, it would surely be quicker and easier to adjust the formulae currently used to make projections of subglacial concentration from accretion ice data than it would be to organise, fund and conduct new drilling operations across the Antarctic continent.

Lastly, it is worth considering that dissolved species are not the only useful clues that TBIS might hold to processes going on beneath the ice sheets. Ice that has been dragged across the subglacial bed will inevitably pick up insoluble sediments. Across all of the studies of microbial life beneath the cryosphere, it has consistently been the sediment that houses the vast majority of biological activity. The reasons for this should be clear: wet sediment is typically richer in terms of nutrients, and provides protection from fast-flowing water that might otherwise break up microbial communities. The TBIS examined in this thesis contained variable amounts of sediment, however the majority of samples contained more than 3 g L^{-1}. This sediment could be utilised for a number of purposes, such as cell counts, fluorescence microscopy, scanning electron microscopy or even analysis of ribosomal DNA. These analyses have the potential to determine the size and structure of the microbial communities under a given region of the AIS. In turn, this can be used to improve our understanding of the kinds of processes taking place in the subglacial environment.

The TBIS from the Marble Hills BIA were also notably full of tiny air bubbles – more densely packed than englacial ice. A similar density of air bubbles has been observed in TBIS from the Patriot Hills BIA, which suggests that this is not a one-off phenomenon. The analysis of these trapped gases could add a very valuable dimension to subglacial studies, as any air bubbles incorporated during regelation will contain a sample of the gases present underneath the ice. This may include traces of metabolic processes such as the

methanogenesis, as is believed to be taking place within the sedimentary basins beneath the AIS [89]. Gas extractions from TBIS could therefore be used to further expand our knowledge of sub-Antarctic biogeochemistry; this is beyond even the scope of our current deep ice drilling operations. To conclude on this first criterion: there is definitely evidence that the data obtained from TBIS could be useful to contemporary researchers.

5.1.2 – Viable sample sites

Antarctica is a large continent, and sampling from the Marble Hills BIA can only inform us of the subglacial environment in the vicinity of Horseshoe Valley. If TBIS are to be useful to future research, then similar sampling sites with regelated terminal blue ice must be found elsewhere on the continent. According to satellite data, wind-driven blue ice areas cover at least 60,000 km^2 (approximately 0.4%) of the Antarctic surface [202]. In addition to this, Winther et al. (2001) identified a further area of 121,000 km^2 with the "potential for blue ice". More than half of this potential blue ice is likely to be "melt-induced", meaning that the blue colouration is a result of successive melting and refreezing, rather than a negative mass balance. Given the ratio of known sublimation-induced and melt-induced blue ice in each of Winther's zones, it can be estimated that up to 40,000 km^2 of this potential blue ice could be formed by sublimation. The area of the Antarctic surface covered by sublimation-driven blue ice is therefore somewhere between 60,000 km^2 and 100,000 km^2 (0.4% - 0.7%). This is consistent with the investigation of SMB by Lenaerts et al. (2012), who found that 0.5% of the surface was subject to net ablation [203].

Of course, not all of this area contains subglacial ice: we have already seen the example of the Allan Hills, where the deepest ice never reaches the subglacial bed. At present, our best indicator of whether or not this is likely to happen is subglacial topography. The best way to estimate the number of viable sample sites would therefore be to assess the bedrock profiles (such as those in BEDMAP2) of each of the BIAs identified by satellite imaging, and determine how many of them feature a sufficiently steep rise in the underlying bedrock. This is, however, beyond the scope of this thesis. A much less quantitative approach would be to make the assumption that this criterion is met in most (if not all) BIAs that are classified as 'closed', defined in Grinsted et al. (2003) as BIAs where "ice flow is forced to terminate because of outcropping nunataks" [138]. This includes all regions of blue ice that flow directly into nunataks (such as those at feet of the Independence Hills, WAIS) as well as those that flow over the top of entirely submerged mountains (such as Scharffenbergbotnen, EAIS). At present, there are no estimates of the relative proportions of open and closed BIAs. However, given that katabatic winds are generated by hills and mountains, it stands that the vast majority of wind-driven BIAs occur in regions with varied topography; any given BIA therefore has a reasonable chance of flowing into submerged nunataks.

BIAs are not evenly distributed across the Antarctic continent: they are concentrated around mountainous regions. Both remote imaging and SMB studies identified suitable BIAs along the Trans-Antarctic, Ellsworth and Prince Charles mountain ranges, as well as a number of nunataks across Dronning Maud Land. This gives good coverage of a lot of the AIS, however there is only limited potential for the collection of TBIS from Dome A (on the East Antarctic plateau) and from Marie Byrd Land. In contrast, ice

cores are typically taken from ice divides, which are typically located on high plateaus of the ice sheet. So does this mean that the distribution of BIAs is inadequate to coincide with contemporary research interests?

The lack of coverage in Marie Byrd Land is particularly pressing. The Amundsen Sea coast is one of the most rapidly melting regions of Antarctica, so it is arguably more important that we understand the subglacial environment of Marie Byrd Land than anywhere else. For instance, it is important to quantify any greenhouse reservoirs that may be breached as the ice melts. Nevertheless, blue ice sampling may still be of use for the investigation of Marie Byrd Land, even though the nearest suitable sampling sites are probably on the western slopes of the Trans-Antarctic Mountains. This is because much of the subglacial hydrology of Antarctica is can be divided into a number of highly-interconnected drainage basins [204]. By comparing the hydrological mapping in Siegert et al. (2009, [204]) with the satellite data from Winther et al. (2001, [202]), it is possible to identify viable BIAs for every major drainage basin underneath the ice sheets (Figure 31). In the case of Mary Byrd Land, blue ice sampling in the Trans-Antarctic Mountains should give some indication of the biogeochemical conditions at the start of the flow path into the subglacial lakes around Byrd Glacier. Similarly, the subglacial hydrology underneath Dome A drains into the basin of the Lambert Glacier, which means that sampling in the Prince Charles Mountains should be representative of the subglacial environment upstream (beneath Dome A) [204]. Given that BIAs are distributed primarily along the top and bottom of each drainage basin, it should be possible to use glaciochemical data from TBIS to identify processes taking place as water flows beneath the ice. Consequently, the relative shortage of BIAs across the Antarctic plateaus should not necessarily limit their potential as a window to the subglacial environment.

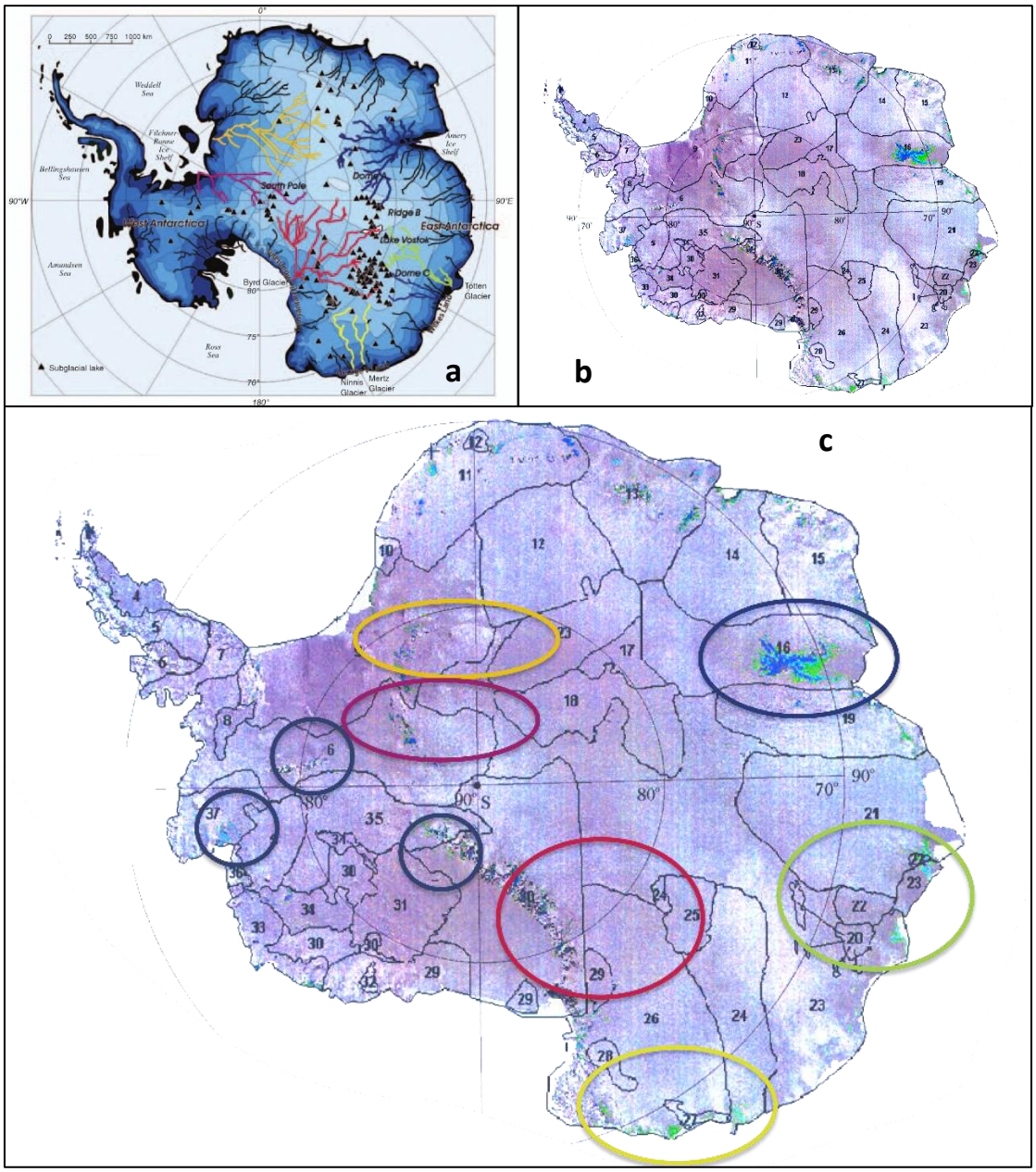

Figure 31 – Maps of BIA distribution across Antarctic drainage basins. a) Map of Antarctic subglacial drainage systems, taken from Siegert et al. (2009, [205]). b) Distribution of Antarctic BIAs as determined by satellite imagery, taken from Winther et al. (2001, [203]). c) Synthesis of above maps, highlighting sublimation-driven BIAs above the largest subglacial drainage basins on the Antarctic continent; this is adapted from the image in Winther et al. (2001), using information from Siegert et al. (2009). The BIAs identified in c) are potential targets for future sampling.

5.2 – Calved Patagonian icebergs

In Chapter 4, the chemistry of calved icebergs was used to make a number of inferences about Steffen Glacier and its influence on the Rio Huemules. However, there were also some notable limitations to the conclusions that were drawn from the iceberg analyses. Once again, it is considered whether or not these limitations are likely to compromise the usefulness of calved iceberg sampling in the context of answering modern research questions. Section 5.2.2 then briefly outlines the global distribution of lake-calving glaciers and evaluates the need for alternative sampling in these locations.

5.2.1 – Usefulness of data

Contemporary research in glaciated regions tends to focus on three broad topics: monitoring glacial mass balance; recording airborne pollution; and examining the influence of glaciers on downstream environments. The first of these topics is largely unrelated to the chemical composition of icebergs, and may be better-estimated by models fed with remote-sensing data. However, these models could potentially be informed by analyses of the stable isotopes of water. For instance, the sublimation signature observed in Lago Steffen icebergs indicates an important SMB process taking place on the glacial surface: quantification of relative sublimation rates in different temperate glaciers could be used to improve the uncertainty in mass balance models. In addition to this, the δ^2H/δ^{18}O signature of icebergs may be compared with that of glacial rivers and used to follow the rate of glacial melt over time. Melt rate proxies could then be compared with meteorological parameters (such as temperature, humidity and wind speed) in order to determine physical relationships controlling mass balance changes. This information could once again be fed back into models in order to improve future projections of glacier mass balance.

It should be noted that δ^2H and δ^{18}O are not straightforward proxies of glacial melt rate. The delta values of non-glacial inputs will fluctuate over time due to changes in air temperature and tropospheric circulation, so not all changes in the isotopic signature of a glacial river are due to changes in glacial input. This is not a problem if there is the opportunity to monitor changes in δ_{NON}, as in this investigation: continuous measurements of the non-glacial Rio Quince alongside the Rio Huemules sampling allowed the calculation of an δ_{NON} value that was representative of the period of sampling. However, this is certainly a consideration for future studies, because not all lake-terminating temperate glaciers will have a convenient non-glacial river adjacent to the outlet river. Furthermore, the need to monitor changes in δ_{NON} doubles the number of samples that need to be collected. This could limit the viability of high-resolution studies of temporal variation in glacial rivers, as it would require that both the glacial and non-glacial sampling points are visited frequently. The potential usefulness of iceberg sampling would consequently be improved if a different proxy of melt rate were found amongst the iceberg data.

One plausible solution might be to calculate a metric of the *meteoric deviation*: the difference between the observed δ^2H-δ^{18}O line and the GMWL. Although the delta values of the Rio Quince exhibit temporal variation, the relationship between δ^2H and δ^{18}O remains more-or-less constant (Figure 32). In contrast, the relationship between δ^2H and δ^{18}O in the Rio Huemules is very variable, and deviates from the meteoric line for periods of several days at a time (Figure 33). If these deviations are shown to coincide with

increased glacial input to the Rio Huemules, then it seems likely that the meteoric deviation could be used as a new proxy for glacial melt rate. This would in turn increase the value of the isotopic data available from iceberg sampling.

Figure 32 – Time series for δ^2H and δ^{18}O in the Rio Quince. The primary and secondary axes have been scaled so that parallel values of δ^2H and δ^{18}O are the corresponding values on the GMWL. This means that the distance between the blue and orange lines corresponds with the meteoric deviation.

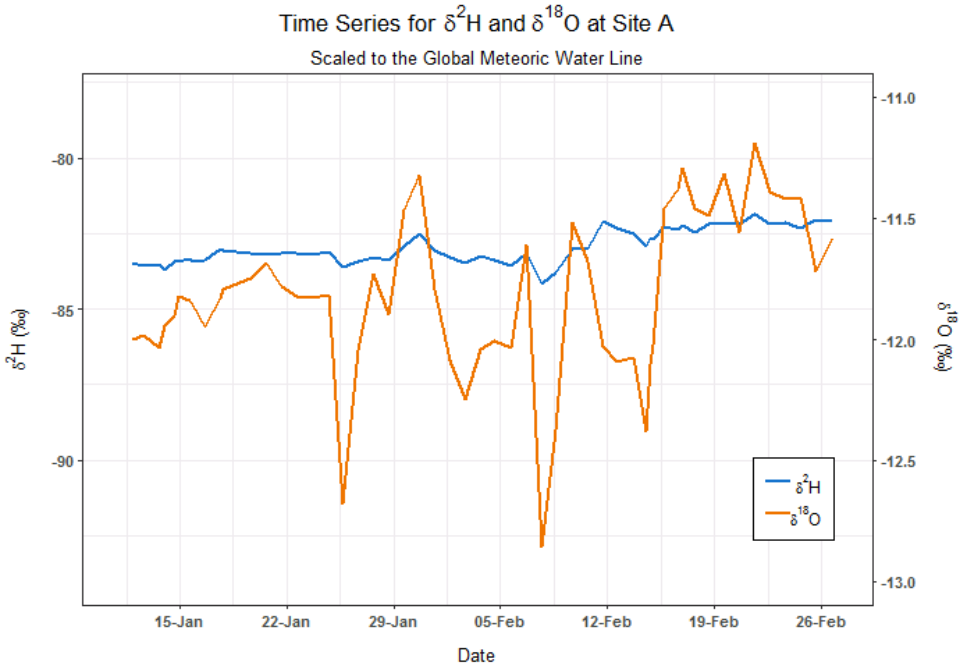

Figure 33 – Time series for δ^2H and δ^{18}O in the Rio Huemules. Once again, this the two axes have been scaled to the GMWL.

Ion chromatography of the iceberg samples suggests that elution is taking place on the surface of the NPI. This supports the findings of previous studies in the SPI and – for the purposes of this thesis – is an interesting result. However, it does limit the usefulness of iceberg studies as a means by which to study atmospheric deposition, as the ionic composition of the icebergs (i.e. englacial ice) is almost certainly different from the precipitation from which it was formed. Whilst this does not support the use of iceberg studies to investigate the record of atmospheric pollution at Steffen Glacier, it is – perhaps counter-intuitively – a very good reason to undertake iceberg sampling elsewhere. A more challenging/expensive field expedition to sample the glacier directly would have made the same finding – that elution has masked the temporal record. Direct sampling may still have some value: for instance, general trends may still be discernible, especially for ions that are slow to elute (e.g. NH_4). Fresh precipitation samples could also be collected and analysed, although this is unlikely to have any advantages over the collection of precipitation from more easily-accessible locations. To summarise on this point, studies of atmospheric composition in temperate glaciers are most valuable when a high-resolution record spanning a number of years is available; iceberg sampling may be used in pilot studies to determine which glaciers are likely to have the most valuable records so that researchers can make better informed decisions when planning difficult or expensive expeditions.

The last research topic considered here is the impact of glaciers on downstream environments; this is becoming an increasingly prominent topic in the face of extensive glacial retreat in many highly populated areas of the world (most notably, the mountainous Third Pole Region, TPR, of central/southern Asia). We have already established that the stable isotopes of water may be used to estimate the relative magnitude of glacial input at a given downstream location. But what of the chemical influence of glaciers? The most obvious drawback with iceberg sampling for this question is that icebergs are mostly comprised of englacial ice, whereas the most nutrient-rich meltwater is found in the subglacial environment. This isn't to say that iceberg sampling is a poor option: the ability to accurately measure one of the two components of glacial input certainly has a place in modern research. However, iceberg sampling in this context is not an alternative method to a more direct approach, and so falls outside the scope of this thesis.

Biological and chemical processes at the subglacial bed both add dissolved species to the melted ice, increasing the concentration of nutrients and altering the relative concentrations of major ions. This means that it is virtually impossible to get a full picture of glacial influence on river chemistry using iceberg sampling alone. The fact that water from the glacial tributary is still significantly diluted when it mixes with water from Lago Steffen suggests that this subglacial input is either less significant than the dilute englacial/supraglacial meltwater input, or less concentrated than local non-glacial sources; iceberg sampling may therefore have a qualitative use in the observation of dissolved species from glacial melt. Nevertheless, the limitations of iceberg sampling may be unattractive to researchers of dissolved ions in freshwater systems.

Despite the low concentration of dissolved nutrients released into Lago Steffen, Steffen Glacier may still deliver nutrients downstream in the form of suspended sediment. Concentrations of suspended sediment in the Rio Huemules are generally high, and peak during the summer melt season (section 4.5.2), while the twenty-four iceberg samples from Lago Steffen were significantly more sediment-rich than the downstream

freshwater. These sediment-bound species may undergo chemical denudation as they travel along the river, or may be bioavailable in their bound state. Either way, the analysis of sediments captured during filtration of the melted iceberg samples may be of value to researchers studying the impact of glaciers on downstream environments. In contrast with dissolved nutrients, there is unlikely to be a significant difference in concentration between iceberg-rafted and subglacial sediments. This is because the rate of subglacial physical weathering is much greater than that of chemical or biological weathering, so the bulk of the subglacial sediments should be relatively unchanged by their different flow path.

Overall, the iceberg glaciochemical data are perhaps less useful than that of TBIS. This is largely due to uncertainty in the composition and relative importance of subglacial meltwater, which is not represented by iceberg samples. Nonetheless, a number of potential uses of iceberg sampling have been identified for future studies: namely, the monitoring of glacial input/melt rate via water isotope signatures (for which iceberg samples *can* be representative of the whole glacier); the analysis of sediment-bound nutrient inputs; and the identification of supraglacial processes (sublimation and elution) for models and low-cost pilot studies.

5.2.2 – Viable sample sites

Calving glaciers are widespread in Patagonia and Tierra del Fuego, where the majority of glaciers terminate in either fjords or proglacial lakes [205]. Calving is an important ablative process in this region: it has been estimated that calving is responsible for two thirds of ablation at the marine-terminating San Rafael Glacier. This single calving front therefore accounts for around 9% of the mass lost from the entire NPI [151]. High ablation is also observed in lacustrine-calving glaciers such as Steffen, which retreated 12 km between 1979 and 2001 – only 2 km less than the much larger San Rafael Glacier [155]. The Carr Austral road runs parallel with the eastern side of the NPI, however few tracks lead west into the steep mountains of the Wet Andes, making the glacier terminus (and iceberg sampling) a much more realistic goal than direct sampling from the supraglacial surface. Few roads at all serve the remaining glaciers of the NPI, SPI or Tierra del Fuego; these are best approached by boat. Once again, this favours iceberg sampling studies. The high connectivity of the fjord system may actually enable sampling from several glaciers at once – something that would be unrealistic for most direct sampling studies. The southern portion of South America is therefore an ideal candidate for future iceberg-centric investigations.

In contrast, the sampling of calved icebergs is unlikely to prove advantageous in the European Alps. For one, historically, very little calving has been witnessed in this region – only a small number of calving glaciers are known, such as Miage Glacier in northern Italy. 20th Century glacier retreat has led to the formation of additional proglacial lakes into which calving events have been observed. However, calving is believed to contribute to only a small proportion of the mass lost from either of these groups of glaciers, meaning that iceberg samples will be less representative of the glacial inputs into the environment. Moreover, access is relatively straightforward in the European Alps: there are reliable roads leading into the majority of glacier valleys and well-documented mountaineering routes covering the entire range. A number of major cities (Geneva, Grenoble, Milan) are situated within the foothills of the Alps, which means that

expeditions to the glacial surface are not as limited in terms of equipment or manpower as they are in Chilean Patagonia, nor are they so expensive. To summarise, although calving activity is on the increase in the European Alps, direct sampling is still preferable because it is likely to yield more useful data for relatively little increase in logistical difficulty.

Outside of the polar ice sheets, most other glaciers sit between the two extremes set by the southern Andes and the European Alps. There are two exceptions to this rule: the glaciers of northern Eurasia and the high mountains of the Asian TPR. Calving is known to be a dominant mass balance process in northern ice caps such as those on Svalbard, where the total calving loss has been estimated to be 4 km^3 ± 1 km^3 per year. In comparison, the annual net surface mass balance (accumulation minus runoff) over the same area is only −0.5 km^3 ± 0.05 km^3 [206]. The sheer magnitude of the calving output may make iceberg sampling more interesting than direct sampling, even if there is better access than for Patagonian glaciers. Moreover, all calving on these Arctic islands is directly into the Arctic Ocean, where access via research vessels is relatively facile (marine iceberg sampling has already been conducted in three locations around Svalbard [207]). However, this approach is not being undertaken as an alternative to direct sampling; it is therefore beyond the scope of this thesis.

Glaciochemical research within the TPR (with the exception of the Tibetan Plateau) is particularly sparse. This is not for lack of importance: the ten great rivers of Asia all originate within this region, and are expected to be affected by significant changes in glacial input this century. As in Patagonia, many glaciers within the TPR are bordered by steep topography, with logistical obstacles such as limited infrastructure and distances to transport equipment. Researchers must also undergo altitude-specific safety training before attempting an ascent, and may be unable to reach a suitable sampling point in the event of bad weather. Routine glacial monitoring in the Tien Shan and Pamir Mountains halted after the collapse of the USSR, however there are now growing efforts to re-establish baseline monitoring in these regions in order to combat water security issues [208]. This new monitoring focuses exclusively on the mass balance and hydrological aspects of glaciology, which could be enhanced by water isotope data from chemical studies. It could also provide a strong foundation from which to build a water quality dimension, akin to the work with Steffen Glacier and the Rio Huemules. At the time of writing, there are no estimates available for the number of calving glaciers within the TPR or the relative importance of calving as an ablative process. However, a recent inventory of lakes within the region indicates that the majority of glacial lakes underwent expansion between 1990 and 2010, most likely due to the retreat of lake-terminating glaciers [209]. Given that the likelihood of calving events is correlated with lake size [210], this suggests that the number of calving glaciers in the TPR is set to increase if the trend of general retreat (excluding the Karakoram Range) continues over the 21st Century. Consequently, there may be opportunity to utilise iceberg sampling at a number of sites within the high mountains of central Asia.

5.3 – Concluding remarks

It is clear that alternative sources of deep ice can indeed yield interesting data. Going forward, the use of TBIS in particular shows promise as a novel approach to a complex problem: how to study the environment beneath the AIS. A number of viable sample sites for future field expeditions have been identified: given the quick and economical protocol required to collected additional samples, further sampling from these locations is strongly recommended. At worst, the samples will represent preserved englacial ice, as used in paleoclimatology. At best, the resulting data will unlock a novel picture of the subglacial environment, with coverage across the Antarctic drainage basins and applicability to several contemporary research questions. As such, the findings of Chapter 3 suggest that the relationship between δ^2H and δ^{18}O may be diagnostic of whether a particular section of the BIA is better suited to paleoclimatic or subglacial study.

Whilst the applicability of iceberg data is perhaps more restricted than that of the TBIS, calved iceberg sampling may prove advantageous in the pursuit of a number of research questions in South America and the TPR. The stable isotopes of water may be used to monitor downstream glacial influence; if the non-glacial input is also monitored then this becomes a useful proxy for glacial melt rate. Analysis of suspended sediment – likely the major source of glacial nutrients in the Rio Huemules – could be used to build a picture of the glacial impact on water quality. Lastly, iceberg sampling could be utilised by pilot studies in order to quickly assess which glaciers are worth targeting for larger direct sampling expeditions – potentially avoiding datasets that have been compromised by post-depositional processes such as elution.

No sampling approach is perfect for all situations. Traditional direct sampling will most likely remain a central part of glaciochemical research for the foreseeable future, because each alternative approach will come with its own set of limitations. For instance, TBIS are unable to provide the same paleoclimatic data as the upper portions of the Vostok ice core. Conversely, these new methods may also provide novel opportunities, such as analysis of the trapped gases in the Marble Hills samples. Most importantly, by exploring alternative sources of deep we open up new opportunities that might otherwise have been limited by constraints on time, funding or practicality. Previous investigations of the subglacial environment have required a significant level of global cooperation in order to acquire the funds and expertise necessary to drill down into the AIS, while no prior glaciochemical investigations have even been conducted on the south side of the NPI. In contrast, the sampling techniques described in this thesis could be organised, funded and undertaken by a small team of scientists – perhaps just a single research group. In this way, these alternative sampling options should increase the collective output of the research community as a whole – which is surely in the best interests of all science.

List of abbreviations

AIS	Antarctic Ice Sheets; the combined EAIS and WAIS.
BIA	Blue Ice Area; a region of exposed glacial ice caused by a negative SMB.
DOC	Dissolved Organic Carbon.
EAIS	East Antarctic Ice Sheet.
GMWL	Global Meteoric Water Line; the common relationship between δ^2H and δ^{18}O in meteoric water.
ITAE	International Trans-Antarctica Expedition
LMWL	Local Meteoric Water Line; an adjustment of the GMWL that takes into account local factors that may affect the stable isotopes of meteoric water.
LOWTEX	The Low Temperature Experimental Facility at the University of Bristol.
NPI	Northern Patagonian Icefield.
PISCES	Patagonian Icefield Shrinkage impacts on Coastal and fjord Ecosystems; an ongoing project investigating the effects of Chilean glaciers on downstream freshwater systems.
SALE	Subglacial Antarctic Lake Exploration; a specialist group founded by SCAR.
SCAR	The Scientific Committee on Antarctic Research; an interdisciplinary committee founded by the International Council for Science (ICSU)s.
SLE	Subglacial Lake Ellsworth; sometimes written *Ellsworth Subglacial Lake* in the literature.
SLV	Subglacial Lake Vostok.
SLW	Subglacial Lake Whillans.
SMB	Surface Mass Balance; the net annual gain or loss of mass from the surface through ablative (e.g. sublimation) and accumulative (e.g. precipitation, wind blow) processes.
SO	Southern Ocean.
SPI	Southern Patagonian Icefield.
TBIS	Terminal Blue Ice Samples; surface ice samples taken from the end of the flow path of a BIA.
TPR	Third Pole Region; the high mountain region of central/southern Asia, comprising the Himalaya, Hindu-Kush, Karakoram, Pamir and Tien Shan mountain ranges, as well as the Tibetan Plateau.
WAIS	West Antarctic Ice Sheet.

Appendices

Appendix 1: Considerations when cleaning ice

Water isotope measurements are particularly susceptible to contamination, as cleaning fluids may affect the outcome. Contaminating alcohols (e.g. from ethanol-cleaned labware) may absorb infrared radiation at the measured frequencies – although some spectroscopic isotope analysers are designed to at least identify when spectral contamination has occurred. Even the chosen cleaning fluid for the ice itself, MilliQ ultrapure water, can affect the measured delta values because it is significantly less depleted in terms of ^{18}O and ^{2}H than glacial ice. Cleaning is nonetheless an essential to the analysis of glacial ice, both because handling in the field is likely to introduce foreign particles, and because the dilute nature of the ice makes it sensitive to contamination.

The initial cleaning step for the Antarctic ice – washing with MilliQ – was designed to remove any water-soluble contaminants (in particular, ions and organic carbon) that had settled on the ice during sectioning. The incubation temperature of -6°C was chosen to minimise the likelihood that samples would take up ultrapure water during cleaning: at lower temperatures, pure water is likely to freeze (accrete) to the surface of the samples; higher temperatures cause the widening of microscopic hydrological channels in the ice, through which water may be taken up. The final step – partial melting and transfer to a fresh bag – was designed to remove the any soluble impurities left behind after washing, as well as the small amount of ultrapure water that remained on the surface.

Incubation was only possible for the ice that was cleaned in LOWTEX; due to Chilean export limitations, the Steffen iceberg samples had to be processed in the field at near-ambient air temperatures. Washing with ultrapure water is not advisable under these conditions, due to the open network of tiny veins that would take up both the cleaning fluid and any impurities carried within it. The alternative cleaning procedure adopted was designed to minimise exposure of the iceberg samples to uncontrolled environments.

As in the laboratory, the tool used to cleave the ice (a commercial ice axe) was made of stainless steel and was cleaned prior to use with ethanol and ultrapure water; acid-washing was deemed inappropriate because the passive chromium oxide layer that forms on stainless steel is vulnerable to acids. The removal of surface material ensured that the ice collected had not been in contact with precipitation or airborne particles. The exposed sample was then extracted directly into its polyethylene bag. All following preparation was conducted within the clean lab tent. In the absence of a washing step, the samples underwent two stages of partial melting (and subsequent transfer to new bags) before being allowed to melt fully. This was designed to remove any foreign particles that had been transferred onto the surface by the ice axe, or during the brief period of exposure to the atmosphere. The drawback of this method is that it requires the ice to warm to around 0°C, allowing the small hydrological channels within each sample to approach their maximum diameter. In theory, surface contaminants may be drawn into such channels during melting. The potential for significant contamination was however limited by the earlier steps minimising exposure and by the formation of meltwater within the channels themselves. On balance, this was deemed preferable to the use of ultrapure water, which is equally likely to enter channels, and is isotopically and chemically different to the ice.

Appendix 2: Analysis of Covariance (ANCOVA)

Comparison of Local Meteoric Water Lines

All statistical analyses were performed in RStudio. ANCOVA was first used to compare the LMWLs calculated from the Ellsworth firn core and from published data derived from the 1990 Trans-Antarctic Research Expedition.

Three variables were created: one for the treatment factor, taking on values of "firn" or "transect"; one vector containing the δ^2H values for both groups, and another containing the corresponding δ^{18}O values. Naturally, the isotope data were paired so that the two measurements from any one sample were stored at equivalent positions. Put another way, the delta values found at the n^{th} position in each of the two vectors are measurements from the same sample.

```
> Deuterium <- c(-244.6,-242.10,-266.27,-251.4,-252.56,-250.56,-272.37,-266.3,-257.13,-267.
09,-265.0,-255.71,-261.77,-255.0,-250.5,-248.4,-251.9,-295.4,-263.3,-296.2,-263.6,-271.0)
> group <- factor(c(rep("Firn", 15), rep("Transect", 7)),
+ levels=c("Firn", "Transect"))
> Oxygen18 <- c(-30.4,-29.8,-33.36,-31.65,-31.55,-30.87,-33.6,-33.3,-31.55,-33.04,-33.1,-3
2.30,-32.95,-31.4,-31.0,-31.8,-32.0,-37.5,-33.2,-37.5,-33.4,-34.9)
```

The data were then plotted within RStudio in a manner equivalent to Figure 4.

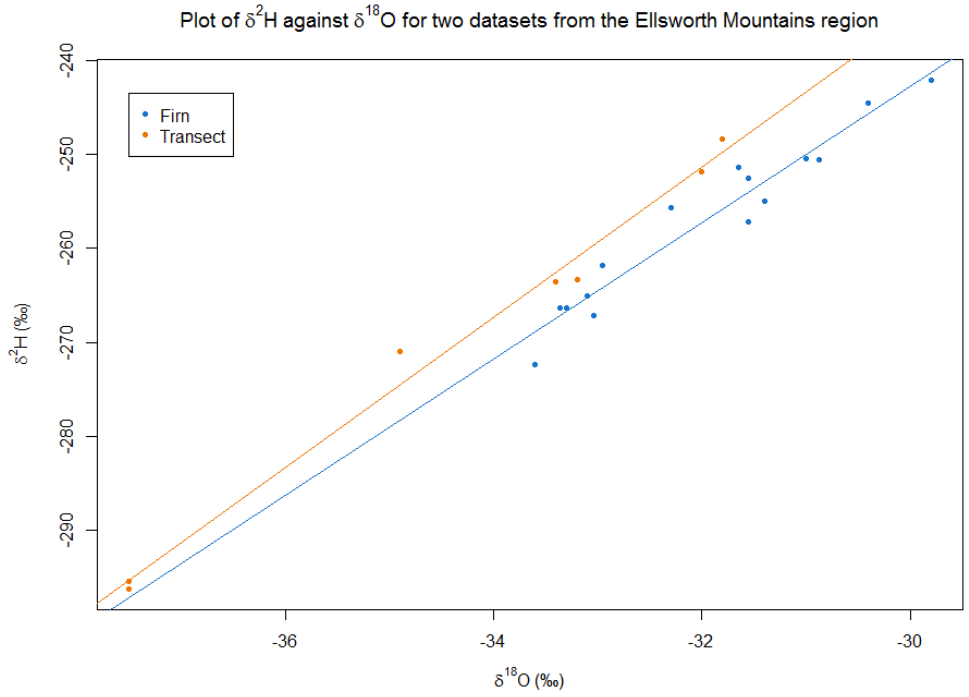

A simplistic one-way ANOVA reveals that the mean δ^2H values for the Ellsworth firn core and the 1990 Trans-Antarctic Expedition were significantly different (F: 4.6645 > 4.3512, $df_1 = 1$, $df_2 = 20$, $\alpha = 0.05$). Consequently, we reject the null hypothesis (p = 0.04311).

```
> mod.1 <- lm(Deuterium ~ group)
> a <- anova(mod.1)
> print(a)
```

```
Analysis of Variance Table

Response: Deuterium
          Df Sum Sq Mean Sq F value  Pr(>F)
group      1  775.6  775.55  4.6645 0.04311 *
Residuals 20 3325.3  166.27
```

Of course, this does nothing to establish whether or not the two groups belong to the same local meteoric line. The one-way ANOVA above assumes that "group" is the only of variance in the δ^2H dataset for which we can account. However, we have already established that both groups exhibit a roughly linear relationship between δ^2H and δ^{18}O. In order to make a meaningful comparison, we must treat δ^{18}O as a covariate – an additional variable that can effect change in the dependent variable.

Before we begin, it is necessary to check for normality in our datasets. ANCOVA is relatively robust to deviations from normality, but it is nonetheless a parametric test and is best used on multivariate normal datasets. A QQ plot reveals no obvious deviation from normality for datasets of this size; the firn core, with 15 data points, is predictably closer to normal.

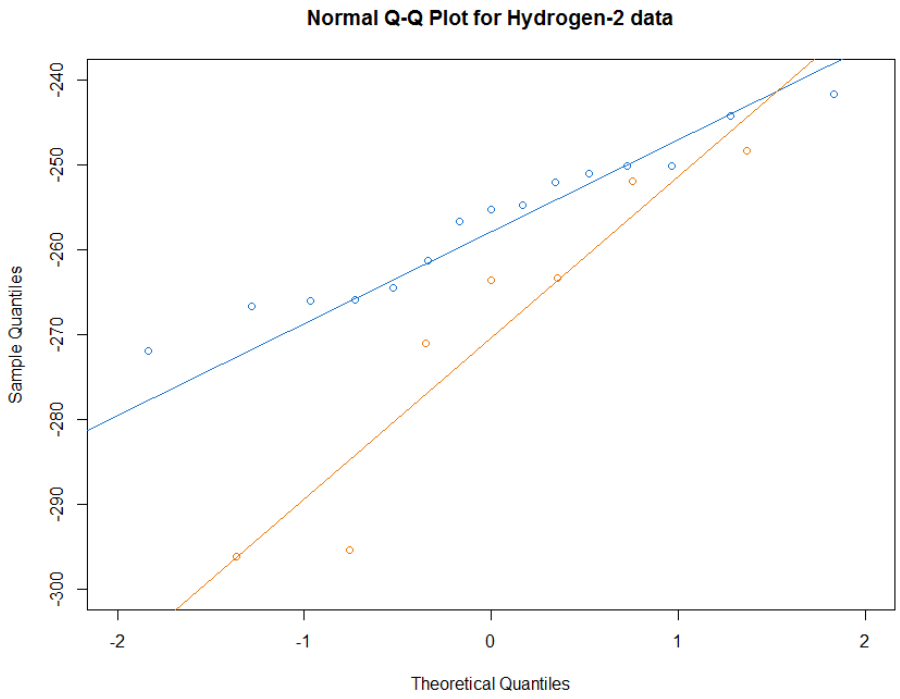

The Shapiro-Wilk test can be used to test for normality. Compared with other common tests for normality, this test tends to retain most power when used in the analysis of small datasets [211].

```
> shapiro.test(Deuterium[1:15])

        Shapiro-Wilk normality test

data:  Deuterium[1:15]
W = 0.9588, p-value = 0.6716

> shapiro.test(Deuterium[16:22])
```

```
        Shapiro-Wilk normality test

data:  Deuterium[16:22]
W = 0.87708, p-value = 0.2138
```

The reported p-value was greater than the significance level for both datasets (0.6716, 0.2138 > 0.05). We accept the two null hypotheses: the firn core and transect datasets are normally distributed with respect to the dependent variable (δ^2H). As ANCOVA requires multivariate normality, we now repeat the process with the covariate.

```
        Shapiro-Wilk normality test

data:  Oxygen18[1:15]
W = 0.93307, p-value = 0.3032

data:  Oxygen18[16:22]
W = 0.8662, p-value = 0.1719
```

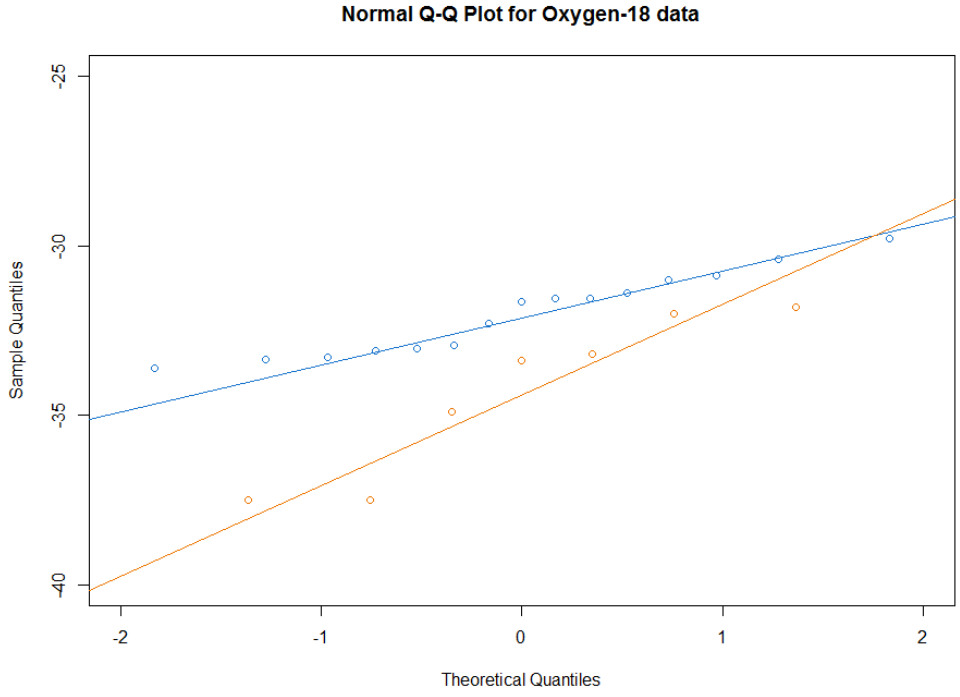

We accept the null hypothesis that the firn core data are normally distributed with respect to the covariate at the 5% significance level (p = 0.3032). We also accept the null hypothesis that the transect data are normally distributed with respect to the covariate (p = 0.1719). It is therefore appropriate to use a parametric test such as ANCOVA in this analysis.

A second assumption of ANCOVA is that there is no interaction between the treatment factor and the covariate. This is known as homogeneity of regression slopes. In effect, this means that the two regression lines (δ^2H vs δ^{18}O for each of the two groups) must not have significantly different gradients. Consequently, it is necessary to test the following null hypothesis:

$$H_0^1: m_2 = m_3$$

To do this, a linear model was created in which δ^2H depends on the treatment factor (group), the covariate (δ^{18}O) and an interaction term between the two. If the interaction term returns a p-value below the significance level, then we can assume that the two meteoric lines have different gradients. Conversely, if it is not significant then we move on to the second null hypothesis.

```
> mod.full <- lm(Deuterium ~ Oxygen18 + group + Oxygen18:group)
> library(car)
> Anova(mod.full, type="II")
Anova Table (Type II tests)

Response: Deuterium
               Sum Sq Df  F value    Pr(>F)
Oxygen18       3226.7  1 634.2973 1.743e-15 ***
group            89.3  1  17.5598 0.0005498 ***
Oxygen18:group    7.1  1   1.3913 0.2535407
Residuals        91.6 18
---
Signif. codes:  0 ‘***’ 0.001 ‘**’ 0.01 ‘*’ 0.05 ‘.’ 0.1 ‘ ’ 1
```

Since the F-value returned for the interaction term is less than the critical value at the 5% significance level (1.3913 < 4.4139, $\alpha = 0.05$, $df_1 = 1$, $df_2 = 18$), we accept H_0^1 ($p = 0.25$). This indicates that there is no significant interaction between the covariate and the treatment factor; put another way, the relationship between δ^2H and δ^{18}O does not differ with the group. Consequently, the two LMWLs may be assumed to have the same gradient.

The above analysis also indicates (as expected) that δ^2H depends on both the covariant and on the treatment factor: the reported F-values were greater than the critical value (634.2973, 17.5598 > 4.4139, $\alpha = 0.05$, $df_1 = 1$, $df_2 = 18$). However, given that the interaction term was insignificant, we should first restrict our linear model before rejecting the corresponding null hypotheses. The resulting model should be more parsimonious, gaining power through the simplification.

```
> #Restricted model (no interaction)
> mod.rest <- lm(Deuterium ~ Oxygen18 + group)
> Anova(mod.rest, type="II")
Anova Table (Type II tests)

Response: Deuterium
          Sum Sq Df F value    Pr(>F)
Oxygen18  3226.7  1 621.498 5.611e-16 ***
group       89.3  1  17.206 0.0005465 ***
Residuals   98.6 19
```

The F-value returned for the group term is greater than the critical value (17.206 > 4.381, $\alpha = 0.05$, $df_N = 1$, $df_D = 19$). We thus reject the null hypothesis at the 5% significance level ($p = 0.0005465$). δ^2H is not independent of group, even when accounting for differences in δ^{18}O. Given that there is no significant difference between the slopes of the two meteoric lines, this must be due to a significant difference in intercept. This is equivalent to rejecting the second null hypothesis of ANCOVA (H_0^2: $\bar{Y}_2 = \bar{Y}_3$).

Appendix 3: Non-parametric linear regression

Simple linear regression is the most common method to test a relationship between continuous dependent and independent variables. It is however not appropriate for datasets with a non-normal distribution. This appendix describes the regression analysis of the Marble Hills water isotope data, starting with a simple least squares linear regression, and then improving the model with a median-based linear model. All analyses were carried out in RStudio.

Regression analysis can be used to quantify the relationship between δ^2H and δ^{18}O observed in samples of blue ice (Figure 4). As per usual, the analysis begins with the creation of two vectors, in which paired data are found at equivalent positions. We then check that these data are suitable for simple least

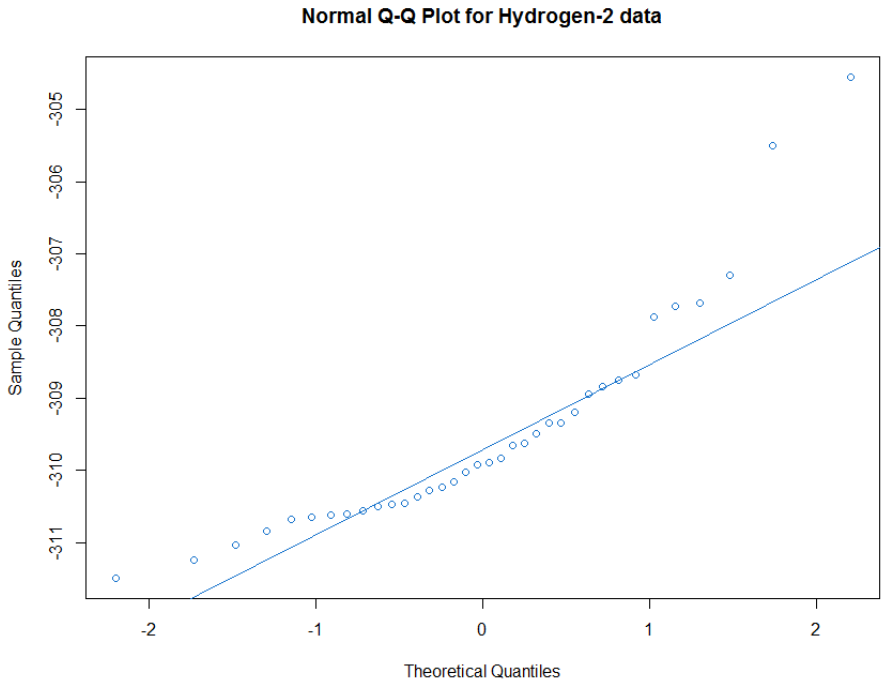

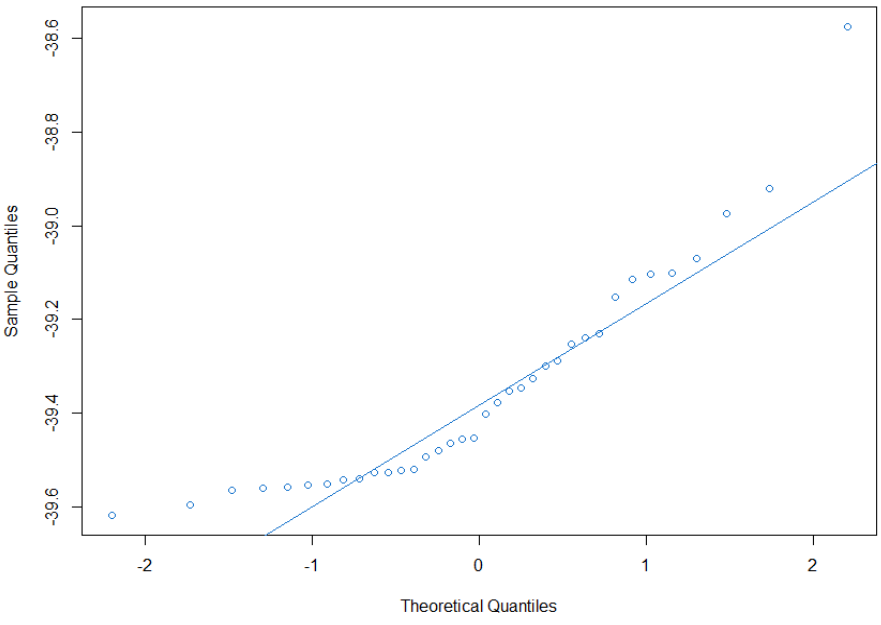

squares linear regression. This assumes covariate normality in the dataset, which can be tested via Q-Q plots and the Shapiro-Wilks normality test.

```
> D <- c(-309.622,-310.463,-307.688,-309.193,-310.231,-308.676,-310.475,-308.943,-309.897,-310.843,-310.616,-311.237,-310.657,-311.494,-311.041,-307.725,-310.167,-309.34,-310.024,-309.648,-310.495,-310.364,-310.61,-309.348,-305.495,-308.838,-309.827,-308.754,-309.486,-307.296,-310.683,-310.562,-310.281,-309.924,-304.548,-307.878)
> O <- c(-39.352,-39.565,-38.974,-39.23,-39.54,-39.327,-39.522,-39.153,-39.299,-39.559,-39.553,-39.494,-39.453,-39.618,-39.595,-39.101,-39.521,-39.464,-39.543,-39.48,-39.551,-39.401,-39.455,-39.346,-38.921,-39.24,-39.561,-39.115,-39.253,-39.071,-39.527,-39.527,-39.377,-39.288,-38.575,-39.104)
> DF9 <- data.frame(D,O)

Shapiro-Wilk normality test

data:  D
W = 0.85777, p-value = 0.0002888

data:  O
W = 0.87218, p-value = 0.0006443
```

On the Q-Q plots above, the outlying values appear to systematically diverge from the linear path expected of a normal dataset. For the dependent variable, the Shapiro-Wilk normality test returns a p-value less than the 5% significance level and so we reject the null hypothesis (p = 0.0002888). The same is found for the δ^{18}O data (p = 0.0006443). We therefore conclude that the dataset does indeed deviate from normality. As the data are unsuited to simple least squares linear regression, it is necessary to choose a non-parametric equivalent.

It is clear from the Q-Q plots that the deviation from normality is due to a number of extreme values. It might therefore be more appropriate to adopt a median-based linear model such as the Theil-Sen estimator (TSE). This approach is resilient to high-leverage extreme values, as it uses median values to calculate a line of best fit. It is also easily performed in R with the *Median-Based Linear Models* package ('mblm').

See below for use of the TSE on the Marble Hills isotope data. For comparison, the parametric approach has also been included underneath.

Theil-Sen Estimator (median-based linear regression)

```
> library(mblm)
> Model9 <- mblm(D ~ O, repeated = FALSE)
> summary.mblm(Model9)

Call:
mblm(formula = D ~ O, repeated = FALSE)

Residuals:
    Min      1Q  Median      3Q     Max
-0.8902 -0.4861  0.0000  0.3834  1.6257

Coefficients:
            Estimate      MAD V value Pr(>|V|)
(Intercept) -87.9885   0.6908       0 1.75e-07 ***
O             5.6302   4.3896  167618  < 2e-16 ***
```

```
---
Signif. codes:  0 ‘***’ 0.001 ‘**’ 0.01 ‘*’ 0.05 ‘.’ 0.1 ‘ ’ 1

Residual standard error: 0.5709 on 34 degrees of freedom
```

Simple least squares method (parametric linear regression)

```
>   <- lm(D ~ O)
> summary(PModel)

Call:
lm(formula = D ~ O)

Residuals:
     Min       1Q   Median       3Q      Max
-0.86140 -0.48607  0.00444  0.35103  1.40031

Coefficients:
            Estimate Std. Error t value Pr(>|t|)
(Intercept) -70.4967    16.0709  -4.387 0.000106 ***
O             6.0738     0.4084  14.873  < 2e-16 ***
---
Signif. codes:  0 ‘***’ 0.001 ‘**’ 0.01 ‘*’ 0.05 ‘.’ 0.1 ‘ ’ 1

Residual standard error: 0.5602 on 34 degrees of freedom
Multiple R-squared:  0.8668, Adjusted R-squared:  0.8629
F-statistic: 221.2 on 1 and 34 DF,  p-value: < 2.2e-16
```

The estimated coefficients of the median-based model give a line with an intercept of -87.9885 and a $\delta^{18}O$ coefficient (gradient) of 5.6302. We reject the null hypotheses that the intercept equals zero ($p << 0.00001$) and that the slope equals zero ($p << 0.00001$). Unsurprisingly, the p-value reported for the model as a whole is also significant ($p << 0.00001$), so we can very confidently reject the null hypothesis that $\delta^{2}H$ is independent of $\delta^{18}O$ in the Marble Hills dataset. The Theil-Sen Estimator models this relationship as:

$$\delta^{2}H = 5.6302 \times \delta^{18}O - 87.9885 \text{ ‰} \qquad \text{Equation 24}$$

It is worth noting that the parametric regression comes to the same conclusions, strongly rejecting both null hypotheses. It does however give markedly different values for the slope (6.0738) and intercept (-70.4967). The two models are compared below.

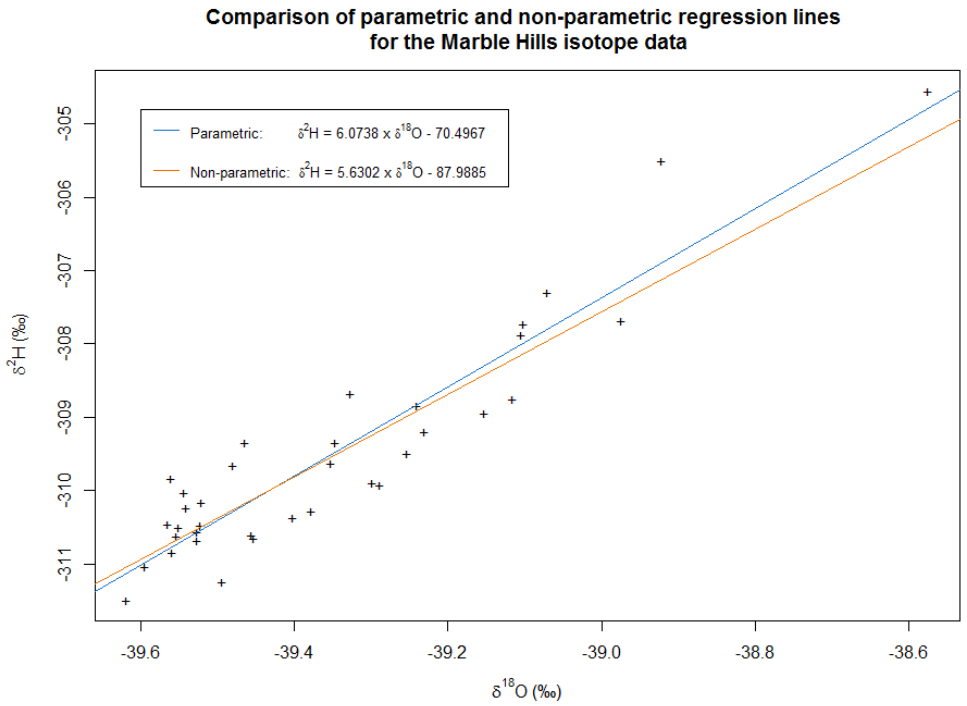

In the figure above, it is evident that the parametric regression line is affected by the two outlying values at the upper right corner of the graph, which have more leverage than the other measurements. In contrast, TSE better predicts the majority of the data, at the cost of higher residuals at extreme values.

Before accepting Equation 9 as our best estimate of the δ^2H / δ^{18}O relationship, we must first validate the model. Due to the choice of a non-parametric regression, the most appropriate measure of goodness of fit is the standard error of the estimate (s_{est}), rather than the square of the Pearson correlation coefficient (R^2). This can be calculated with the following formula:

$$s_{est} = \sqrt{\frac{1}{N}\sum_{X}(Y_X - \hat{Y}_X)^2}$$

Where $\hat{Y}_X$ is the value of Y predicted by the regression for a given value X; N is number of X values.

```
Fit9 <- predict(Model9, newdata = DF9)
Res9 <- D-Fit9
SEE9 <- sqrt((sum(Res9^2))/36)
[1] 0.5548362
```

The standard error of the estimate for the non-parametric model is: s_{est} = 0.5548362. This is very low, suggesting that the equation is a good fit to the data. However, it is important to note that this measure of goodness of fit is still affected by outliers (it is in effect a cousin of standard deviation). It is therefore not suited to comparing parametric and non-parametric models generated from the same dataset: most parametric models are designed to minimise the square of the residuals, thus any parametric technique based upon this dataset will return a low score, even though they are inappropriate for the distribution.

An alternative method of model validation is to draw plots based on residuals and fitted values. For instance, the relationship between observed values of δ^2H and those predicted from δ^{18}O observations can be used to evaluate the accuracy of a given model. In the first plot below, we see that the distribution of data

is fairly close to the line of best fit. This demonstrates that the model can predict δ^2H with tolerable accuracy. The second plot (residuals vs fitted values) demonstrates a relatively random distribution of residuals. This plot does highlight the two least-depleted measurements as potential outliers, however as this is does not have a significant effect on non-parametric regression then we are safe to include these data. With all checks complete, we may now accept Equation 9 as the best model for our Marble Hills isotope data.

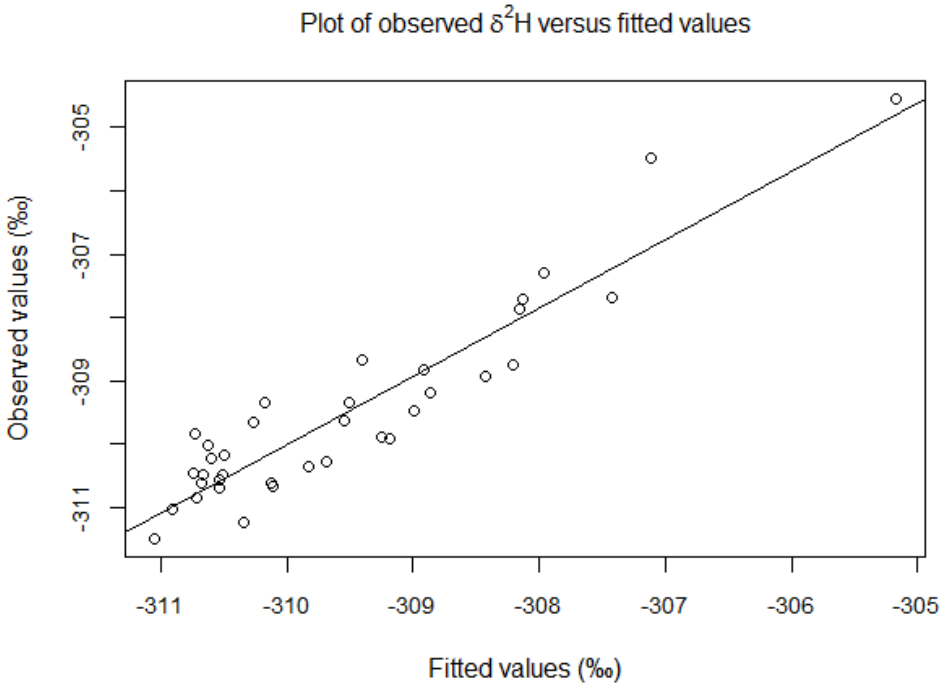

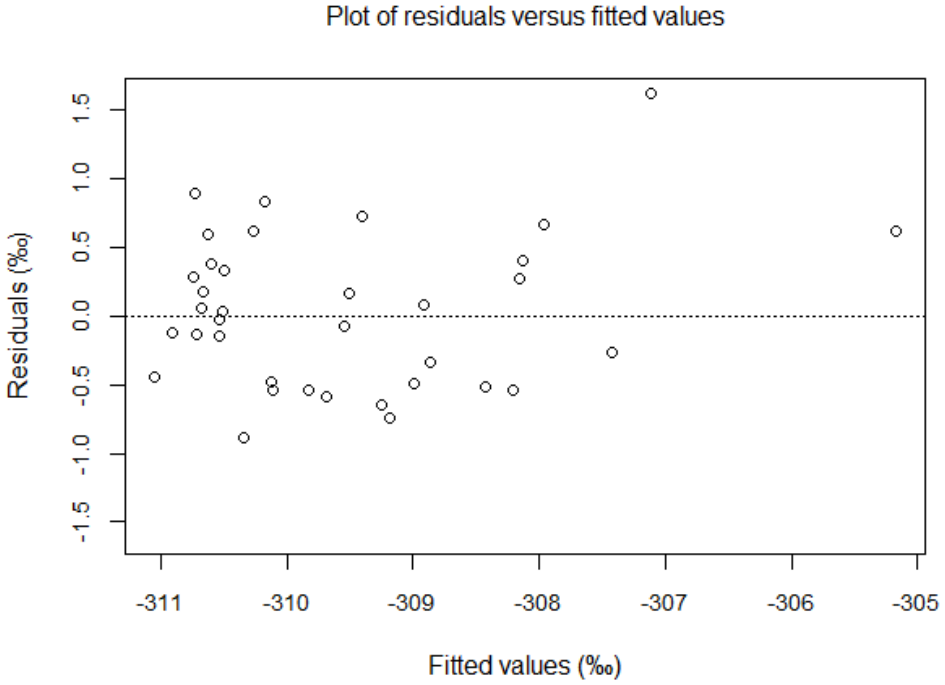

Appendix 4: Comparing residuals arising from Equations 7, 8 and 9

It is mathematically complicated to directly compare the linear models behind Equations 7, 8 and 9: the unbalanced design, lack of normality and need to factor in a covariate rule out all commonly used statistical tests. It is however easy to calculate the difference between the experimentally derived values and those predicted by the three equations (i.e. the residuals). We can then test the null hypothesis that the residuals for the three equations arise from the same population (H_0: $\mu_9 = \mu_8 = \mu_7$).

First, we must generate the residual datasets:

```
> #Models
> library(mblm)
> Model7 <- lm(D~O,data=DF7)
> Model8 <- lm(D~O,data=DF8)
> Model9 <- mblm(D~O,data=DF9, repeated = FALSE)
> #Fitted values
> DF <- data.frame(O)
> Fit7 <- predict(Model7,newdata=DF);
> Fit8 <- predict(Model8,newdata=DF);
> Fit9 <- predict(Model9,newdata=DF);
> #Residuals
> Res7 <- D-Fit7;
> Res8 <- D-Fit8;
> Res9 <- D-Fit9;
> #Boxplots
> Residuals <- c(Res7,Res8,Res9)
> Equation <- factor(c(rep("Equation 7",36),rep("Equation 8",36),rep("Equation 9",36)))
> levels=c("Equation 7","Equation 8","Equation 9")
> DATA <- data.frame(Residuals,Equation)
> require(ggplot2)
> ggplot(DATA, aes(x = Equation, y = Residuals)) + geom_boxplot() + scale_x_discrete(name =
"Model")+ scale_y_continuous(name = "Residual / \u2030")
```

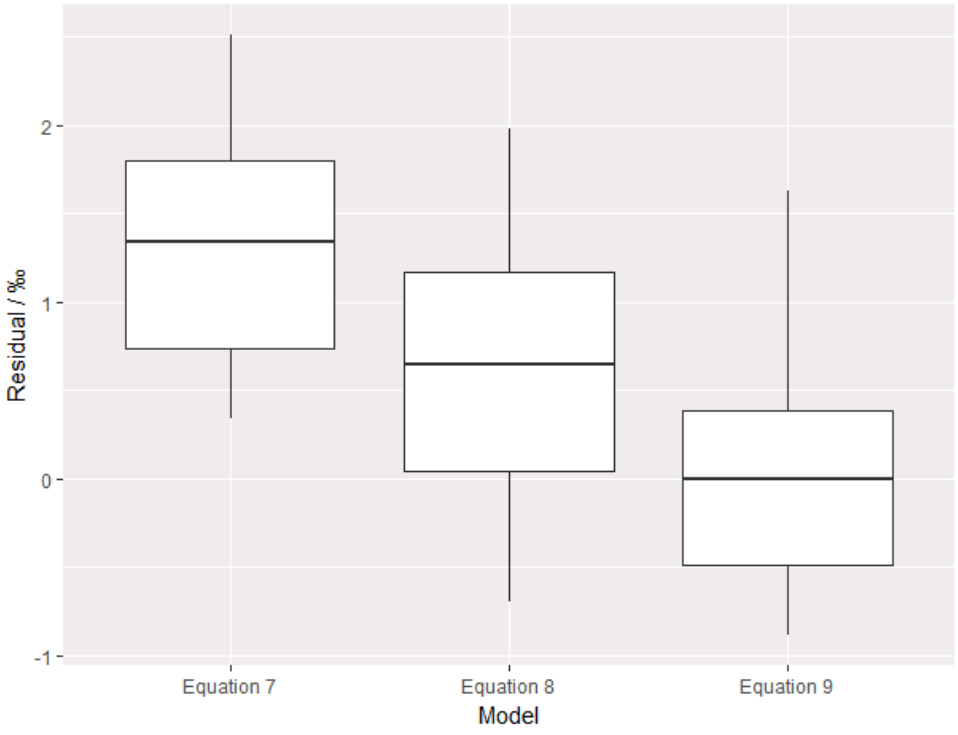

We then test for normality in our datasets. If residuals arise only due to random error – as should be the case for any appropriate model – then they should be normally distributed. Conversely, non-normal distributions may indicate systematic error in a model, causing fitted values to deviate more over certain ranges.

```
> shapiro.test(Res7)

        Shapiro-Wilk normality test
data:  Res7
W = 0.95872, p-value = 0.1962

> shapiro.test(Res8)
        Shapiro-Wilk normality test
data:  Res8
W = 0.97192, p-value = 0.4803

> shapiro.test(Res9)
        Shapiro-Wilk normality test
data:  Res9
W = 0.95976, p-value = 0.2114
```

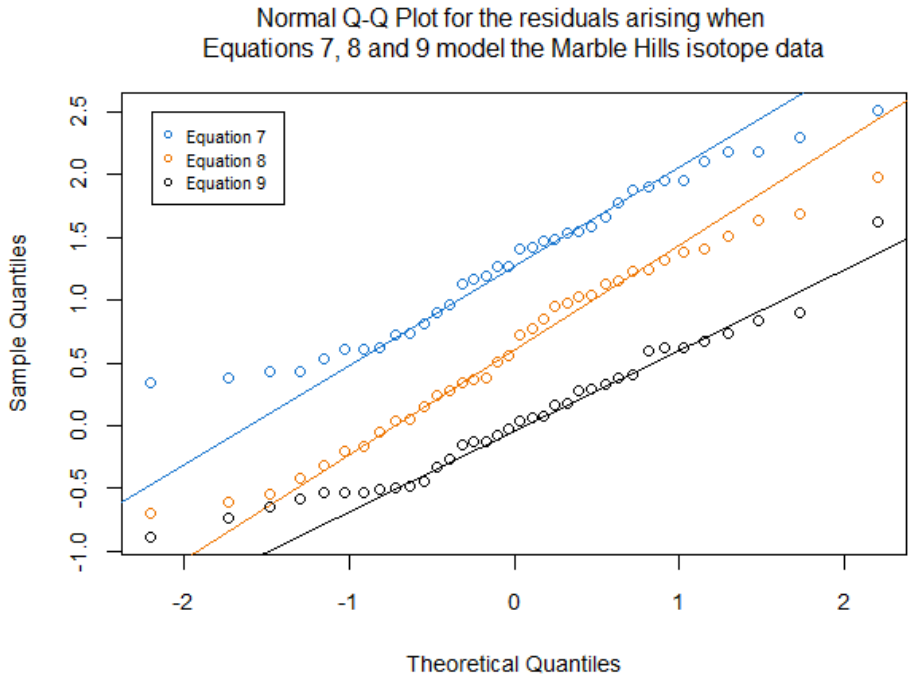

All of the datasets are normal within the 95% confidence level. Whilst a normal distribution of residuals does not necessarily indicate an appropriate model, it does at the very least indicate that any of the equations *could* be appropriate for the Marble Hills data.

Now that the datasets have been created and normality has been confirmed, we can proceed with our first one-way ANOVA. This tests whether or not all three groups of residuals are likely to be from the same population (i.e. none of the models fit the data significantly better than the others).

```
> Residuals <- c(Res7,Res8,Res9)
> Equation <- factor(c(rep("Equation 7",36),rep("Equation 8",36),rep("Equation 9",36)))
> levels=c("Equation 7","Equation 8","Equation 9")
```

```
> DATA <- data.frame(Residuals,Equation)
> fit <- anova(lm(Residuals ~ Equation, data=DATA))
> cbind(fit, 'CriticalValue' = qf(1-.05, fit[1,1], fit[2,1]))
           Df   Sum Sq    Mean Sq F value       Pr(>F) CriticalValue
Equation    2 29.13886 14.5694300 35.8534 1.354072e-12      3.082852
Residuals 105 42.66792  0.4063612      NA           NA      3.082852
```

The F-statistic is greater than the critical value at the 5% significance level (35.8534 > 3.0829, df_1 = 2, df_2 = 105, α = 0.05). We therefore reject the null hypothesis (p << 0.0001). This means that at least one of the groups of residuals is statistically different from the others; to find out which groups differ, we run Tukey's Honest Significant Difference test:

```
> TukeyHSD(aov(Residuals ~ Equation, data=DATA),conf.level=0.95)
  Tukey multiple comparisons of means
    95% family-wise confidence level

Fit: aov(formula = Residuals ~ Equation, data = DATA)

$Equation
                            diff        lwr        upr     p adj
Equation 8-Equation 7 -0.6960300 -1.0532396 -0.3388205 0.0000308
Equation 9-Equation 7 -1.2703901 -1.6275997 -0.9131805 0.0000000
Equation 9-Equation 8 -0.5743601 -0.9315696 -0.2171505 0.0006518
```

This test confirms that all groups of residuals are significantly different. From this we can infer that, when modelling the Marble Hills isotope data, one equation must be more appropriate than the others. From the boxplot above, it is evident that Equation 9 has smaller residuals than the other equations. We can quantify this by calculating the sum of the squared residuals (RSS) for each of the three equations:

$$RSS = \sum_X (Y_X - \hat{Y}_X)^2$$

where Y_x is the measured δ^2H and $\hat{Y}_x$ is the predicted δ^2H for a given value of X ($\delta^{18}O$). The difference in goodness of fit can also be expressed as the standard error of the estimate, s_{est} (see Appendix 3).

```
> RSS7 <- sum(Res7^2)
> RSS8 <- sum(Res8^2)
> RSS9 <- sum(Res9^2)
> SEE7 <- sqrt((RSS7)/36)
> SEE8 <- sqrt((RSS8)/36)
> SEE9 <- sqrt((RSS9)/36)
>
> summarise <- data.frame("Equation 7"=c(coef(Model7)["O"],coef(Model7)["(Intercept)"],RSS
7,SEE7),"Equation 8"=c(coef(Model8)["O"],coef(Model8)["(Intercept)"],RSS8,SEE8),"Equation 9
"=c(coef(Model9)["O"],coef(Model9)["(Intercept)"],RSS9,SEE9),row.names=c("Slope","Intercept
","Residual sum of squares","Standard error of the estimate"))


> summarise
                              Equation.7 Equation.8  Equation.9
Slope                        7.285290  7.9805616   5.6301775
Intercept                   -24.128573  3.9898488 -87.9885488
Residual sum of squares      74.799096 28.2893639  11.0823567
Standard error of the estimate  1.441441  0.8864624   0.5548362
```

The much lower residual sum of squares (and subsequent standard error of the estimate) demonstrates that Equation 9 is a better fit for the data than equations 7 and 8.

While these analyses have verified that Equation 9 is the best of the available equations for modelling the Marble Hills isotope data, and that it is indeed a good fit for the data, they have not strictly proven that it is significantly better than all linear models with a gradient consistent with meteoric water (the intercept could, in theory, be the dominant factor). Consequently, it is important to examine other glaciochemical signatures before concluding that the TBIS are definitely of subglacial origin.

Appendix 5: Spatial analysis of TBIS

The original block of blue ice was sectioned along three perpendicular axes: these were denoted x, y and z, where low x-values indicate proximity to the Marble Hills; low y-values indicate proximity to the mouth of Horseshoe Valley; and low z-values indicate proximity to the surface. Hereafter, x, y and z will be referred to as width, length and depth, respectively.

Trends

Multivariate analysis of covariance was run on a linear model predicting $\delta^{18}O$ from x, y, z and their interaction terms. This founds that there are no linear relationships between $\delta^{18}O$ and location.

```
> summary(lma_O)

Call:
lm(formula = O.BIA ~ x * y * z, data = SpatialData_NoOut)

Residuals:
     Min       1Q   Median       3Q      Max
-0.30256 -0.12122 -0.00356  0.06615  0.42638

Coefficients:
              Estimate Std. Error  t value Pr(>|t|)
(Intercept) -3.955e+01  2.958e-01 -133.717   <2e-16 ***
x            1.991e-02  2.940e-02    0.677    0.504
y            1.662e-02  1.484e-02    1.120    0.273
z           -1.172e-02  2.144e-02   -0.547    0.589
x:y         -2.151e-03  1.477e-03   -1.456    0.157
x:z          2.088e-03  2.139e-03    0.976    0.338
y:z          8.050e-04  1.079e-03    0.746    0.462
x:y:z       -1.594e-04  1.090e-04   -1.462    0.155
---
Signif. codes:  0 ‘***’ 0.001 ‘**’ 0.01 ‘*’ 0.05 ‘.’ 0.1 ‘ ’ 1

Residual standard error: 0.1881 on 27 degrees of freedom
  (1 observation deleted due to missingness)
Multiple R-squared:  0.2426, Adjusted R-squared:  0.04623
F-statistic: 1.235 on 7 and 27 DF,  p-value: 0.3184
```

Equivalent analyses found no significant spatial trend for $\delta^{2}H$, Na^{+}, K^{+}, Mg^{2+}, F^{-}, NO_3^{-} and DOC. However, p-values of less than 0.05 were observed for Ca^{2+}, Cl^{-} and SO_4^{2-}:

	p-values						
Variable	x	y	z	x*y	x*z	y*z	x*y*z
Ca^{2+}	0.0912	**0.0186**	**0.0005**	0.3415	0.3415	**0.0084**	0.1365
Cl^{-}	0.4095	0.1129	0.1797	0.1425	0.1425	**0.0462**	0.0702
SO_4^{2-}	0.0509	0.0831	**0.0173**	0.2071	0.2071	**0.0488**	0.1532

Ca^{2+} and SO_4^{2-} ions both correlated with depth. This may be due to the angle at which ice arrives at the sampling site: ice arriving at different depths may have had different lengths of contact time with the subglacial environment, and therefore picked up more for Ca^{2+} (liberated from bedrock) and SO_4^{2-} (oxidised under subglacial conditions). However, if this were the case then a similar correlation with DOC would also be expected, and none was observed. One alternative explanation is that the TBIS taken from a given depth happen to contain the remnants of a temporal spike in Ca^{2+} or SO_4^{2-} concentration. For instance, a rock fall higher up Horseshoe Valley may lead to the local enrichment of Ca^{2+} ions as the limestone debris and surrounding ice sink into the glacier. A spike in the concentration of SO_4^{2-}, meanwhile, may be caused by temporary elevation in atmospheric SO_4^{2-}, as may occur due to major volcanic activity. Nevertheless, it is unlikely that any of these trends could be determined from one sampling site alone: a dedicated study spanning a significantly greater range in x, y and z values would be necessary.

See below for a scatterplot of calcium concentration versus 3D location within the original block of terminal blue ice. This has been scaled so that the z-axis is negative: samples closest to the surface are at the top of the plot (away from the origin), because that seems more intuitive for the observer.

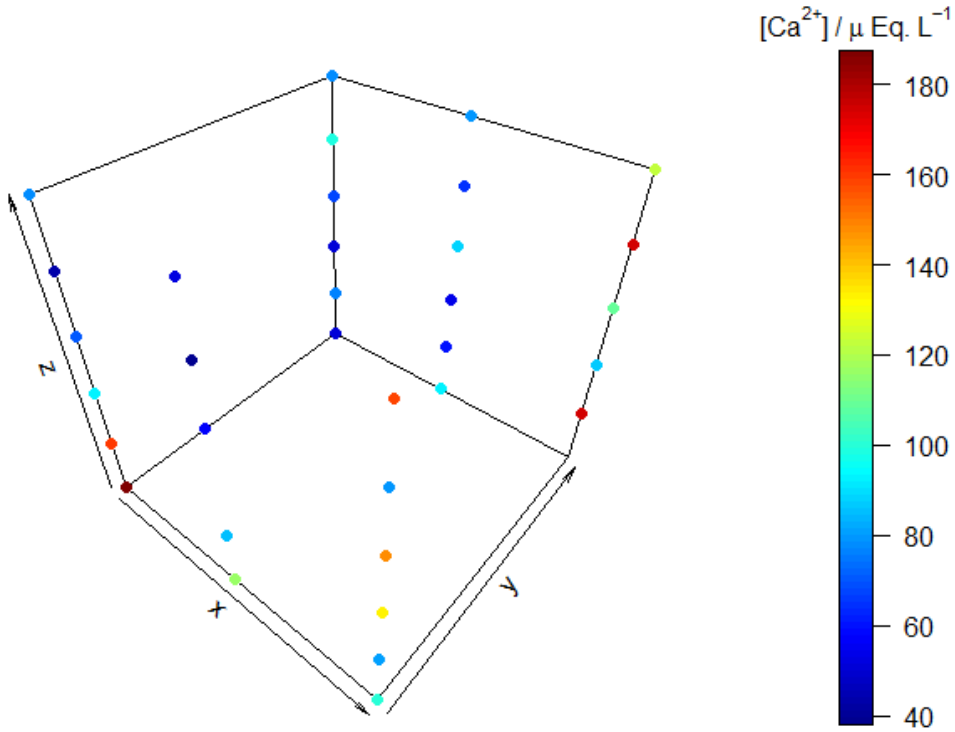

The plot shows that even if a statistical relationship exists between Ca^{2+} concentration and the z-axis, there is not an enrichment of Ca^{2+} ions closer to the surface, as would be expected if the ions were deposited by katabatic winds (see section 3.2.3). This can be seen more clearly in a scatterplot of calcium concentration against depth (below). There is at least as much variation in Ca^{2+} concentration between samples taken from the same depth than between different depths, and the top samples show no enrichment at all.

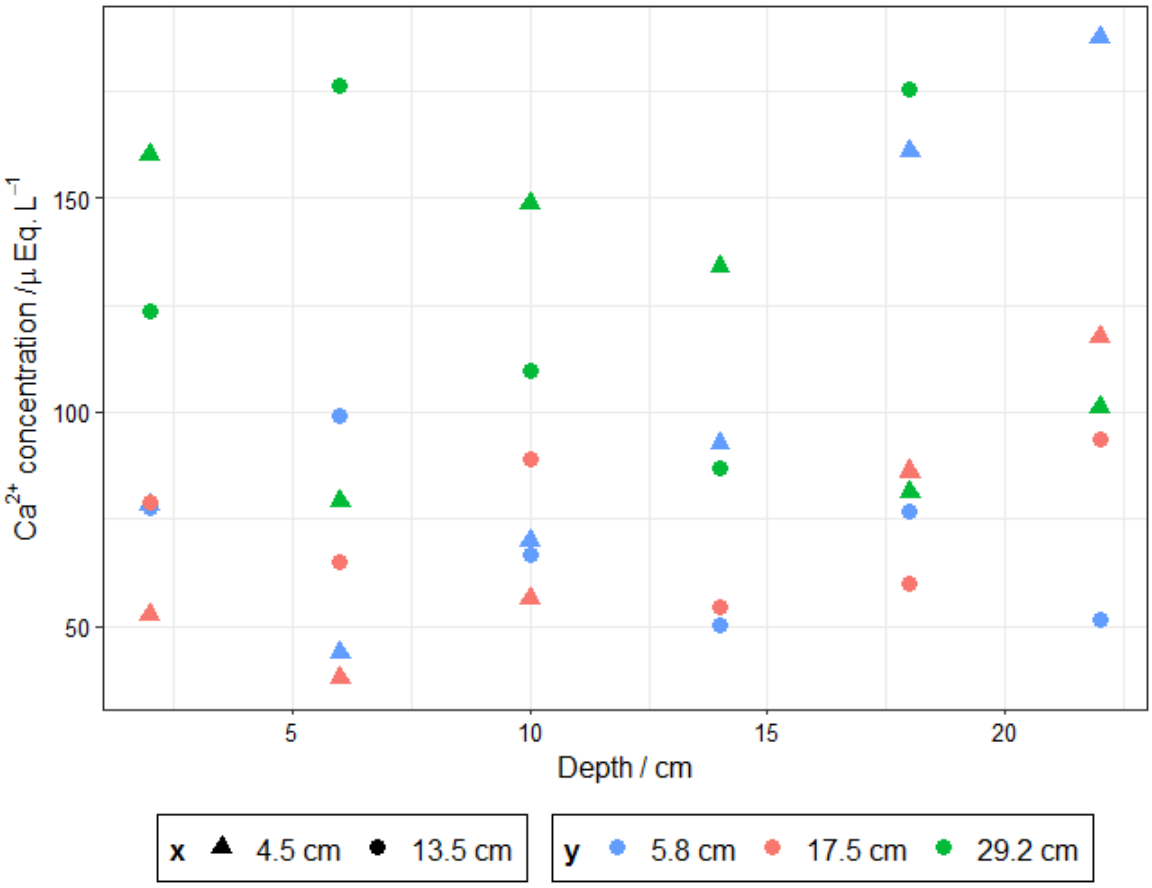
Ca2+ concentration /µ Eq. L−1
150
100
50
5
10
15
20
Depth / cm
x
4.5 cm
13.5 cm
y
5.8 cm
17.5 cm
29.2 cm

Appendix 6: Comparison of blue, white and grey icebergs

The icebergs observed in Lago Steffen are notably variable in certain physical characteristics. They can be loosely classified according to their colouration, density and structure. White icebergs are fairly colourless, with a high albedo and a moderate density; they contained a few pockets of suspended sediment, but were generally clear enough to see miniature hydrological channels running throughout the structure. Blue icebergs had a moderate albedo (and reflected blue light) and an extremely high density – unlike their white counterparts, there were no veins running through the blue icebergs. Grey icebergs contained clay-like deposits and were rich in suspended sediment. They were lowest in terms of both density and albedo.

These categories are subjective: certain regions of ice had characteristics lying between different classifications. For instance, some white icebergs had regions with an intermediate concentration of suspended sediment. However, the majority of icebergs could be classified without difficulty. Analysis of variance was used to test whether or not these classifications could be used to predict the chemical characteristics of the ice better than the average values of the whole population.

Suspended sediment

The dry mass of sediment filtered out of each sample was estimated as per section 2.6. These data are far from being normally-distributed ($p = 1.192 \times 10^{-8}$, Shapiro-Wilk), and so the non-parametric Kruskal-Wallis test is the most appropriate statistical technique for a comparison between the different populations of icebergs. Unsurprisingly, the Kruskal-Wallis test produced a χ^2 value that was greater than the critical value at the 5% significance level ($\chi^2 = 21.294$, $\chi^2_{crit} = 14.067$) and so we reject the null hypothesis ($p = 0.003358$). This means that not all samples originate from the same distribution (i.e. sediment content is affected by iceberg classification).

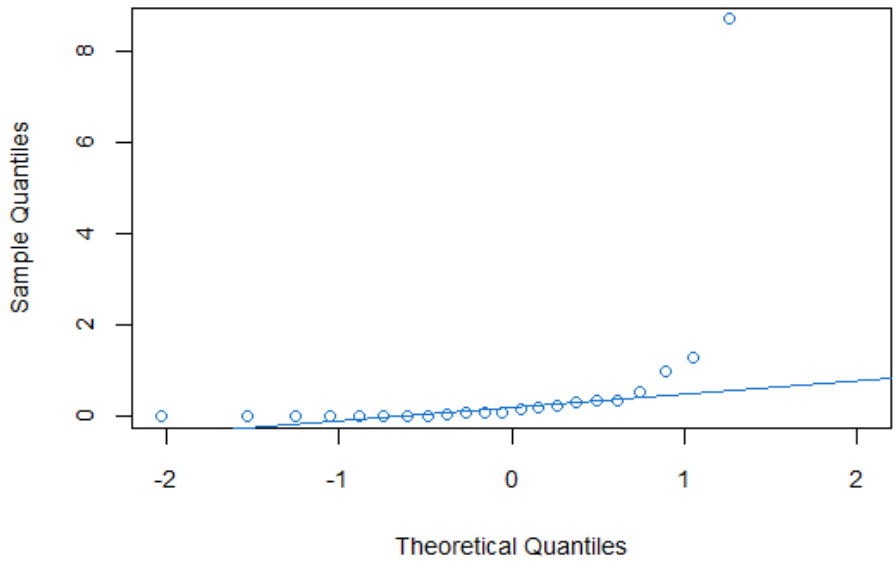


```
> kruskal.test(Sed ~ Iceberg, data = SGDF)

        Kruskal-Wallis rank sum test
```

```
data:  Sed by Iceberg
Kruskal-Wallis chi-squared = 21.294, df = 7, p-value = 0.003358
```

Knowing that there is a significant relationship between iceberg classification and sediment content, we can perform a post-hoc Dunn test in order to investigate which pairs are significantly different:

```
> dunn.test(x=Sed,g=Type)
  Kruskal-Wallis rank sum test

data: Sed and Type
Kruskal-Wallis chi-squared = 13.8676, df = 2, p-value = 0


                           Comparison of Sed by Type
                                (No adjustment)
Col Mean-|
Row Mean |       Blue       Grey
---------+----------------------
    Grey |  -3.633637
         |    0.0001*
         |
   White |  -0.896034   2.353989
         |     0.1851    0.0093*

alpha = 0.05
Reject Ho if p <= alpha/2
```

At this significance level ($\alpha = 0.05$), we reject the null hypothesis for both the grey-blue and grey-white pairings ($p_{Grey\text{-}Blue} = 0.0001$; $p_{Grey\text{-}White} = 0.0093$). Conversely, we accept the null hypothesis for the white-blue pairing ($p_{White\text{-}Blue} = 0.1851$). This indicates that the population of grey icebergs has significant stochastic dominance over both the blue and white populations. Neither the blue or white icebergs shows stochastic dominance over the other at the 5% significance level: samples from blue and white icebergs are therefore assumed to share the same distribution.

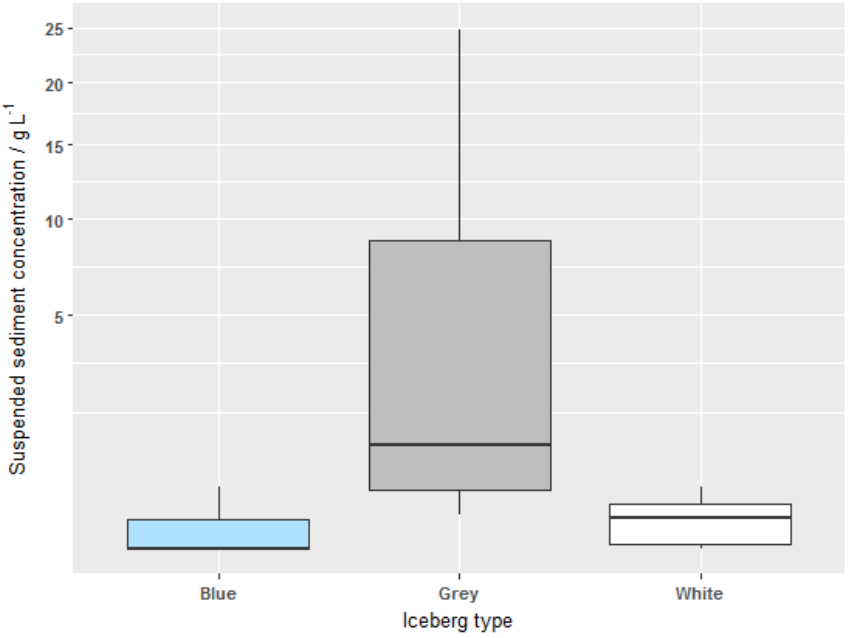

Stable isotopes of water

The first characteristics tested were the stable isotopes of water: δ^2H, δ^{18}O and δ^{17}O. The delta values observed for each of the three classifications of ice were initially displayed as three boxplots (see following pages). These plots demonstrate a large amount of overlap between the white icebergs and the other populations; the blue and the grey icebergs do however appear more distinct. One-way ANOVA was then used to compare the mean δ^2H value of the three different populations:

```
> # Test for normality in the entire dataset
> shapiro.test(SGDF$O17)

         Shapiro-Wilk normality test

 data:  SGDF$D
 W = 0.97935, p-value = 0.8836

> # Test for normality within each of the three populations

> shapiro.test(c(SGDF$D [1:3],SGDF$D [19:21]))

         Shapiro-Wilk normality test

 data:  c(SGDF$D[1:3], SGDF$D[19:21])
 W = 0.9205, p-value = 0.5089

 > shapiro.test(c(SGDF$D [4:6],SGDF$D [10:12],SGDF$D [16:18]))

         Shapiro-Wilk normality test

 data:  c(SGDF$D[4:6], SGDF$D[10:12], SGDF$D[16:18])
 W = 0.95728, p-value = 0.7695

 > shapiro.test(c(SGDF$D [7:9],SGDF$D [13:15],SGDF$D [22:24]))

         Shapiro-Wilk normality test

 data:  c(SGDF$D[7:9], SGDF$D[13:15], SGDF$D[22:24])
 W = 0.88484, p-value = 0.1764

> # Data appear normally distributed

> # Proceed with parametric analysis of variance

> SG.D <- aov(D~Type,data=SGDF)
 > summary(SG.D)

             Df Sum Sq Mean Sq F value Pr(>F)
 Type         2  841.6   420.8   5.348 0.0133 *
 Residuals   21 1652.3    78.7
 ---
 Signif. codes:  0 ‘***’ 0.001 ‘**’ 0.01 ‘*’ 0.05 ‘.’ 0.1 ‘ ’ 1
```

The F-statistic was greater than the critical value at the 5% significance level (5.348 > 4.349, $df_N = 2$, $df_D = 21$) and so we reject the null hypothesis ($p = 0.0133$, $\alpha = 0.05$). The analysis therefore found that there is a significant relationship between δ^2H and the classification of an iceberg.

This test indicates that iceberg colour should be taken into consideration when estimating the average composition of a group of icebergs. However, it does not indicate *how* these categories should be taken into consideration: we know that some population means are different, but not which populations. Having established that classification is in fact a useful predictor for δ^2H, it is now possible to apply a post-hoc test to investigate which of the population means are significantly different. Tukey's HSD (Honest Significant Difference test) is chosen for this; it is a standard multistep comparison procedure, which tests each possible pair of means (white vs blue, white vs grey, and blue vs grey) for a significant difference.

```
> # Post-hoc testing
> TukeyHSD(x=SG.D)

  Tukey multiple comparisons of means
    95% family-wise confidence level

Fit: aov(formula = D ~ Type, data = SGDF)

$Type
         diff        lwr       upr     p adj
G-B 13.299222   2.759488 23.838956 0.0120023
W-B  3.464778  -8.319003 15.248558 0.7421690
W-G -9.834444 -21.618225  1.949336 0.1132543
```

Tukey's HSD indicates that there is a significant difference between the grey and blue population means ($p = 0.0120023$, $\alpha = 0.05$). Conversely, we accept the other two null hypotheses at the 5% significance level: the population of white icebergs does not differ significantly the blue population ($p = 0.7421690$); nor is there a significant difference between the white and the grey populations ($p = 0.1132543$). This finding can be seen quite clearly on the boxplot for the measurements of δ^2H within the three populations.

The same procedure was carried out for the $\delta^{18}O$ and $\delta^{17}O$ datasets. As with the measurements of $\delta^{2}H$, it was found that there was a significant relationship between iceberg classification and $\delta^{18}O$ ($5.559 > 4.349$, $df_N = 2$, $df_D = 21$) and so we reject the null hypothesis ($p = 0.0115$, $\alpha = 0.05$). Once again, Tukey's HSD indicates that the only significantly different pair was the comparison of grey and blue populations of iceberg samples ($p = 0.0103262$, $\alpha = 0.05$). Analysis of the $\delta^{17}O$ data produces the same findings, only with a stronger likelihood of significance: one-way ANOVA revealed a relationship between classification and $\delta^{17}O$ at the 1% significance level ($6.027 > 4.349$, $df_N = 2$, $df_D = 21$, $p = 0.00854$, $\alpha = 0.01$). Lastly, Tukey's HSD confirmed that this is due to a significant difference between the grey and the blue populations ($p = 0.0082437$, $\alpha = 0.05$).

The purpose of these analyses was to examine whether or not certain physical characteristics of a calved iceberg are associated with certain variations in isotopic signature. This is an important consideration if iceberg sampling is to be used to form a representative idea of glacial composition. To illustrate, if 40% of the icebergs that calve of a particular glacier happen to be blue – and blue icebergs are associated with more depleted delta values for $\delta^{2}H$, $\delta^{18}O$ and $\delta^{17}O$ – then the sampling protocol should ensure that 40% of the samples are from blue icebergs. Alternatively, researchers could calculate representative values for each of the classifications of iceberg, and then use their relative abundances to calculate a weighted mean that is representative of the glacier.

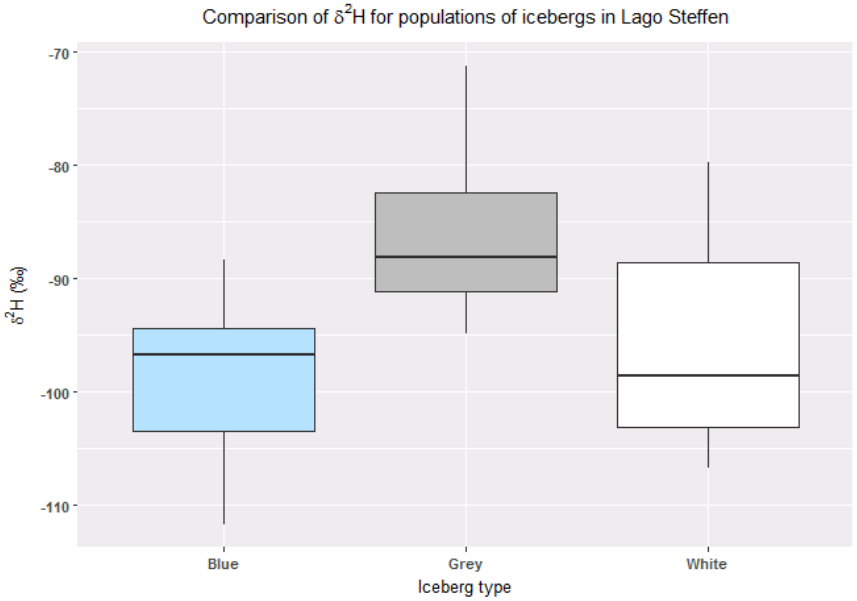

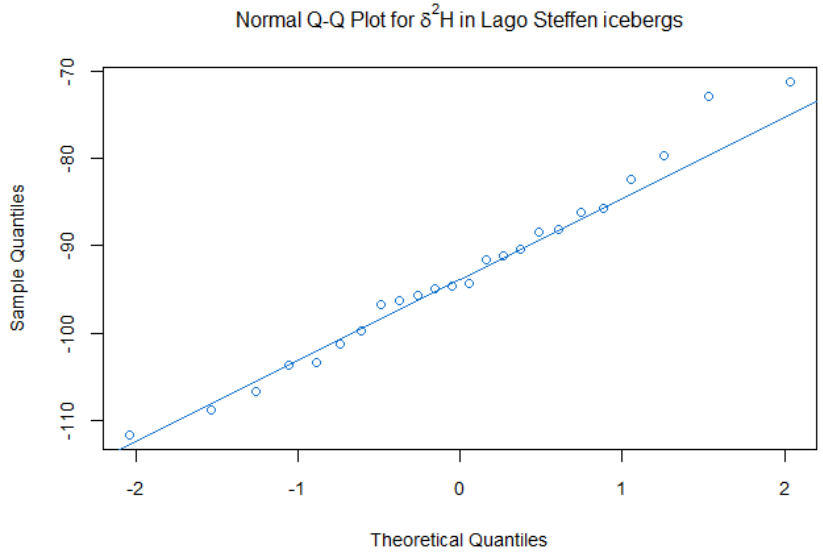

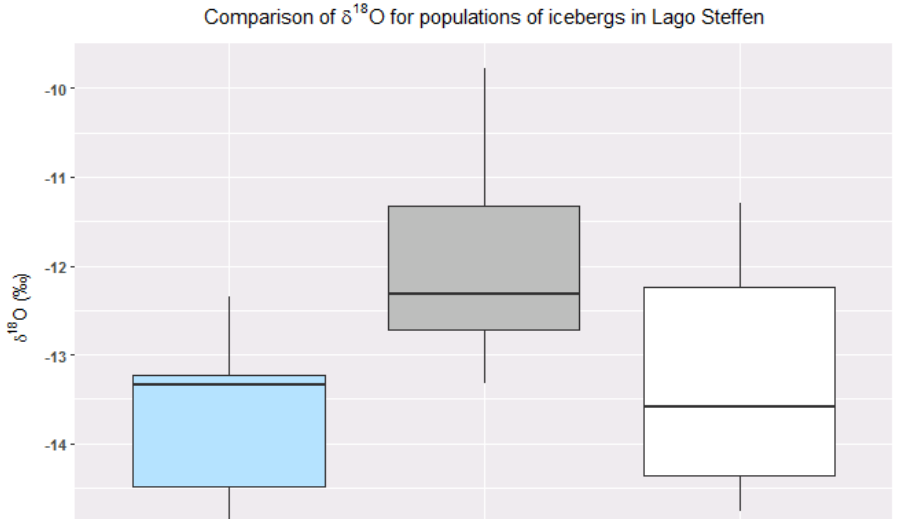
Comparison of δ18O for populations of icebergs in Lago Steffen
δ18O (‰)
-10
-11
-12
-13
-14

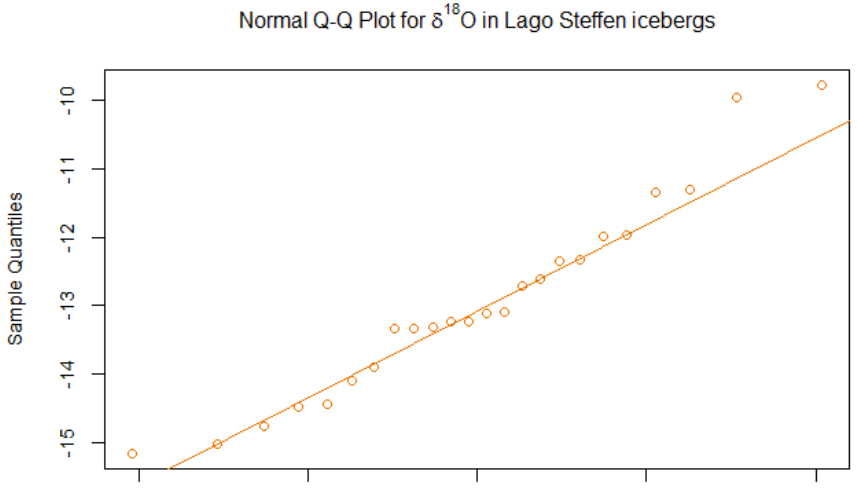
Normal Q-Q Plot for δ18O in Lago Steffen icebergs
Sample Quantiles
-10
-11
-12
-13
-14
-15

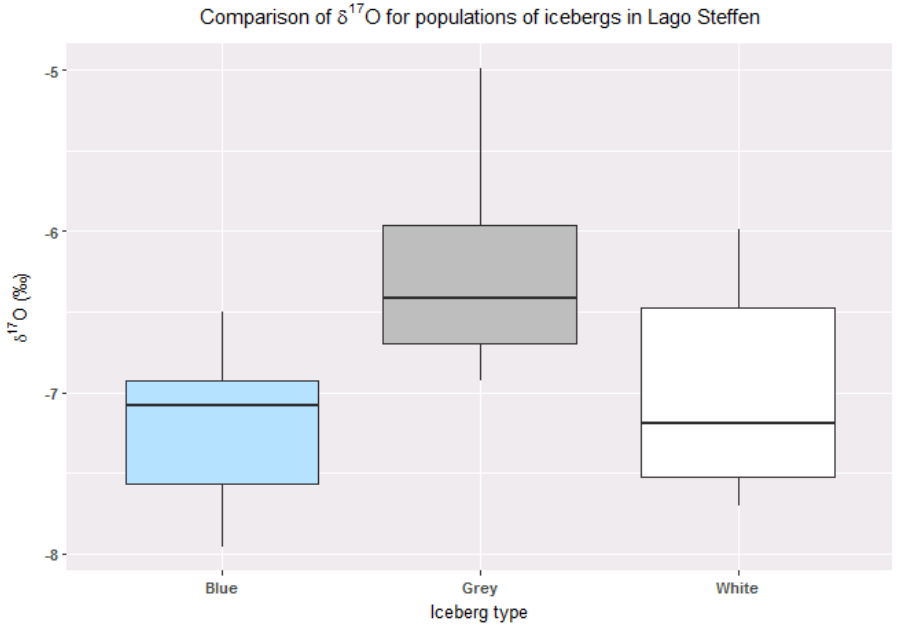
Comparison of δ17O for populations of icebergs in Lago Steffen
δ17O (‰)
-5
-6
-7
-8
Blue
Grey
White
Iceberg type

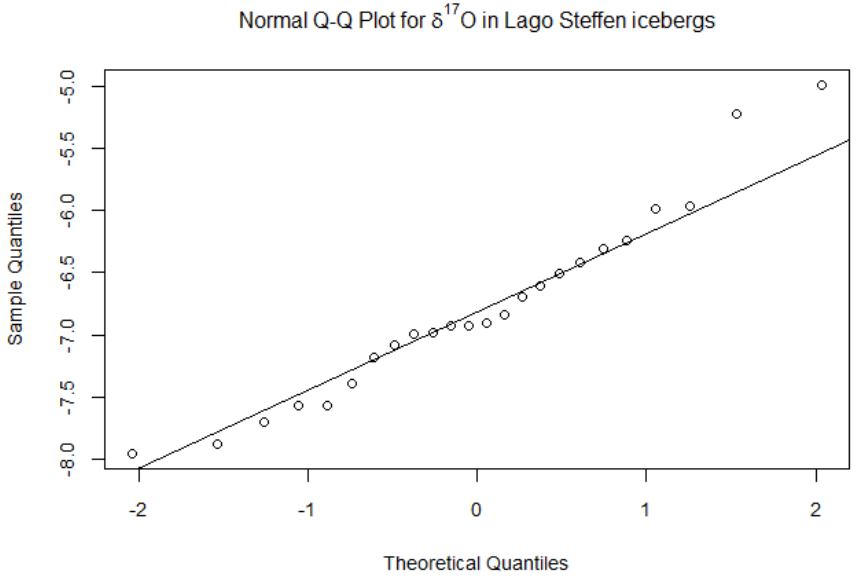
Normal Q-Q Plot for δ17O in Lago Steffen icebergs
Sample Quantiles
-5.0
-5.5
-6.0
-6.5
-7.0
-7.5
-8.0
-2
-1
0
1
2
Theoretical Quantiles

Dissolved Organic Carbon

Unlike for the water isotopes, the DOC data are not normally distributed (p = 0003628, Shapiro-Wilk). This is almost entirely due to the high value of 198.6 ppb for sample SG13. Although this first appears to be an outlier, it has not been excluded from the dataset. This is because SG13 also contained an extremely large quantity of suspended sediment (almost 25 g L^{-1}) and was notably enriched in Ca^{2+} relative to the other samples. Moreover, it is not uncommon to see DOC observations higher than 200 ppb in other temperate glaciers. Consequently, the most likely explanation is that the high concentrations of sediment were collected from a wet glacier-rock interface, a process in which DOC was also acquired. Note that this does not confirm that SG13 is a basal sample, as similar glacier-rock interfaces are found along the margins of the glacier.

```
Shapiro-Wilk normality test

data:  SGDF$DOC
W = 0.8055, p-value = 0.0003628
```

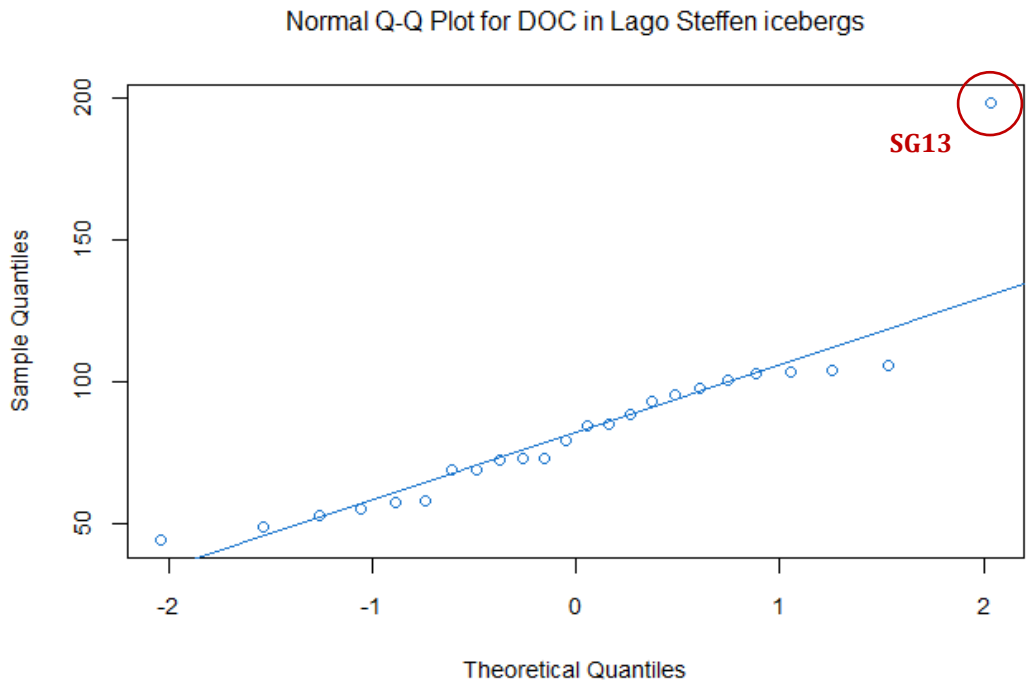

Due to this non-normal distribution, ANOVA is not an appropriate test of population means. A non-parametric Kruskal-Wallis test was instead performed to compare DOC data from blue, grey and white icebergs:

```
> kruskal.test(DOC ~ Iceberg, data = SGDF)

        Kruskal-Wallis rank sum test

data:  DOC by Iceberg
Kruskal-Wallis chi-squared = 7.52, df = 7, p-value = 0.3768
```

The null hypothesis was accepted ($p = 0.3768$, $\alpha = 0.05$). This indicates that there is not a significant relationship between the classification of an iceberg and its DOC content. This is reflected in the great deal of overlap between the boxplots for blue, grey and white icebergs below.

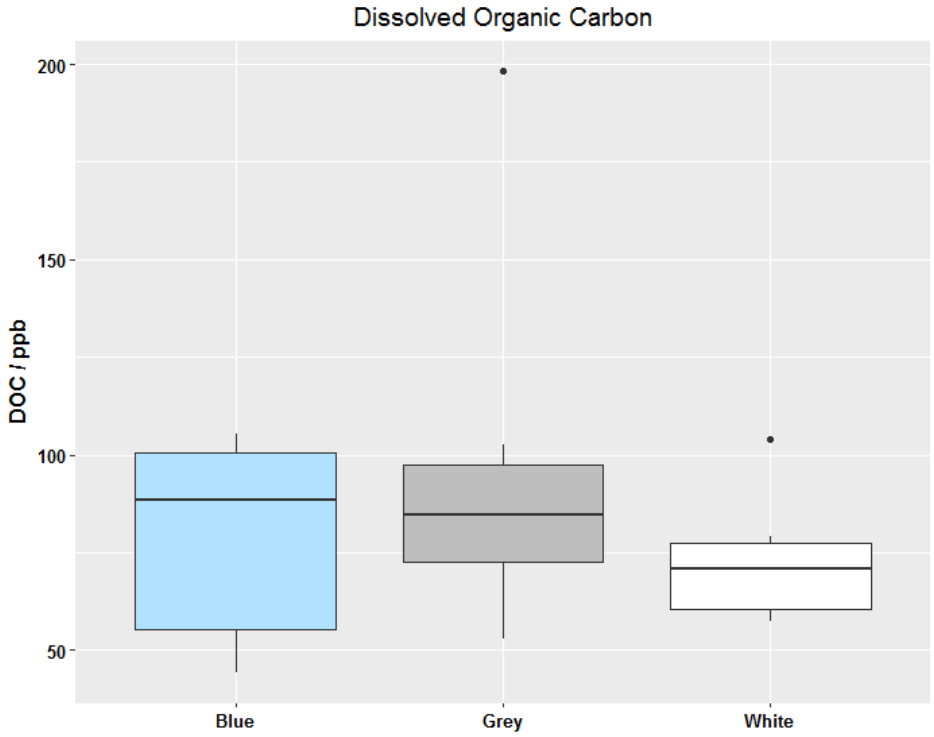

Major ions

None of the observations of major ions have normal distributions – the Shapiro-Wilk p-value is actually approaching zero in all eight species measured in notable quantities (see table below). In most cases, this deviation from normality is due to a high value in a single iceberg sample. For Na^+, K^+, Mg^{2+}, F^- and NO_2^-, this peak measurement was observed in SG5, a sample of extremely dense blue ice with no observable suspended sediment load. Ca^{2+} and Cl^- both peaked in SG13 – the grey ice sample with the highest amount of suspended sediment (almost 25 g L^{-1}) – while the highest sulphate concentration was observed in SG7, the grey sample with the second greatest mass of suspended sediment (around 12 g L^{-1}). As with the DOC, none of these observations have been excluded from the analysis on the basis that they are well within the normal range for temperate glaciers and can be explained by the history of the given ice sample.

The Kruskal-Wallis test was again chosen as the most appropriate test with which to compare population means. The χ^2 values of the analyses were all less than the critical value at the 5% significance level (χ^2_{crit} = 14.067), and so the null hypothesis was accepted ($p > 0.05$). Iceberg colour is therefore not a significant predictor of the concentration of dissolved major ions. See below for χ^2 values, boxplots and scatterplots for the individual ions.

Ion	Shapiro-Wilk Normality	Kruskal-Wallis Rank Sum Test (df = 7)	
	p-value	χ^2	p-value
Na^+	6.338×10^{-7}	6.6729	0.4637
K^+	1.831×10^{-6}	9.2982	0.2319
Ca^{2+}	1.792×10^{-8}	11.941	0.1025
Mg^{2+}	2.102×10^{-5}	8.4913	0.2913
Cl^-	2.153×10^{-5}	6.3912	0.4949
F^-	1.749×10^{-9}	10.119	0.1819
NO_2^-	1.063×10^{-6}	13.9000	0.0530
SO_4^{2-}	2.100×10^{-6}	6.7968	0.4503

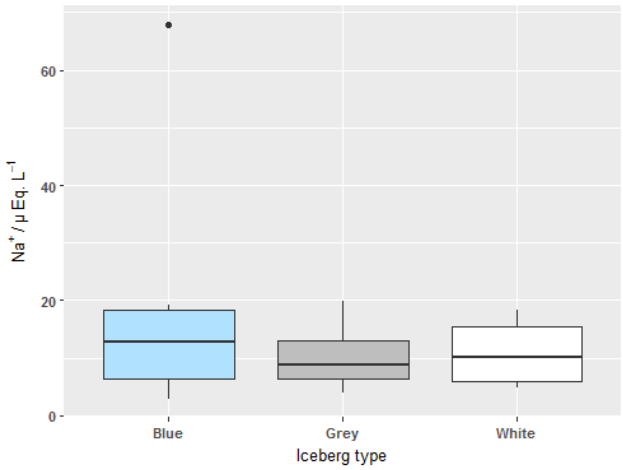
60
40
20
0
Na+ / µ Eq. L−1
Blue
Grey
White
Iceberg type

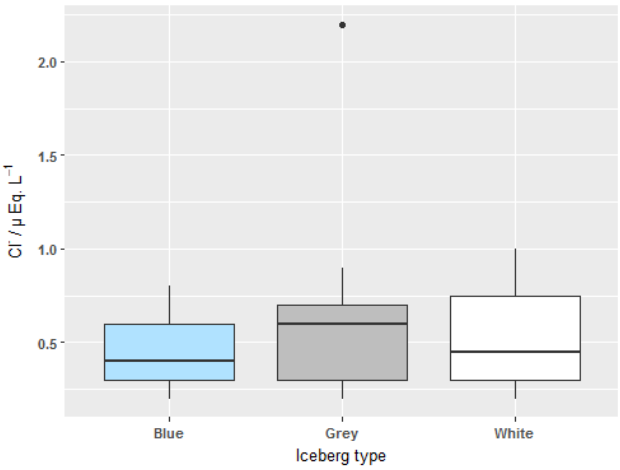
2.0
1.5
1.0
0.5
Cl- / µ Eq. L−1
Blue
Grey
White
Iceberg type

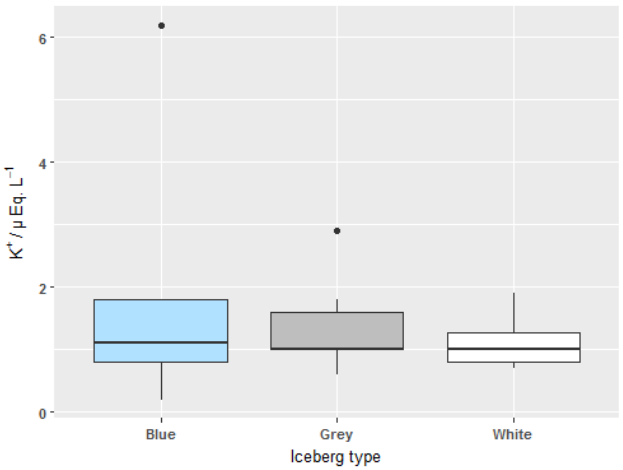
6
4
2
0
K+ / µ Eq. L−1
Blue
Grey
White
Iceberg type

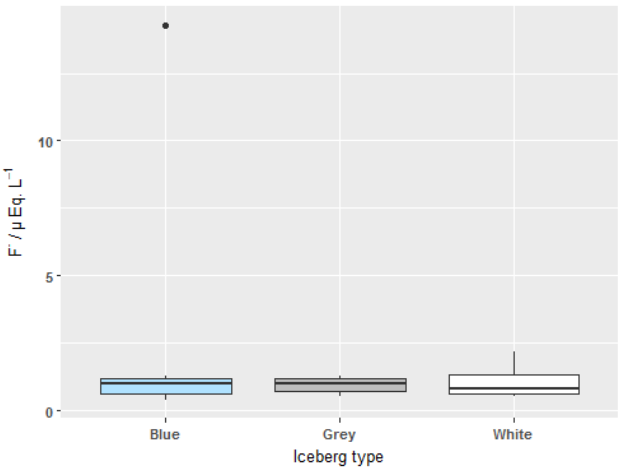
10
5
0
F- / µ Eq. L−1
Blue
Grey
White
Iceberg type

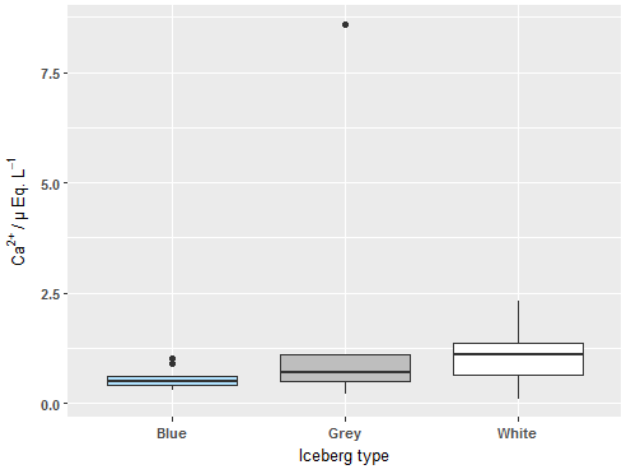
7.5
5.0
2.5
0.0
Ca2+ / µ Eq. L−1
Blue
Grey
White
Iceberg type

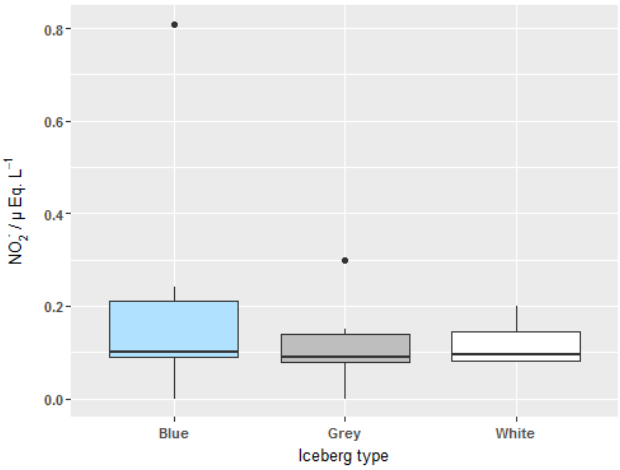
0.8
0.6
0.4
0.2
0.0
NO2- / µ Eq. L−1
Blue
Grey
White
Iceberg type

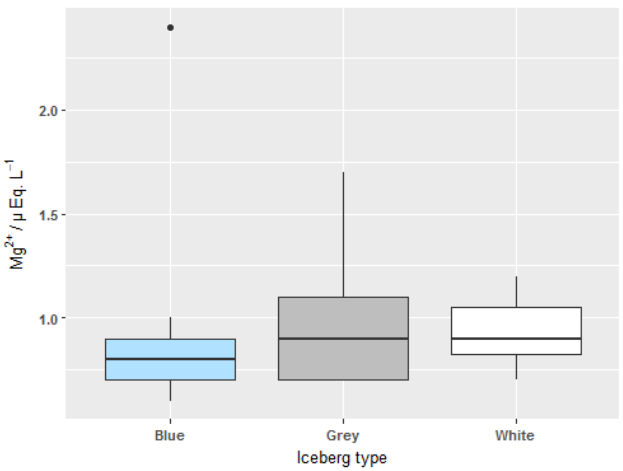
2.0
1.5
1.0
Mg2+ / µ Eq. L−1
Blue
Grey
White
Iceberg type

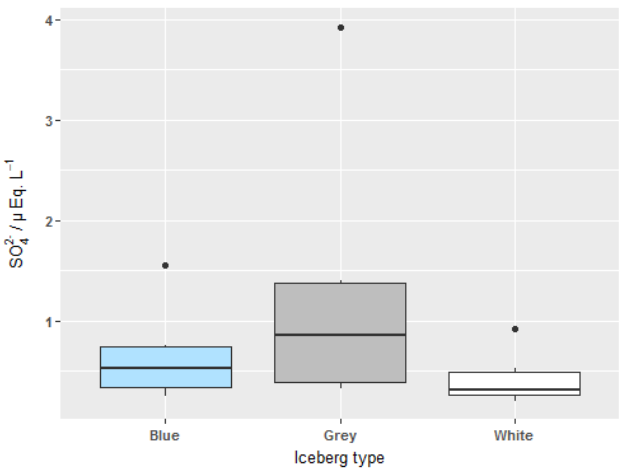
4
3
2
1
SO42- / µ Eq. L−1
Blue
Grey
White
Iceberg type

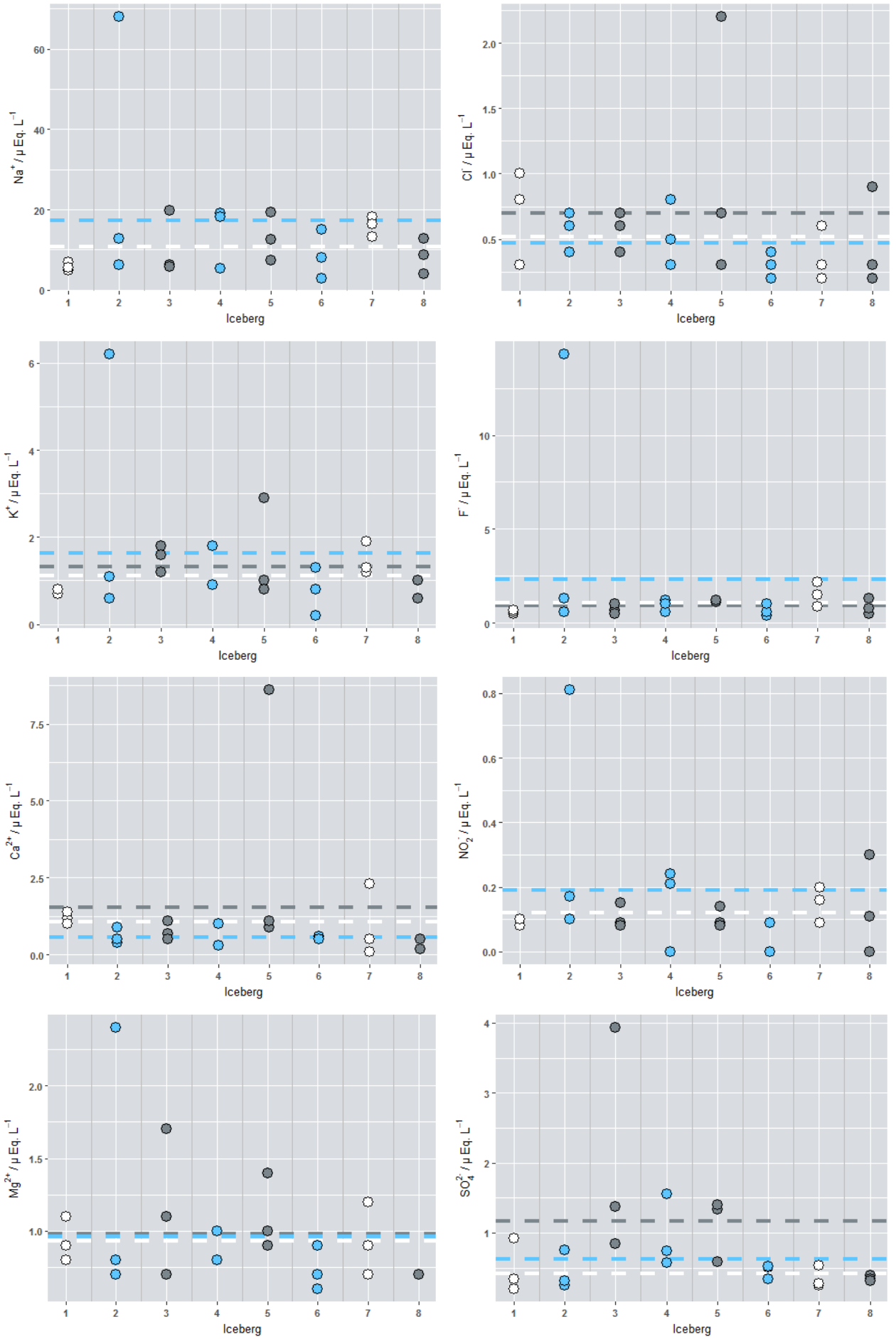
Na+ / µ Eq. L−1
Cl− / µ Eq. L−1
K+ / µ Eq. L−1
F− / µ Eq. L−1
Ca2+ / µ Eq. L−1
NO2− / µ Eq. L−1
Mg2+ / µ Eq. L−1
SO42− / µ Eq. L−1
Iceberg

Appendix 7: Deriving a two-component model for glacial contribution

This model considers the following parameters:

- R_{SAM} (the isotope ratio of a given semi-glacial sample);
- R_{GLA} (the average isotope ratio of all glacial inputs);
- R_{NON} (the average isotope ratio of all non-glacial inputs).

Each of these is just a number between 0 and 1, depending on the ratio of heavier isotopes (^{2}H, ^{18}O or ^{17}O) to their more-common counterparts (^{1}H or ^{16}O). R_{GLA} and R_{NON} are both averages of the isotopic ratios of individual inputs (e.g. a given stream), weighted by the relative magnitude of each input. Similarly, R_{SAM} is just a weighted average of R_{GLA} and R_{NON}:

$$R_{SAM} = \frac{xR_{GLA} + yR_{NON}}{x + y} \quad \text{Eq. 19}$$

where x and y are the relative magnitudes of the glacial and non-glacial inputs, respectively. As these represent the total input to the water body, we can write a second equation:

$$x + y = 1 \quad \text{Eq. 20}$$

This can be used to simplify Equation 19:

$$R_{SAM} = xR_{GLA} + yR_{NON} \quad \text{Eq. 19b}$$

Equation 20 can be arranged to show that:

$$x = 1 - y \quad \text{Eq. 20b}$$

And

$$y = 1 - x \quad \text{Eq. 20c}$$

Either of these can then be substituted into Equation 19b. Using Equation 20c gives:

$$R_{SAM} = xR_{GLA} + (1 - x)R_{NON} \quad \text{Eq. 19c}$$

This can be rearranged as follows:

$$R_{SAM} = xR_{GLA} + R_{NON} - xR_{NON}$$

$$R_{SAM} - R_{NON} = xR_{GLA} - xR_{NON}$$

$$R_{SAM} - R_{NON} = x(R_{GLA} - R_{NON})$$

Hence:

$$x = \frac{R_{SAM} - R_{NON}}{R_{GLA} - R_{NON}} \quad \text{Eq. 20d}$$

Similarly, substituting 20b into Equation 19b gives:

$$y = \frac{R_{SAM} - R_{GLA}}{R_{NON} - R_{GLA}} \quad \text{Eq. 20e}$$

Given the convention for expressing isotopic ratios as delta values, it would be more useful if Equations 20d and 20e were written in terms of δ_{SAM}, δ_{GLA} and δ_{NON}. Delta values and isotope ratios are related as follows:

$$R = \left(\frac{\delta}{1000} + 1\right) \times R_{STD} \qquad \text{Eq. 21}$$

where R is the isotope ratio of a sample, δ is the delta value of a sample and R_{STD} is the isotope ratio of the standard. Substituting Equation 21 into Equation 19b gives:

$$\left(\frac{\delta_{SAM}}{1000} + 1\right) \times R_{STD} = x\left(\frac{\delta_{GLA}}{1000} + 1\right) \times R_{STD} + y\left(\frac{\delta_{NON}}{1000} + 1\right) \times R_{STD} \qquad \text{Eq. 19d}$$

Which can be rearranged as follows:

$$\frac{\delta_{SAM}}{1000} + 1 = x\left(\frac{\delta_{GLA}}{1000} + 1\right) + y\left(\frac{\delta_{NON}}{1000} + 1\right) \qquad \text{Eq. 19e}$$

$$\delta_{SAM} + 1000 = x\,\delta_{GLA} + 1000\,x + y\,\delta_{NON} + 1000\,y \qquad \text{Eq. 19f}$$

$$\delta_{SAM} + 1000 = x\,\delta_{GLA} + y\,\delta_{NON} + 1000\,(x + y) \qquad \text{Eq. 19g}$$

Given that $x + y = 1$ (Eq. 20), we can simplify this to show that:

$$\delta_{SAM} = x\,\delta_{GLA} + y\,\delta_{NON} \qquad \text{Eq. 19h}$$

This is the same as Equation 13b, except that isotopic ratios have been replaced by delta values. Consequently, the simultaneous equations 14 and 18 can be combined to show that:

$$x = \frac{\delta_{SAM} - \delta_{NON}}{\delta_{GLA} - \delta_{NON}} \qquad \text{Eq. 22}$$

$$y = \frac{\delta_{SAM} - \delta_{GLA}}{\delta_{NON} - \delta_{GLA}} \qquad \text{Eq. 23}$$

References

1. Augustin, L., et al., *Eight glacial cycles from an Antarctic ice core.* Nature, 2004. **429**(6992): p. 623-628.

2. Siegert, M.J., et al., *Physical, chemical and biological processes in Lake Vostok and other Antarctic subglacial lakes.* Nature, 2001. **414**(6864): p. 603-609.

3. Heegaard, E., H.J.B. Birks, and R.J. Telford, *Relationships between calibrated ages and depth in stratigraphical sequences: an estimation procedure by mixed-effect regression.* Holocene, 2005. **15**(4): p. 612-618.

4. Dansgaard, W., et al., *One Thousand Centuries of Climatic Record from Camp Century on Greenland Ice Sheet.* Science, 1969. **166**(3903): p. 377-380.

5. Epstein, S., R.P. Sharp, and A.J. Gow, *Antarctic Ice Sheet - Stable Isotope Analyses of Byrd Station Cores and Interhemispheric Climatic Implications.* Science, 1970. **168**(3939): p. 1570-1572.

6. Motoyama, H., *The Second Deep Ice Coring Project at Dome Fuji, Antarctica.* Scientific Drilling, 2007. **No. 5**: p. 41-43.

7. Flower, B.P. and J.P. Kennett, *The Middle Miocene Climatic Transition - East Antarctic Ice-Sheet Development, Deep-Ocean Circulation and Global Carbon Cycling.* Palaeogeography Palaeoclimatology Palaeoecology, 1994. **108**(3-4): p. 537-555.

8. Shevenell, A.E., J.P. Kennett, and D.W. Lea, *Middle Miocene Southern Ocean cooling and Antarctic cryosphere expansion.* Science, 2004. **305**(5691): p. 1766-1770.

9. Craig, H. and C. Chou, *Methane: The record in polar ice cores.* Geophysical Research Letters, 1982. **9**(11): p. 1221-1224.

10. Barnola, J.M., et al., *Vostok Ice Core Provides 160,000-Year Record of Atmospheric Co2.* Nature, 1987. **329**(6138): p. 408-414.

11. Petit, J.-R., et al., *Climate and atmospheric history of the past 420,000 years from the Vostok ice core, Antarctica.* Nature, 1999. **399**(6735): p. 429-436.

12. Luthi, D., et al., *High-resolution carbon dioxide concentration record 650,000-800,000 years before present.* Nature, 2008. **453**(7193): p. 379-382.

13. Bradley, R.S., et al., *Low latitude ice cores record Pacific sea surface temperatures.* Geophysical Research Letters, 2003. **30**(4).

14. Thompson, L.G., et al., *Annually Resolved Ice Core Records of Tropical Climate Variability over the Past similar to 1800 Years.* Science, 2013. **340**(6135): p. 945-950.

15. Simoes, J.C. and V.S. Zagorodnov, *The record of anthropogenic pollution in snow and ice in Svalbard, Norway.* Atmospheric Environment, 2001. **35**(2): p. 403-413.

16. Isaksson, E., et al., *Ice cores from Svalbard - useful archives of past climate and pollution history.* Physics and Chemistry of the Earth, 2003. **28**(28-32): p. 1217-1228.

17. Preunkert, S., M. Legrand, and D. Wagenbach, *Sulfate trends in a Col du Dome (French Alps) ice core: A record of anthropogenic sulfate levels in the European midtroposphere over the twentieth century.* Journal of Geophysical Research-Atmospheres, 2001. **106**(D23): p. 31991-32004.

18. Jenk, T.M., et al., *Radiocarbon analysis in an Alpine ice core: record of anthropogenic and biogenic contributions to carbonaceous aerosols in the past (1650-1940).* Atmospheric Chemistry and Physics, 2006. **6**: p. 5381-5390.

19. Osterberg, E., et al., *Ice core record of rising lead pollution in the North Pacific atmosphere.* Geophysical Research Letters, 2008. **35**(5).

20. International Partnerships in Ice Core Sciences, I.P.I.C.S. *White Paper: the IPICS 2k Array: a network of ice core climate and climate forcing records for the last two millennia*. 2005.

21. Cullather, R.I., D.H. Bromwich, and M.L.V. Woert, *Spatial and Temporal Variability of Antarctic Precipitation from Atmospheric Methods.* Journal of Climate, 1998. **11**(3): p. 334-367.

22. Preunkert, S., D. Wagenbach, and M. Legrand, *A seasonally resolved alpine ice core record of nitrate: Comparison with anthropogenic inventories and estimation of preindustrial emissions of NO in Europe.* Journal of Geophysical Research-Atmospheres, 2003. **108**(D21).

23. Butz, D., *The Agricultural Use of Melt Water in Hopar Settlement, Pakistan.* Annals of Glaciology, 2017. **13**: p. 35-39.

24. Bradley, R.S., et al., *Threats to water supplies in the tropical Andes.* Science, 2006. **312**(5781): p. 1755-1756.

25. Bolch, T., *Hydrology: Asian glaciers are a reliable water source.* Nature, 2017. **545**(7653): p. 161-162.

26. Pritchard, H.D., *Asia's glaciers are a regionally important buffer against drought.* Nature, 2017. **545**(7653): p. 169-174.

27. Leavell, D. *The consequences of climate change for the water resources of Peru*. in *World Water Congress, Montpelier, France*. 2008.

28. Hood, E., et al., *Glaciers as a source of ancient and labile organic matter to the marine environment.* Nature, 2009. **462**(7276): p. 1044-U100.

29. Slemmons, K.E.H., J.E. Saros, and K. Simon, *The influence of glacial meltwater on alpine aquatic ecosystems: a review.* Environmental Science-Processes & Impacts, 2013. **15**(10): p. 1794-1806.

30. Hood, E., et al., *Storage and release of organic carbon from glaciers and ice sheets.* Nature Geoscience, 2015. **8**(2): p. 91-96.

31. Xu, J., et al., *The melting Himalayas: regional challenges and local impacts of climate change on mountain ecosystems and livelihoods*. 2007, Kathmandu: International Centre for Integrated Mountain Development (ICIMOD). vi + 15 pp.

32. Mark, B.G., et al., *Climate Change and Tropical Andean Glacier Recession: Evaluating Hydrologic Changes and Livelihood Vulnerability in the Cordillera Blanca, Peru.* Annals of the Association of American Geographers, 2010. **100**(4): p. 794-805.

33. Slemmons, K.E.H. and J.E. Saros, *Implications of nitrogen-rich glacial meltwater for phytoplankton diversity and productivity in alpine lakes.* Limnology and Oceanography, 2012. **57**(6): p. 1651-1663.

34. Martin, J.H., *Glacial-Interglacial Co2 Change: The Iron Hypothesis.* Paleoceanography, 1990. **5**(1): p. 1-13.

35. Martin, J.H., S.E. Fitzwater, and R.M. Gordon, *Iron deficiency limits phytoplankton growth in Antarctic waters.* Global Biogeochemical Cycles, 1990. **4**(1): p. 5-12.

36. Martin, J.H., R.M. Gordon, and S.E. Fitzwater, *Iron in Antarctic Waters.* Nature, 1990. **345**(6271): p. 156-158.

37. Sedwick, P.N. and G.R. DiTullio, *Regulation of algal blooms in Antarctic shelf waters by the release of iron from melting sea ice.* Geophysical Research Letters, 1997. **24**(20): p. 2515-2518.

38. Bhatia, M.P., et al., *Greenland meltwater as a significant and potentially bioavailable source of iron to the ocean.* Nature Geoscience, 2013. **6**(4): p. 274-278.

39. Hawkings, J.R., et al., *Ice sheets as a significant source of highly reactive nanoparticulate iron to the oceans.* Nat Commun, 2014. **5**: p. 3929.

40. Moline, M.A. and B.B. Prezelin, *Long-term monitoring and analyses of physical factors regulating variability in coastal Antarctic phytoplankton biomass, in situ productivity and taxonomic composition over subseasonal, seasonal and interannual time scales.* Marine Ecology Progress Series, 1996. **145**(1-3): p. 143-160.

41. Dierssen, H.M., M. Vernet, and R.C. Smith, *Optimizing models for remotely estimating primary production in Antarctic coastal waters.* Antarctic Science, 2000. **12**(1): p. 20-32.

42. Hylander, S., et al., *Climate-induced input of turbid glacial meltwater affects vertical distribution and community composition of phyto- and zooplankton.* Journal of Plankton Research, 2011. **33**(8): p. 1239-1248.

43. Arrigo, K.R., et al., *Phytoplankton community structure and the drawdown of nutrients and CO2 in the Southern Ocean.* Science, 1999. **283**(5400): p. 365-367.

44. Frajka-Williams, E. and P.B. Rhines, *Physical controls and interannual variability of the Labrador Sea spring phytoplankton bloom in distinct regions.* Deep-Sea Research Part I-Oceanographic Research Papers, 2010. **57**(4): p. 541-552.

45. Collins, D., *Hydrology of an alpine glacier as indicated by the chemical composition of meltwater.* Zeitschrift für Gletscherkunde und Glazialgeologie, 1977. **13**: p. 219-238.

46. Nordstrom 1, D.K., *Aqueous Pyrite Oxidation and the Consequent Formation of Secondary Iron Minerals*, in *Acid Sulfate Weathering*, J.A. Kittrick, D.S. Fanning, and L.R. Hossner, Editors. 1982, Soil Science Society of America: Madison, WI. p. 37-56.

47. Chillrud, S., et al., *Chemical weathering of phosphate and germanium in glacial meltwater streams: effects of subglacial pyrite oxidation.* Limnology and Oceanography, 1994. **39**(5): p. 1130-1140.

48. Tranter, M., et al., *A conceptual model of solute acquisition by Alpine glacial meltwaters.* Journal of Glaciology, 2017. **39**(133): p. 573-581.

49. Lemmens, M. and M. Roger, *Influence of ion exchange on dissolved load of alpine meltwaters.* Earth Surface Processes, 1978. **3**(2): p. 179-187.

50. Gooseff, M.N., D.M. Mcknight, and R.L. Runkel, *Reach-Scale Cation Exchange Controls on Major Ion Chemistry of an Antarctic Glacial Meltwater Stream.* Aquatic Geochemistry, 2004. **10**(3): p. 221-238.

51. Tranter, M., et al., *A conceptual model of solute acquisition by Alpine glacial meltwaters.* Journal of Glaciology, 1993. **133**: p. 573-581.

52. Reynolds, R.C. and N.M. Johnson, *Chemical weathering in the temperate glacial environment of the Northern Cascade Mountains.* Geochimica et Cosmochimica Acta, 1972. **36**(5): p. 537-554.

53. Singh, P. and N. Kumar, *Impact assessment of climate change on the hydrological response of a snow and glacier melt runoff dominated Himalayan river.* Journal of Hydrology, 1997. **193**(1): p. 316-350.

54. Hall, M.H.P. and D.B. Fagre, *Modeled Climate-Induced Glacier Change in Glacier National Park, 1850–2100.* BioScience, 2003. **53**(2): p. 131-140.

55. Anderson, S.P., *Glaciers show direct linkage between erosion rate and chemical weathering fluxes.* Geomorphology, 2005. **67**(1-2): p. 147-157.

56. Petrovich, R., *Kinetics of Dissolution of Mechanically Comminuted Rock-Forming Oxides and Silicates .1. Deformation and Dissolution of Quartz under Laboratory Conditions.* Geochimica Et Cosmochimica Acta, 1981. **45**(10): p. 1665-1674.

57. Prestrud Anderson, S., J.I. Drever, and N.F. Humphrey, *Chemical weathering in glacial environments.* Geology, 1997. **25**(5): p. 399-402.

58. Yde, J.C., et al., *Basal ice microbiology at the margin of the Greenland ice sheet.* Annals of Glaciology, 2010. **51**(56): p. 71-79.

59. Skidmore, M.L., J.M. Foght, and M.J. Sharp, *Microbial life beneath a high arctic glacier.* Appl Environ Microbiol, 2000. **66**(8): p. 3214-20.

60. Foght, J., et al., *Culturable Bacteria in Subglacial Sediments and Ice from Two Southern Hemisphere Glaciers.* Microbial Ecology, 2004. **47**(4): p. 329-340.

61. Rondón, J., et al., *Diversity of culturable bacteria recovered from Pico Bolívar's glacial and subglacial environments, at 4950 m, in Venezuelan tropical Andes.* Canadian Journal of Microbiology, 2016. **62**(11): p. 904-917.

62. Price, P.B., *A habitat for psychrophiles in deep Antarctic ice.* Proceedings of the National Academy of Sciences, 2000. **97**(3): p. 1247-1251.

63. Priscu, J.C., et al., *Geomicrobiology of subglacial ice above Lake Vostok, Antarctica.* Science, 1999. **286**(5447): p. 2141-2144.

64. Lanoil, B., et al., *Bacteria beneath the West Antarctic ice sheet.* Environmental Microbiology, 2009. **11**(3): p. 609-615.

65. Christner, B.C., et al., *A microbial ecosystem beneath the West Antarctic ice sheet.* Nature, 2014. **512**(7514): p. 310-313.

66. Boetius, A., et al., *Microbial ecology of the cryosphere: sea ice and glacial habitats.* Nature Reviews Microbiology, 2015.

67. Wharton Jr, R., et al., *Algae in cryoconite holes on Canada Glacier in southern Victorialand, Antarctica.* Phycologia, 1981. **20**(2): p. 208-211.

68. Säwström, C., et al., *The microbial communities and primary productivity of cryoconite holes in an Arctic glacier (Svalbard 79 N).* Polar Biology, 2002. **25**(8): p. 591-596.

69. Price, P.B., et al., *Temperature profile for glacial ice at the South Pole: Implications for life in a nearby subglacial lake.* Proceedings of the National Academy of Sciences, 2002. **99**(12): p. 7844-7847.

70. Pattyn, F., *Antarctic subglacial conditions inferred from a hybrid ice sheet/ice stream model.* Earth and Planetary Science Letters, 2010. **295**(3): p. 451-461.

71. Bottrell, S.H. and M. Tranter, *Sulphide oxidation under partially anoxic conditions at the bed of the Haut Glacier d'Arolla, Switzerland.* Hydrological Processes, 2002. **16**(12): p. 2363-2368.

72. Wadham, J.L., et al., *Stable isotope evidence for microbial sulphate reduction at the bed of a polythermal high Arctic glacier.* Earth and Planetary Science Letters, 2004. **219**(3): p. 341-355.

73. Tranter, M., et al., *Geochemical weathering at the bed of Haut Glacier d'Arolla, Switzerland—a new model.* Hydrological Processes, 2002. **16**(5): p. 959-993.

74. Wynn, P.M., A. Hodson, and T. Heaton, *Chemical and Isotopic Switching within the Subglacial Environment of a High Arctic Glacier.* Biogeochemistry, 2006. **78**(2): p. 173-193.

75. Lamb, H.R.T., M.; Brown, H.; Hubbard, B. P.; Sharp, M. J.; Gordon, S.; Smart C. C.; Willis, I. C.; Nielsen M. K., *The composition of subglacial meltwaters sampled from boreholes at the Haut Glacier d'Arolla, Switzerland.* Biogeochemislry of Seasonally Snow-Covered Catchments (Proceedings of a Boulder Symposium), 1995. **IAHSPubl.no. Ï28**: p. 395-403.

76. Tranter, M., et al., *VARIABILITY IN THE CHEMICAL COMPOSITION OF IN SITU SUBGLACIAL MELTWATERS.* Hydrological Processes, 1997. **11**(1): p. 59-77.

77. Tranter, M., M. Skidmore, and J. Wadham, *Hydrological controls on microbial communities in subglacial environments.* Hydrological Processes, 2005. **19**(4): p. 995-998.

78. Mitchell, A.C., et al., *Influence of bedrock mineral composition on microbial diversity in a subglacial environment.* Geology, 2013. **41**(8): p. 855-858.

79. Wadham, J., et al., *The potential role of the Antarctic Ice Sheet in global biogeochemical cycles.* Earth and Environmental Science Transactions of the Royal Society of Edinburgh, 2013. **104**(01): p. 55-67.

80. Raiswell, R. and D.E. Canfield, *The Iron Biogeochemical Cycle Past and Present.* Geochemical Perspectives, 2012. **1**(1): p. 1-2.

81. Schroth, A.W., et al., *Glacial influence on the geochemistry of riverine iron fluxes to the Gulf of Alaska and effects of deglaciation.* Geophysical Research Letters, 2011. **38**(16): p. n/a-n/a.

82. Raiswell, R., et al., *Bioavailable iron in the Southern Ocean: the significance of the iceberg conveyor belt.* Geochemical Transactions, 2008. **9**(1): p. 7.

83. Death, R., et al., *Antarctic ice sheet fertilises the Southern Ocean.* Biogeosciences, 2014. **11**(10): p. 2635-2643.

84. Alderkamp, A.C., et al., *Iron from melting glaciers fuels phytoplankton blooms in the Amundsen Sea (Southern Ocean): Phytoplankton characteristics and productivity.* Deep-Sea Research Part Ii-Topical Studies in Oceanography, 2012. **71-76**: p. 32-48.

85. Millero, F.J., S. Sotolongo, and M. Izaguirre, *The oxidation kinetics of Fe(II) in seawater.* Geochimica et Cosmochimica Acta, 1987. **51**(4): p. 793-801.

86. Misumi, K., et al., *The iron budget in ocean surface waters in the 20th and 21st centuries: projections by the Community Earth System Model version 1*. 2014.

87. McKay, R., et al., *Antarctic Cenozoic climate history from sedimentary records: ANDRILL and beyond.* Phil. Trans. R. Soc. A, 2016. **374**(2059): p. 20140301.

88. Stibal, M., et al., *Methanogenic potential of Arctic and Antarctic subglacial environments with contrasting organic carbon sources.* Global Change Biology, 2012. **18**(11): p. 3332-3345.

89. Wadham, J., et al., *Potential methane reservoirs beneath Antarctica.* Nature, 2012. **488**(7413): p. 633-637.

90. Wadham, J., et al., *Subglacial methanogenesis: a potential climatic amplifier?* Global Biogeochemical Cycles, 2008. **22**(2).

91. Boyd, E.S., et al., *Methanogenesis in subglacial sediments.* Environmental microbiology reports, 2010. **2**(5): p. 685-692.

92. Achberger, A.M., et al., *Microbial Community Structure of Subglacial Lake Whillans, West Antarctica.* Frontiers in Microbiology, 2016. **7**.

93. Anesio, A.M. and J. Laybourn-Parry, *Glaciers and ice sheets as a biome.* Trends in Ecology & Evolution, 2012. **27**(4): p. 219-225.

94. Christner, B.C., et al., *Glacial ice cores: A model system for developing extraterrestrial decontamination protocols.* Icarus, 2005. **174**(2): p. 572-584.

95. Robin, G.d.Q., C. Swithinbank, and B. Smith, *Radio echo exploration of the Antarctic ice sheet.* International Association of Scientific Hydrology Publication, 1970. **86**: p. 97-115.

96. Oswald, G.K.A. and G.D.Q. Robin, *Lakes beneath Antarctic Ice Sheet.* Nature, 1973. **245**(5423): p. 251-254.

97. Pearce, D.A., et al., *Preliminary analysis of life within a former subglacial lake sediment in Antarctica.* Diversity, 2013. **5**(3): p. 680-702.

98. Engelhardt, H., et al., *Physical conditions at the base of a fast moving Antarctic ice stream.* Science, 1990. **248**(4951): p. 57-59.

99. Wingham, D.J., et al., *Rapid discharge connects Antarctic subglacial lakes.* Nature, 2006. **440**(7087): p. 1033-1036.

100. Fretwell, P., et al., *Bedmap2: improved ice bed, surface and thickness datasets for Antarctica.* The Cryosphere, 2013. **7**(1).

101. Priscu, J., et al., *Exploring subglacial Antarctic lake environments.* Eos, Transactions American Geophysical Union, 2005. **86**(20): p. 193-197.

102. Siegert, M.J., et al., *Antarctic subglacial lake exploration: first results and future plans.* Phil. Trans. R. Soc. A, 2016. **374**(2059): p. 20140466.

103. Kapitsa, A., et al., *A large deep freshwater lake beneath the ice of central East Antarctica.* Nature, 1996. **381**(6584): p. 684.

104. Siegert, M., et al., *An inventory of Antarctic sub-glacial lakes.* Antarctic Science, 1996. **8**(03): p. 281-286.

105. Priscu, J.C., et al., *An International Plan for Antarctic Subglacial Lake Exploration.* Polar Geography, 2003. **27**(1): p. 69-83.

106. Talalay, P., et al., *Ice-core drilling problems and solutions.* Cold Regions Science and Technology, 2015. **120**: p. 1-20.

107. Bulat, S., et al., *Cell concentrations of microorganisms in glacial and lake ice of the Vostok ice core, East Antarctica.* Microbiology, 2009. **78**(6): p. 808.

108. Bulat, S.A., et al., *DNA signature of thermophilic bacteria from the aged accretion ice of Lake Vostok, Antarctica: implications for searching for life in extreme icy environments.* International Journal of Astrobiology, 2004. **3**(01): p. 1-12.

109. Bulat, S.A., et al., *Searching for life in extreme environments relevant to Jovian's Europa: Lessons from subglacial ice studies at Lake Vostok (East Antarctica).* Advances in Space Research, 2011. **48**(4): p. 697-701.

110. Alekhina, I., et al., *Chemical characteristics of the ice cores obtained after the first unsealing of subglacial Lake Vostok.* Geological Society, London, Special Publications, 2017. **461**.

111. Lukin, V. and S. Bulat, *Vostok subglacial lake: details of Russian plans/activities for drilling and sampling.* Antarctic Subglacial Aquatic Environments, Geophys. Monogr. Ser, 2011. **192**: p. 187-197.

112. Pomelov, V., *Water sampling of the subglacial Lake Vostok: Final Comprehensive Environmental Evaluation.* Report, Russian Antarctic Expedition, Arctic and Antarctic Research Institute, St-Petersburg, Russia, 2010.

113. Talalay, P., *Russian researchers reach subglacial Lake Vostok in Antarctica.* Adv. Polar Sci, 2012. **23**(3): p. 176-180.

114. Alekhina, I.A., et al., *Molecular analysis of bacterial diversity in kerosene-based drilling fluid from the deep ice borehole at Vostok, East Antarctica.* FEMS microbiology ecology, 2007. **59**(2): p. 289-299.

115. Bulat, S.A., *Microbiology of the subglacial Lake Vostok: first results of borehole-frozen lake water analysis and prospects for searching for lake inhabitants.* Phil. Trans. R. Soc. A, 2016. **374**(2059): p. 20140292.

116. Lukin, V.V. and N.I. Vasiliev, *Technological aspects of the final phase of drilling borehole 5G and unsealing Vostok Subglacial Lake, East Antarctica.* Annals of Glaciology, 2014. **55**(65): p. 83.

117. Talalay, P. and A. Markov, *Thermobaric Conditions at Ice-Water Interface in Subglacial Lake Vostok, East Antarctica.* Natural Resources, 2015. **6**(06): p. 423.

118. Siegert, M.J., et al., *An assessment of deep hot-water drilling as a means to undertake direct measurement and sampling of Antarctic subglacial lakes: experience and lessons learned from the Lake Ellsworth field season 2012/13.* Annals of Glaciology, 2014. **55**(65): p. 59-73.

119. Siegert, M.J., et al., *Clean access, measurement, and sampling of Ellsworth Subglacial Lake: A method for exploring deep Antarctic subglacial lake environments.* Reviews of Geophysics, 2012. **50**(1): p. n/a-n/a.

120. Schiermeier, Q., *Polar drilling problems revealed: report into failings of expedition to explore Antarctic lake finds equipment to blame--but complications can be fixed.* Nature, 2014. **505**(7484): p. 463-464.

121. Lake Ellsworth Consortium, U.K., *Final Comprehensive Environmental Evaluation for the Proposed Exploration of Lake Ellsworth, Antarctica.* 2012.

122. Siegert, M.J., *A 60-year international history of Antarctic subglacial lake exploration.* Geological Society, London, Special Publications, 2017. **461**: p. SP461. 5.

123. Augustin, L., S. Panichi, and F. Frascati, *EPICA Dome C 2 drilling operations: performances, difficulties, results.* Annals of Glaciology, 2007. **47**(1): p. 68-72.

124. Melles, M., et al., *The Lake El'gygytgyn Scientific Drilling Project–Conquering Arctic Challenges through Continental Drilling.* Scientific Drilling, 2011. **11**: p. 29-40.

125. Slawny, K.R., et al., *Production drilling at WAIS Divide.* Annals of Glaciology, 2014. **55**(68): p. 147.

126. Kummu, M. and O. Varis, *The world by latitudes: A global analysis of human population, development level and environment across the north–south axis over the past half century.* Applied Geography, 2011. **31**(2): p. 495-507.

127. Kaab, A., et al., *Remote sensing of glacier- and permafrost-related hazards in high mountains: an overview.* Natural Hazards and Earth System Sciences, 2005. **5**(4): p. 527-554.

128. Racoviteanu, A.E., M.W. Williams, and R.G. Barry, *Optical remote sensing of glacier characteristics: A review with focus on the Himalaya.* Sensors, 2008. **8**(5): p. 3355-3383.

129. Schwikowski, M., et al., *A new thermal drilling system for high-altitude or temperate glaciers.* Annals of glaciology, 2014. **55**(68): p. 131-136.

130. Bintanja, R., *On the glaciological, meteorological, and climatological significance of Antarctic blue ice areas.* Reviews of Geophysics, 1999. **37**(3): p. 337-359.

131. Sinisalo, A. and J.C. Moore, *Antarctic blue ice areas-towards extracting palaeoclimate information.* Antarctic Science, 2010. **22**(02): p. 99-115.

132. Liston, G.E. and J.-G. Winther, *Antarctic surface and subsurface snow and ice melt fluxes.* Journal of Climate, 2005. **18**(10): p. 1469-1481.

133. Hui, F., et al., *Mapping blue-ice areas in Antarctica using ETM+ and MODIS data.* Annals of Glaciology, 2014. **55**(66): p. 129-137.

134. Yoshida, M., et al., *Discovery of meteorites near Yamato Mountains, East Antarctica.* Antarctic Record, 1971. **39**: p. 62-65.

135. Hey, M.H., *Catalogue of Meteorites: With Special Reference to Those Represented in the Collection of the British Museum (Natural History).* 1966: British Museum (Natural History).

136. Harvey, R., *The origin and significance of Antarctic meteorites.* Chemie der Erde-Geochemistry, 2003. **63**(2): p. 93-147.

137. Whillans, I.M. and W. Cassidy, *Catch a falling star: Meteorites and old ice.* Science, 1983. **222**(4619): p. 55-57.

138. Grinsted, A., et al., *Dating Antarctic blue ice areas using a novel ice flow model.* Geophysical research letters, 2003. **30**(19).

139. Sinisalo, A., et al., *Inferences from stable water isotopes on the Holocene evolution of Scharffenbergbotnen blue-ice area, East Antarctica.* Journal of Glaciology, 2007. **53**(182): p. 427-434.

140. Moore, J.C., et al., *Interpreting ancient ice in a shallow ice core from the South Yamato (Antarctica) blue ice area using flow modeling and compositional matching to deep ice cores.* Journal of Geophysical Research: Atmospheres, 2006. **111**(D16).

141. Korotkikh, E.V., et al., *The last interglacial as represented in the glaciochemical record from Mount Moulton Blue Ice Area, West Antarctica.* Quaternary Science Reviews, 2011. **30**(15): p. 1940-1947.

142. Spaulding, N.E., et al., *Climate archives from 90 to 250ka in horizontal and vertical ice cores from the Allan Hills Blue Ice Area, Antarctica.* Quaternary Research, 2013. **80**(3): p. 562-574.

143. Rignot, E., A. Rivera, and G. Casassa, *Contribution of the Patagonia Icefields of South America to Sea Level Rise.* Science, 2003. **302**(5644): p. 434-437.

144. Paul, F., et al., *Rapid disintegration of Alpine glaciers observed with satellite data.* Geophysical research letters, 2004. **31**(21).

145. Duprat, L.P.A.M., G.R. Bigg, and D.J. Wilton, *Enhanced Southern Ocean marine productivity due to fertilization by giant icebergs.* Nature Geosci, 2016. **9**(3): p. 219-221.

146. Smith, K.L., et al., *Free-drifting icebergs: Hot spots of chemical and biological enrichment in the Weddell Sea.* Science, 2007. **317**.

147. Casassa, G., et al., *Mass balance of the Antarctic ice sheet at Patriot Hills.* Annals of Glaciology, Vol 27, 1998, 1998. **27**: p. 130-134.

148. Casassa, G., et al., *Elevation change and ice flow at Horseshoe Valley, Patriot Hills, West Antarctica.* Annals of Glaciology, Vol 39, 2004, 2004. **39**: p. 20-28.

149. Carrasco, J., G. Casassa, and A. Rivera. *A warm event at Patriot Hills, Antarctica: an ENSO related phenomenon*. in *Sixth International Conference on Southern Hemisphere Meteorology and Oceanography*. 2000.

150. Turney, C., et al., *Late Pleistocene and early Holocene change in the Weddell Sea: a new climate record from the Patriot Hills, Ellsworth Mountains, West Antarctica.* Journal of Quaternary Science, 2013. **28**(7): p. 697-704.

151. Warren, C.R. and D.E. Sugden, *The Patagonian Icefields: A Glaciological Review.* Arctic and Alpine Research, 1993. **25**(4): p. 316-331.

152. Meier, M.F. and A. Post, *Fast tidewater glaciers.* Journal of Geophysical Research: Solid Earth, 1987. **92**(B9): p. 9051-9058.

153. Warren, C.R., *Iceberg calving and the glacioclimatic record.* Progress in Physical Geography, 1992. **16**(3): p. 253-282.

154. Lopez, P., et al., *A regional view of fluctuations in glacier length in southern South America.* Global and Planetary Change, 2010. **71**(1–2): p. 85-108.

155. Rivera, A., et al., *Ice elevation and areal changes of glaciers from the Northern Patagonia Icefield, Chile.* Global and Planetary Change, 2007. **59**(1): p. 126-137.

156. Aniya, M. and H. Sato, *Recent glacier variations in the Patagonia Icefield.* Journal of the Japanese Society of Snow and Ice, 1996. **58**(1): p. 43-52.

157. JAXA, E. *Significant retreats of huge glaciers in Patagonia, South America (Part 4)*. 2011 27/05/2017]; Available from: http://www.eorc.jaxa.jp/en/earthview/2011/tp110525.html.

158. Glasser, N.F., et al., *Global sea-level contribution from the Patagonian Icefields since the Little Ice Age maximum.* Nature Geosci, 2011. **4**(5): p. 303-307.

159. Ross, N., et al., *Ellsworth Subglacial Lake, West Antarctica: A Review of Its History and Recent Field Campaigns.* Antarctic Subglacial Aquatic Environments (eds M. J. Siegert and M. C. Kennicutt), 2011: p. 221-233.

160. Baer, D.S., et al., *Sensitive absorption measurements in the near-infrared region using off-axis integrated-cavity-output spectroscopy.* Applied Physics B: Lasers and Optics, 2002. **75**(2): p. 261-265.

161. Berman, E.S., et al., *Measurement of δ18O, δ17O, and 17O-excess in water by off-axis integrated cavity output spectroscopy and isotope ratio mass spectrometry.* Analytical chemistry, 2013. **85**(21): p. 10392-10398.

162. Paul, J.B., L. Lapson, and J.G. Anderson, *Ultrasensitive absorption spectroscopy with a high-finesse optical cavity and off-axis alignment.* Applied optics, 2001. **40**(27): p. 4904-4910.

163. Armbruster, D.A. and T. Pry, *Limit of Blank, Limit of Detection and Limit of Quantitation.* The Clinical Biochemist Reviews, 2008. **29**(Suppl 1): p. S49-S52.

164. Craig, H., *Isotopic variations in meteoric waters.* Science, 1961. **133**(3465): p. 1702-1703.

165. Souchez, R.A. and J. Jouzel, *On the Isotopic Composition in δD and δ18O of Water and Ice During Freezing.* Journal of Glaciology, 1984. **30**(106): p. 369-372.

166. Hubbard, B. and M. Sharp, *Weertman regelation, multiple refreezing events and the isotopic evolution of the basal ice layer.* Journal of Glaciology, 1993. **39**(132): p. 275-291.

167. Gordon, J.E., et al., *δD-δ18O Relationships and the Thermal History of Basal Ice Near the margins of two Glaciers in Lyngen, North Norway.* Journal of Glaciology, 1988. **34**(118): p. 265-268.

168. Masson-Delmotte, V., et al., *A review of Antarctic surface snow isotopic composition: Observations, atmospheric circulation, and isotopic modeling.* Journal of Climate, 2008. **21**(13): p. 3359-3387.

169. Qin, D., et al., *Distribution of stable isotopes in surface snow along the route of the 1990 International Trans-Antarctica Expedition.* Journal of Glaciology, 1994. **40**(134): p. 107-118.

170. Kirchner, S. and R.J. Delmas, *A 1000 year glaciochemical study at the South Pole.* Annals of Glaciology, 1988. **10**: p. 80-84.

171. Wake, C.P., *Glaciochemical investigations as a tool for determining the spatial and seasonal variation of snow accumulation in the central Karakoram, northern Pakistan.* Annals of Glaciology, 1989. **13**: p. 279-284.

172. Legrand, M. and P. Mayewski, *Glaciochemistry of polar ice cores: A review.* Reviews of Geophysics, 1997. **35**(3): p. 219-243.

173. Monahan, E.C., D.E. Spiel, and K.L. Davidson, *A model of marine aerosol generation via whitecaps and wave disruption*, in *Oceanic whitecaps*. 1986, Springer. p. 167-174.

174. Fischer, H., et al., *Glacial/interglacial changes in mineral dust and sea-salt records in polar ice cores: Sources, transport, and deposition.* Reviews of Geophysics, 2007. **45**(1): p. n/a-n/a.

175. Pilson, M.E., *An Introduction to the Chemistry of the Sea*. 2nd ed. 2012: Cambridge University Press.

176. Jourdain, B. and M. Legrand, *Year-round records of bulk and size-segregated aerosol composition and HCl and HNO3 levels in the Dumont d'Urville (coastal Antarctica) atmosphere: Implications for sea-salt aerosol fractionation in the winter and summer.* Journal of Geophysical Research: Atmospheres, 2002. **107**(D22): p. ACH 20-1-ACH 20-13.

177. Qin, D., et al., *The Weddell Sea region: an important precipitation channel to the interior of the Antarctic ice sheet as revealed by glaciochemical investigation of surface snow along the longest trans-Antarctic route.* Annals of Glaciology, 1999. **29**(1): p. 55-60.

178. Legrand, M., *Chemistry of Antarctic snow and ice.* Le Journal de Physique Colloques, 1987. **48**(C1): p. C1-77-C1-86.

179. Mulvaney, R. and E.W. Wolff, *Spatial variability of the major chemistry of the Antarctic ice sheet.* Annals of Glaciology, 1994. **20**: p. 440-447.

180. Legrand, M.R., et al., *Vostok (Antarctica) ice core: Atmospheric chemistry changes over the last climatic cycle (160,000 years).* Atmospheric Environment (1967), 1988. **22**(2): p. 317-331.

181. Legrand, M. and R.J. Delmas, *Spatial and temporal variations of snow chemistry in Terre Adélie (East Antarctica).* Annals of Glaciology, 1985. **7**(1): p. 20-25.

182. Antony, R., et al., *Organic carbon in Antarctic snow: spatial trends and possible sources.* Environmental science & technology, 2011. **45**(23): p. 9944-9950.

183. Christner, B.C., et al., *Limnological conditions in subglacial Lake Vostok, Antarctica.* Limnology and Oceanography, 2006. **51**(6): p. 2485-2501.

184. Legrand, M., et al., *Water-soluble organic carbon in snow and ice deposited at Alpine, Greenland, and Antarctic sites: a critical review of available data and their atmospheric relevance.* Climate of the Past, 2013. **9**(5): p. 2195.

185. Higgins, J.A., et al., *Atmospheric composition 1 million years ago from blue ice in the Allan Hills, Antarctica.* Proceedings of the National Academy of Sciences, 2015. **112**(22): p. 6887-6891.

186. Aristarain, A.J. and R.J. Delmas, *Firn-core study from the southern Patagonia ice cap, South America.* Journal of Glaciology, 1993. **39**(132): p. 249-254.

187. Herreros, J., et al., *Environmental records from temperate glacier ice on Nevado Coropuna saddle, southern Peru.* Advances in Geosciences, 2009. **22**: p. 27-34.

188. Maupetit, F. and R.J. Delmas, *Snow chemistry of high altitude glaciers in the French Alps.* Tellus B: Chemical and Physical Meteorology, 1994. **46**(4): p. 304-324.

189. SHIRAIWA, T., et al., *High net accumulation rates at Campo de Hielo Patagonico Sur, South America, revealed by analysis of a 45.97 m long ice core.* Annals of Glaciology, 2002. **35**: p. 84-90.

190. Davies, T., C. Vincent, and P. Brimblecombe, *Preferential elution of strong acids from a Norwegian ice cap.* Nature, 1982. **300**(5888): p. 161.

191. Brimblecombe, P., et al., *Observations of the preferential loss of major ions from melting snow and laboratory ice.* Water Research, 1987. **21**(10): p. 1279-1286.

192. Eichler, A., M. Schwikowski, and H.W. Gäggeler, *Meltwater-induced relocation of chemical species in Alpine firn.* Tellus B: Chemical and Physical Meteorology, 2001. **53**(2): p. 192-203.

193. Li, Z., et al., *Seasonal variability of ionic concentrations in surface snow and elution processes in snow–firn packs at the PGPI site on Ürümqi glacier No. 1, eastern Tien Shan, China.* Annals of Glaciology, 2006. **43**: p. 250-256.

194. Vimeux, F., et al., *A promising location in Patagonia for paleoclimate and paleoenvironmental reconstructions revealed by a shallow firn core from Monte San Valentín (Northern Patagonia Icefield, Chile).* Journal of Geophysical Research: Atmospheres, 2008. **113**(D16).

195. Shichang, K., et al., *Monsoon and dust signals recorded in Dasuopu glacier, Tibetan Plateau.* Journal of Glaciology, 2000. **46**(153): p. 222-226.

196. Edwards, R. and P. Sedwick, *Iron in East Antarctic snow: implications for atmospheric iron deposition and algal production in Antarctic waters.* Geophys Res Lett, 2001. **28**.

197. Clark, I.D. and P. Fritz, *Environmental Isotopes in Hydrogeology*. 1997: CRC Press.

198. Grabczak, J., J. Niewodniczański, and K. Różański, *Isotope stratification in high mountain glaciers: Examples from the Peruvian Andes and Himalaya.* Journal of Glaciology, 1983. **29**(103): p. 417-424.

199. Escobar, V., et al., *Water balance in the Patagonian Icefield*, in *Glaciological researches in Patagonia, 1990*, R. Naruse and M. Aniya, Editors. 1992, Japanese Society of Snow and Ice: Institute of Low Temperature Science, Hokkaido University. p. 109–19.

200. Bromwich, D.H., J.P. Nicolas, and A.J. Monaghan, *An assessment of precipitation changes over Antarctica and the Southern Ocean since 1989 in contemporary global reanalyses.* Journal of Climate, 2011. **24**(16): p. 4189-4209.

201. Raiswell, R., et al., *Contributions from glacially derived sediment to the global iron (oxyhydr)oxide cycle: implications for iron delivery to the oceans.* Geochim Cosmochim Acta, 2006. **70**.

202. Winther, J.-G., M.N. Jespersen, and G.E. Liston, *Blue-ice areas in Antarctica derived from NOAA AVHRR satellite data.* Journal of Glaciology, 2001. **47**(157): p. 325-334.

203. Lenaerts, J., et al., *A new, high-resolution surface mass balance map of Antarctica (1979–2010) based on regional atmospheric climate modeling.* Geophysical Research Letters, 2012. **39**(4).

204. Siegert, M.J., A. Le Brocq, and A.J. Payne, *Hydrological connections between Antarctic subglacial lakes, the flow of water beneath the East Antarctic Ice Sheet and implications for sedimentary processes.* 2009.

205. Warren, C. and M. Aniya, *The calving glaciers of southern South America.* Global and Planetary Change, 1999. **22**(1-4): p. 59-77.

206. Dowdeswell, J.A. and J.O. Hagen, *Arctic ice caps and glaciers*, in *Mass Balance of the Cryosphere: Observations and Modelling of Contemporary and Future Changes*, A.J. Payne and J.L. Bamber, Editors. 2004, Cambridge University Press: Cambridge. p. 527-558.

207. Raiswell, R., et al., *Potentially bioavailable iron delivery by iceberg-hosted sediments and atmospheric dust to the polar oceans.* Biogeosciences, 2016. **13**(13): p. 3887-3900.

208. Hoelzle, M., et al., *Re-establishing glacier monitoring in Kyrgyzstan and Uzbekistan, Central Asia.* Geoscientific Instrumentation, Methods and Data Systems, 2017. **6**(2): p. 397-418.

209. Zhang, G., et al., *An inventory of glacial lakes in the Third Pole region and their changes in response to global warming.* Global and Planetary Change, 2015. **131**: p. 148-157.

210. Sakai, A., et al., *Onset of calving at supraglacial lakes on debris-covered glaciers of the Nepal Himalaya.* Journal of Glaciology, 2009. **55**(193): p. 909-917.

211. Öztuna, D., A.H. Elhan, and E. Tüccar, *Investigation of four different normality tests in terms of type 1 error rate and power under different distributions.* Turkish Journal of Medical Sciences, 2006. **36**(3): p. 171-176.

Copyright declaration

Figure 4 and Figure 22 were created using basemap data from ArcGIS online. I therefore declare that portions of this document include intellectual property of Esri and its licensors and are used under license.